

eRD14 - EIC PID Consortium

- An integrated program for particle identification (PID) for a future Electron-Ion Collider (EIC) detector.

M. Alfred¹⁰, B. Azmoun³, F. Barbosa¹⁵, W. Brooks²¹, T. Cao²⁷, M. Chiu³, E. Cisbani^{13,14}, M. Contalbrigo¹², S. Danagoulian¹⁸, A. Datta²⁴, A. Del Dotto¹³, M. Demarteau², A. Denisov¹¹, J.M. Durham¹⁷, A. Durum¹¹, R. Dzhygadlo⁹, C. Fanelli^{15,16}, D. Fields²⁴, Y. Furletova¹⁵, C. Gleason²⁵, M. Grosse-Perdekamp²³, J. Harris²⁶, M. Hattawy¹⁹, X. He⁸, H. van Hecke¹⁷, T. Horn⁴, J. Huang³, C. Hyde¹⁹, Y. Ilieva²⁵, G. Kalicy⁴, A. Kebede¹⁸, B. Kim⁵, E. Kistenev³, M. Liu¹⁷, R. Majka²⁶, J. McKisson¹⁵, R. Mendez²¹, I. Mostafanezhad²², P. Nadel-Turonski²⁰, K. Peters⁹, W. Roh⁸, R. Pisani³, P. Rossi¹⁵, M. Sarsour⁸, C. Schwarz⁹, J. Schwiening⁹, C.L. da Silva¹⁶, N. Smirnov²⁶, J. Stevens⁶, A. Sukhanov³, X. Sun⁸, S. Syed⁸, R. Towell¹, G. Varner²², R. Wagner², C. Woody³, C.-P. Wong⁸, J. Xie², Z.W. Zhao⁷, B. Zihlmann¹⁵, C. Zorn¹⁵.

Contacts: P. Nadel-Turonski <turonski@jlab.org>, Y. Ilieva <ilieva@sc.edu>

¹) Abilene Christian University, Abilene, TX 79601

²) Argonne National Lab, Argonne, IL 60439

³) Brookhaven National Lab, Upton, NY 11973

⁴) Catholic University of America, Washington, DC 20064

⁵) City College of New York, New York, NY 10031

⁶) College of William & Mary, Williamsburg, VA 2318

⁷) Duke University, Durham, NC 27708

⁸) Georgia State University, Atlanta, GA 30303

⁹) GSI Helmholtzzentrum für Schwerionenforschung GmbH, 64291 Darmstadt, Germany

¹⁰) Howard University, Washington, DC 20059

¹¹) Institute for High Energy Physics, Protvino, Russia

¹²) INFN, Sezione di Ferrara, 44100 Ferrara, Italy

¹³) INFN, Sezione di Roma, 00185 Rome, Italy

¹⁴) Istituto Superiore di Sanità, 00161 Rome, Italy

¹⁵) Jefferson Lab, Newport News, VA 23606

¹⁶) Laboratory for Nuclear Science, Massachusetts Institute of Technology, Cambridge, MA 02139

¹⁷) Los Alamos National Lab, Los Alamos, NM 87545

¹⁸) North Carolina A&T State University, Greensboro, NC 27411

¹⁹) Old Dominion University, Norfolk, VA 23529

²⁰) Stony Brook University, Stony Brook, NY 11794

²¹) Universidad Técnica Federico Santa María, Valparaíso, Chile

²²) University of Hawaii, Honolulu, HI 96822

²³) University of Illinois, Urbana-Champaign, IL 61801

²⁴) University of New Mexico, Albuquerque, NM 87131

²⁵) University of South Carolina, Columbia, SC 29208

²⁶) Yale University, New Haven, CT 06520

²⁷) University of New Hampshire, Durham, NH 03824

²⁷) Indiana University, Bloomington, IN 47405

Table of Contents

1. Introduction	3
2. Hadron identification	5
2.1 PID requirements and implementation options	5
2.1.1 Hadron ID requirements	5
2.1.2 Integrated PID solution for the EIC (concept) detector(s)	6
2.2 Dual-radiator RICH (dRICH)	9
Figure 2.2.6: The expected performance of the dRICH prototype: number of photons (left) and Cherenkov angle resolution (right) for the two radiators (aerogel and gas).	15
2.2.4 FY19 Progresses and Achievements	15
2.3 Modular Aerogel RICH (mRICH)	16
2.3.1 FY19 Progress and Achievements	17
2.3.2 Proposed mRICH R&D Activities	22
2.3.3 mRICH R&D Deliverables	22
2.4 High-Performance DIRC (hpDIRC)	23
2.4.2 FY19 Progress and Achievements	24
2.4.3 Proposed DIRC R&D Activities	30
2.4.4 DIRC R&D Deliverables	32
3. Lepton (electron) Identification	32
3.1 Electron ID	33
3.2 Muon ID	35
4. Photosensors & Electronics	35
4.1.1 FY19 Progress and Achievements	36
4.1.2 Proposed High-B R&D Activities	41
4.1.3 High-B R&D Deliverables	42
4.2 LAPPD™ MCP-PMTs	43
4.2.1 FY19 Progress and Achievements	43
4.2.2 Proposed LAPPD R&D Activities	44
4.2.3 LAPPD R&D Deliverables	45
4.3 Readout Sensors and Electronics for Detector Prototypes	45
4.3.3 Proposed R&D Deliverables	51
5. Budget	52
Appendices	55

Abstract

The EIC PID consortium (eRD14) has been formed to develop an integrated program for particle identification (PID) for a future Electron-Ion Collider (EIC) detector, for which excellent particle identification is an essential requirement. For instance, identification of hadrons in the final state is needed for understanding how different quark flavors contribute to the properties of hadrons, and reliable identification of the scattered electron is important for covering kinematics where pion backgrounds are large. The PID systems also have the greatest overall impact on the layout of the central detector and put important constraints on the magnetic field. It is thus essential to conduct the relevant R&D at an early stage of the development of a complete EIC detector. In addition to providing solutions addressing the broader EIC requirements, the PID consortium has worked closely with BNL and JLab to ensure that the R&D projects are compatible with the specific EIC detector concepts that are being pursued there.

1. Introduction

The ability to identify hadrons in the final state is a key requirement for the physics program of the EIC. Being able to tag the flavor of the struck quark in semi-inclusive DIS can, for instance, tell us something about the transverse momentum distributions (and potentially orbital angular momentum) of the strange sea, while open charm (with subsequent decays into kaons) is important for probing the distribution of gluons in protons and nuclei. While the distribution of produced particles depends on the specific process, broadly speaking the kinematics for meson production follows the energies of the colliding beams. If the reaction produces a meson traveling in the direction of the proton (ion) beam, this meson can have a momentum which is a significant fraction of that of the beam. If the meson is produced in the opposite (electron) direction, it cannot acquire more momentum than that carried by the electron beam. In the central region it is possible to produce mesons over a wide range of momenta, but the distribution is driven by the kinematics of the process (Q^2, p_T) rather than the energies of the colliding beams¹. Here, a greater reach of the PID coverage directly translates into, for instance, a larger lever arm in Q^2 – a key goal for the EIC – as well as an ability to probe deeper into the high- p_T region of semi-inclusive DIS. In both cases (high Q^2 and high p_T) the event rates are low, but the physics impact is high. The Q^2 coverage of the detector at central angles (mid rapidity) does, however, grow quickly with the momentum of the detected (and identified) particles. To fully satisfy the physics goals of the EIC, it is thus essential to provide coverage above 5 GeV/ c for hadrons (π/K) in the barrel region, with 6 – 7 GeV/ c being ideal. In the electron endcap, one would need to provide hadron ID up to a significant fraction of the electron beam energy (~ 10 GeV/ c), while in the hadron endcap one would need to reach a significant fraction of the proton or ion beam momentum (~ 50 GeV/ c).

To address the different requirements associated with the three different parts of the detector, the consortium is pursuing R&D on (and requesting funding for) three different technologies for imaging Cherenkov detectors: a dual-radiator (gas/aerogel) RICH (dRICH) for the hadron endcap, a high-performance DIRC (hpDIRC) for the central (barrel) region, and a modular aerogel RICH (mRICH) for the electron endcap, which could also be used in the hadron endcap in conjunction with a single-radiator gas RICH such as the

¹ Note that p_T is defined with respect to the virtual photon direction in the rest frame of the proton (ion) rather than the beam direction in the detector frame. A large p_T will, generally, give rise to a higher momentum, as well as a larger component transverse to the beam, but the boost smears the distribution.

one developed by eRD6. A time-of-flight (TOF) measurement, or dE/dx information from a TPC, is also needed for PID in the momentum range below the thresholds of the Cherenkov detectors, for which the consortium has performed R&D on mRPC and MCP-PMT-based TOF systems.

The Cherenkov systems also have a significant potential for e/π identification. When combined with an EM calorimeter, the mRICH and hpDIRC could provide excellent suppression of the low-momentum charged-pion backgrounds, which limit the ability to measure the scattered electron in kinematics where it loses most of its energy (in the detector frame). The progress of the R&D for these systems is very promising, and may in the future eliminate the need for other supplementary e/π identification systems (for instance, the hadronic calorimeter on the electron endcap proposed for the BeAST or an e/π Cherenkov/HBD proposed for the JLab detector). Being able to eliminate such potentially redundant systems would make the EIC detector simpler, more compact, and cheaper. Further improvement of the e/π capabilities of the Cherenkov detectors may thus be a natural extension of the current R&D effort (for the mRICH it could mean slightly increasing the focal length and reducing pixel size, while for the hpDIRC it could imply improving the time resolution and ensuring that the radiator bar length is kept as short as possible). On the hadron side, the dRICH provides a significant e/π identification capability (~ 15 GeV on its own, and more than 20 GeV when combined with the EM calorimeter), which is sufficient for the detection of, for instance, decays of charmonium states. An important recent result is that the performance does not suffer greatly even as the size of the detector is reduced. This was seen when the dRICH design was adapted to the slightly smaller space available in the BNL detectors concepts.

The PID consortium is also carrying out R&D on photosensors for the Cherenkov detectors. The challenges addressed by the PID consortium are: operations inside the magnetic field of the central detector; and cost reduction. The former is carried out using the high-B test facility at JLab and at the g-2 magnet test facility at ANL, while the latter focuses on adaptation and optimization of LAPPD™ MCP-PMT's to EIC requirements (pixelated readout, UV photocathodes, high-B capabilities), as well as characterization of early-production sensors.

In FY18 we also started a new effort within the consortium to develop cutting-edge readout electronics for all the small-pixel photosensors (including the LAPPDs) that will be used by the Cherenkov detectors. This work is being led by U. Hawaii and INFN, with support from JLab. The initial version of this electronics is already being used in the 2018 mRICH beam test at Fermilab. Later versions, based on the new SiREAD chip, which is developed under DOE SBIR program by Nalu Scientific in collaboration with University of Hawaii, are intended to form a common readout for all Cherenkov prototypes, as well as the basis for the readout of the final Cherenkov systems to be used the future EIC detector.

2. Hadron identification

2.1 PID requirements and implementation options

2.1.1 Hadron ID requirements

The physics program of the EIC, as described in the White Paper, the 2010 INT report, the 2015 NSAC Long Range Plan, and elsewhere, is very broad and multifaceted – and so are the corresponding detector requirements. The most basic particle distribution is that from inclusive Deep Inelastic Scattering (DIS),

which essentially sums over all combinations of final-state hadrons for a given kinematics (x, Q^2) of the scattered electron. As one looks at specific subsets of the data, the particle distributions can be quite different. For example, the analysis of events at the exclusive limit leads to transverse spatial imaging of the quarks and gluons in the target nucleon or ion beam, for which flavor sensitivity is crucial to unravel the chiral-symmetry-breaking structure of the sea. Here, the struck quark hadronizes into a pion or a kaon, taking essentially all of the momentum transferred from the scattered electron. In this subprocess, the kaon momenta are much higher than the average momenta for kaon production in DIS. Similarly, the intermediate case of semi-inclusive DIS allows the creation of transverse images in momentum space. Here it is also important to cover a wide range in meson momentum fraction (*vis a vis* the ‘jet’), with PID for flavor separation. Failing to do so will restrict the kinematical reach of the EIC regardless of the beam energies provided by the accelerator.

Another important case to consider is when the kaons are not produced in the primary process, but are decay products of heavier mesons. For instance, the kaons from the decay of the ϕ -meson, which is important for studies of gluon saturation, have higher momenta than kaons from the decay of D-mesons (open charm), which also provide information on gluon distributions.

A compilation of a catalogue of processes and kinematics illustrating the impact of various kaon identification options on the full EIC physics program goes beyond the scope of this R&D proposal. A lot of information can be found in the EIC White Paper, to which we refer. However, we note that for the purpose of understanding the general hadron ID requirements at EIC, this level of detail is not necessary. As long as one keeps in mind that a lot of the information lies in the tails of the distributions, where the number of particles is small, the meson distributions from inclusive DIS provide a good guidance. Figure 2.1.1 shows these distributions for pions and kaons in a common BNL/JLab kinematics (10 GeV/ c electrons on 100 GeV/ c protons), in a broad but typical bin of Q^2 .

As discussed in the introduction, with higher beam energies, the meson energies in the endcaps become correspondingly higher, while the distribution in the central barrel, is less affected. Figure 2.1.1 clearly shows the need for PID over a very wide momentum range (up to about 50 GeV/ c) in the hadron endcap, and a moderate range up to 5 – 7 GeV/ c in the central barrel. In the electron endcap, which also sees hadrons with higher momenta produced at lower values of Q^2 , the desired range would reach somewhat higher limit than the one suggested by the Q^2 -bin shown in Fig. 2.1.1, approaching the electron beam energy. Thus, an upper limit of about 10 GeV/ c is a relatively site-independent requirement. In addition, we note that the π/K ratios are not excessive – and become smaller for higher momenta, making identification easier. However, while the momentum reach for each system is conventionally quoted at the 3σ level, the analysis of each specific channel can use PID cuts such that the uncertainty from PID would match other uncertainties. Since the curves of separation vs momentum are provided for each system, a user can easily estimate the momentum reach for the level of purity required for their specific channel of interest.

It is also worth noting that AI tools have been introduced for the optimization of the dRICH configuration, with preliminary results showing a net improvement in performance. The same tools can also be extended to other systems, making the EIC detector R&D one of the first programs systematically exploiting AI.

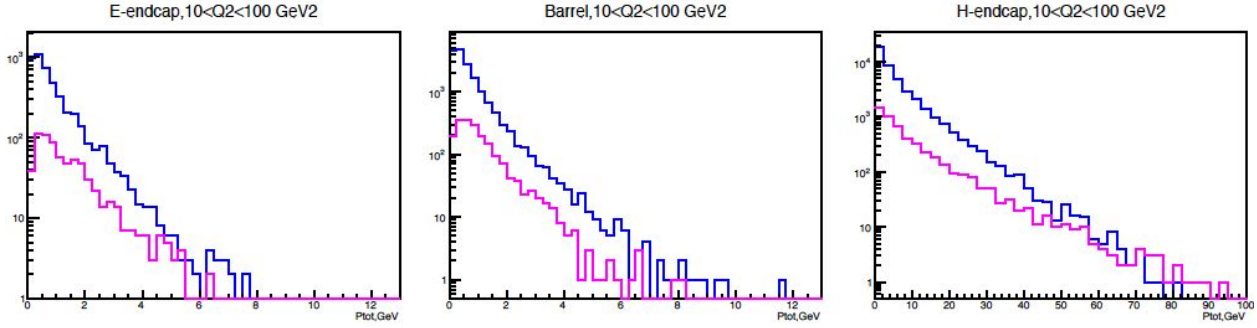


Figure 2.1.1: Momentum distributions of pions (blue) and kaons (magenta) from Pythia for DIS events corresponding to collisions between 10 GeV/c electrons and 100 GeV/c protons, a common BNL/JLab kinematics, shown for a bin of $10 < Q^2 < 100 \text{ GeV}^2$ (without imposing cuts related to any specific physics channel or analysis).

2.1.2 Integrated PID solution for the EIC (concept) detector(s)

The three model detectors developed at BNL and JLab originally had slightly different layouts of the hadron ID systems, but the configurations have converged. In particular, the layout of the BeAST detector changed in 2016, making it compatible with all the PID systems being developed by eRD14, and implementation of all three Cherenkov systems (dRICH, mRICH, and hpDIRC) is currently underway. The configuration of the EIC detector concept based on sPHENIX was also updated very recently. It now includes the mRICH in both the electron and hadron endcaps as well as the DIRC in the barrel. The psTOF is also an option for, in particular, the small angles on the hadron side. The inner Hcal, which is a particular feature of sPHENIX, makes it easier to use a gas-only RICH such as the one developed by eRD6, but a dual-radiator RICH (dRICH) could be used if the collision point was shifted, creating more space on the hadron endcap. The JLab detector concept incorporated all eRD14 technologies already from the start of the PID consortium activities. Thus, the consortium strategy of developing an integrated PID solution suited for the EIC physics requirements has not only resulted in significant progress of the hardware R&D, but also contributed to the evolution of the various EIC detector concepts proposed at BNL and JLab (shown in Figures 2.1.2 – 2.1.4).

Central Barrel

In addition to meeting the performance requirements, the PID system for the central detector has to cover a large area but with a minimal radial footprint. A DIRC detector offers an attractive solution as it can meet all three requirements. It is the most radially compact PID detector (the radiator bar thickness is less than 2 cm), and the bars can cover a large area while the sensor area remains small. Such a reduction in area can be accomplished in a conventional RICH detector by using mirrors, but this solution is not compatible with the requirement for compactness. Using recent estimates for the cost per unit area, polished fused silica is cheaper than low-cost photosensors, making the DIRC overall more suitable for the barrel than, say, the mRICH. The ongoing R&D has also shown that performance can be pushed well beyond the 4 GeV/c achieved in BaBar, up to 5 – 6 GeV/c using advanced optics (eRD4) and to 6 – 7 GeV/c by optimizing the system for time-based reconstruction (eRD14), making the hpDIRC a very good match for the EIC requirements. The DIRC has thus now been adopted as a baseline solution by the three detector concepts developed at BNL and JLab, although a high-resolution TOF could also be considered for the PID in the barrel as it is relatively compact and affordable.

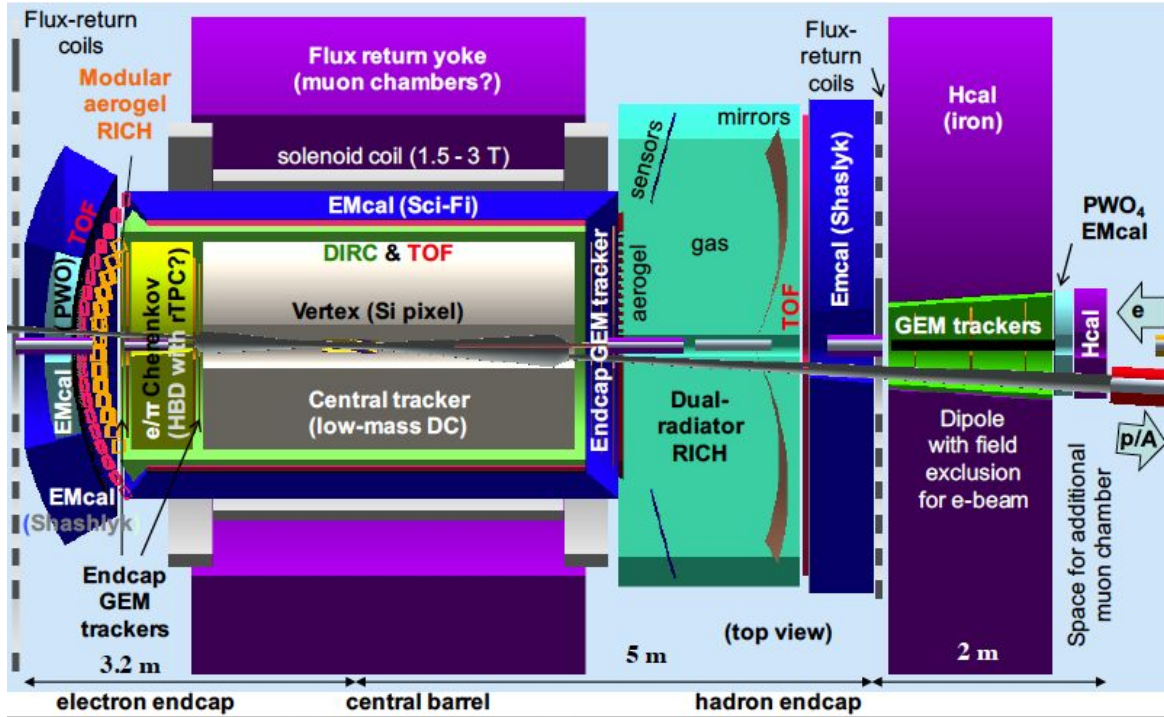


Figure 2.1.2: The JLab central detector concept uses the DIRC, dual-radiator, and modular aerogel RICH detectors from the eRD14 R&D, and has 4π TOF coverage. It also includes an e/π Cherenkov detector in the electron endcap for suppression of low-momentum charged pions, although the supplementary e/π capability of the latest version of the mRICH may turn out to be sufficient for this task.

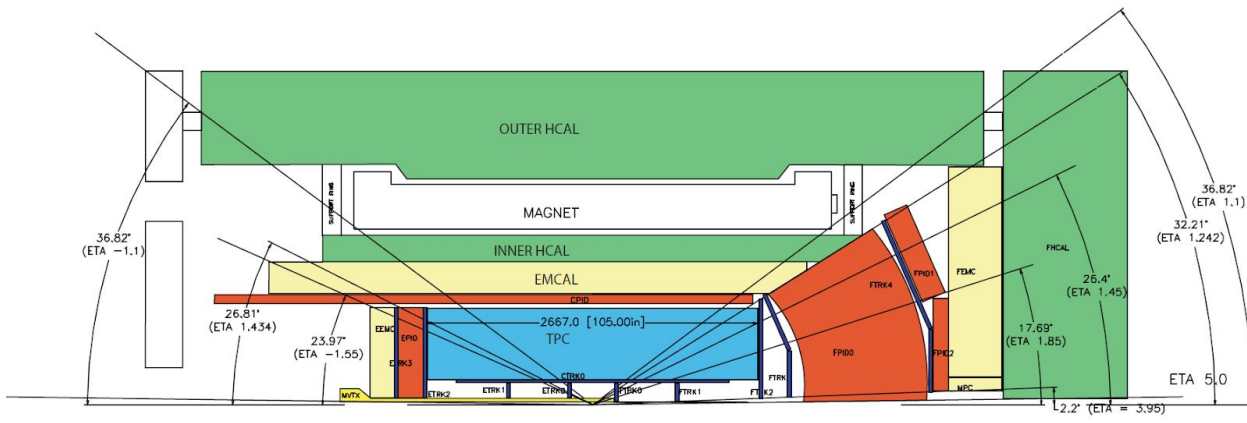


Figure 2.1.3: The 2018 version of the BNL EIC detector based on sPHENIX (which uses the BaBar solenoid) includes a DIRC at mid-rapidity and the mRICH in the electron endcap. In the hadron endcap, the current concept uses the single-radiator gas RICH developed by eRD6 in combination with the mRICH, but is also compatible with a dual-radiator RICH, such as the one developed by eRD14.

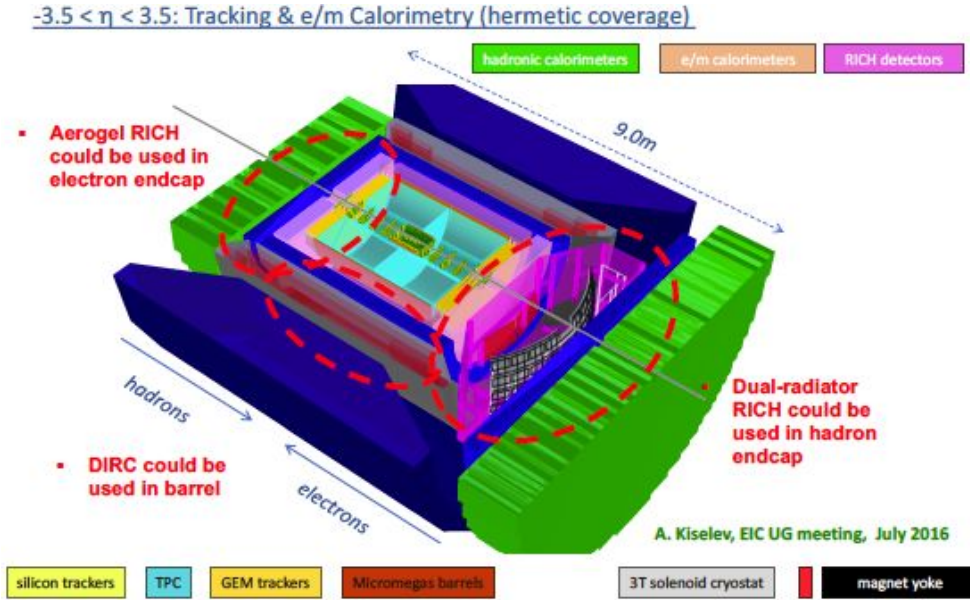


Figure 2.1.4: The BNL BeAST detector concept reserves space for several types of PID systems. Currently, all three eRD14 Cherenkov systems (DIRC, mRICH, and dRICH) are being implemented (although the figure above shows the CMB RICH from GSI which came with the simulation package).

(Outgoing) electron-side endcap

The EIC is designed to support a wide range of electron beam energies (currently assumed to be 3 – 12 GeV in the JLab design and up to 18 GeV at BNL). However, hadron ID for momenta up to about 10 GeV/c would satisfy both the BNL and JLab requirements, making a compact, high-performance aerogel RICH a natural choice. Over the last year, such a system has become part of the baseline for all three major EIC detector concepts (JLab, ePHENIX, BeAST). In terms of implementation, there are three options. A mirror-based design, a proximity-focused design using two aerogel indices, and a lens-based aerogel RICH. However, the mirror-based option is not compact, and the proximity-focused alternative is only compact if the momentum coverage is modest. The lens-focused mRICH design, on the other hand, offers both a compact design and the desired momentum range. The lens-focusing also reduces the sensor area required per unit of solid angle, which is important since photosensors are the main cost driver of the RICH detectors.

(Outgoing) hadron-side endcap

Due to the large span of hadron momenta, ranging from a few GeV to a large fraction of the beam energy, the PID requirements on the hadron endcap are in many ways the most demanding. The difference in the maximum proton-beam energies considered at the two sites is also significant (250 GeV for BNL and 100 GeV for JLab). However, even for lower beam energies the maximum hadron momenta are so large that it is important to provide good π/K separation up to several tens of GeVs. Thus, any future EIC detector will need to incorporate a mirror-based, focusing gas RICH as part of the hadron-side PID solution. From a technological point of view, the R&D path that needs to be pursued for the hadron ID is thus relatively site-independent, and a nominal 3σ π/K coverage up to 50 GeV/c is reasonable for both sites.

The key challenge is instead how to best cover the full momentum range. The most straightforward solution is to have a dual-radiator (gas and aerogel) RICH covering the high and mid momentum range, with

supplementary coverage by TOF (or dE/dx) for the lower momenta. However, no such RICH has yet been built for a collider experiment with the strong limitations due to space and magnetic field expected for an EIC detector, making the ongoing R&D undertaken by eRD14 imperative. By combining $n=1.02$ aerogel and C_2F_6 gas, the dual-radiator RICH (dRICH) design pursued by eRD14 provides continuous coverage in RICH mode over the full momentum range (see Fig 2.1.5), and the layout with sector-based, outward-reflecting mirrors makes it possible to move the photosensors away from the beam.

However, the natural geometry for a dRICH is almost cylindrical, and if the layout of the other subsystems favor a more conical shape, the CF_4 gas-only RICH with inward-reflecting mirrors developed by eRD6 could be favorable. The gas-only RICH could be supplemented by separate detectors such as the mRICH (used in the current version of ePHENIX) or TOF to cover the lower momenta. The lack of continuous PID coverage in this configuration suggests, however, that further R&D may be needed, perhaps considering the use of a heavier gas with a slightly higher index of refraction.

Aerogel ($n = 1.02$) | $e_{th}(GeV/c) = 0.0025$ | $\pi_{th}(GeV/c) = 0.67$ | $K_{th}(GeV/c) = 2.46$ | $p_{th}(GeV/c) = 4.89$
C₂F₆ ($n = 1.00082$) | $e_{th}(GeV/c) = 0.0123$ | $\pi_{th}(GeV/c) = 3.48$ | $K_{th}(GeV/c) = 12.3$ | $p_{th}(GeV/c) = 23.4$

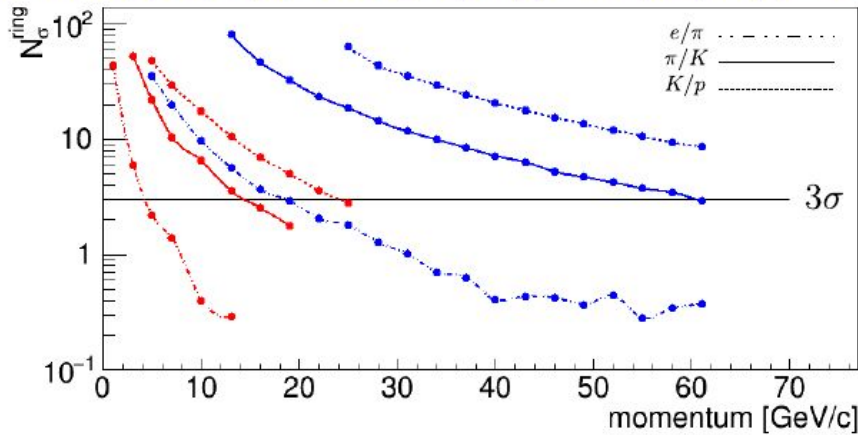


Figure 2.1.5: C_2F_6 gas/aerogel dual-radiator RICH performance for a particle scattered at 15 degrees. There is a good overlap between the PID coverage of the aerogel (red) and the gas (blue) for all three pairs of particle species.

2.2 Dual-radiator RICH (dRICH)

Contacts: Z.W. Zhao <zwzhao@jlab.org>, E. Cisbani <evaristo.cisbani@roma1.infn.it>, M. Contalbrigo <marco.contalbrigo@fe.infn.it>

The dual-radiator Ring Imaging Cherenkov (dRICH) detector has been designed to provide continuous full hadron identification ($\pi/K/p$ better than 3 sigma apart) from ~ 3 GeV/c to ~ 60 GeV/c, and electron identification (e/π) up to about 15 GeV/c, at the (outgoing) ion-side endcap of the EIC detector, covering angles up to 25° . Achieving such a momentum coverage in the ion-side region is a key requirement for the EIC physics program. Currently, the dRICH is the only hadron identification detector in EIC able to provide continuous coverage in RICH mode over the full momentum range required for the forward endcap.

The dRICH baseline configuration has been consolidated in the first half of 2018; it consists of two radiators

(aerogel and gas) sharing the same outward focusing mirror and highly segmented photosensors ($\sim 3 \text{ mm}^2$ pixels). The focal plane is away from the beam and ensures that the UV photons radiated in the gas have a direct path to the photosensors without passing through the aerogel. A spherical mirror combined with a flat focal plane creates aberrations, in particular at small angles. These can be addressed by building a correction into the mirror itself (as is done in applications for astronomy), or by arranging the arrangement of the photosensors on a curved surface in a way that minimizes aberrations. While both approaches work, the latter seems simpler and was implemented in the dRICH, as shown in Fig. 2.2.1.

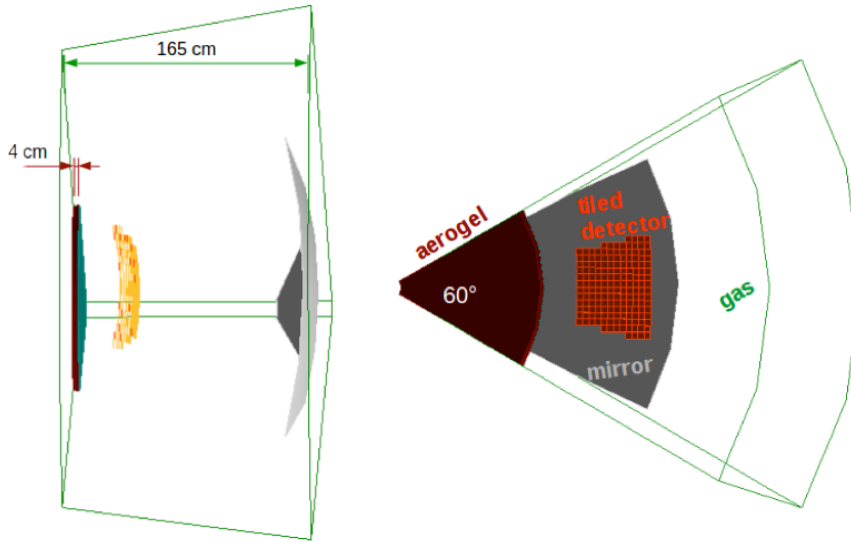


Figure 2.2.1: A single dRICH sector with slightly curved optical sensor detector surface. **Left:** side view of aerogel (dark red), mirror (light grey) and sensors (yellow); indicated are the aerogel thickness and the gas gap. **Right:** front view of aerogel (dark red), mirror (light grey) and sensors (light red).

2.2.1 Design optimization based on Bayesian Approach

Every detector consists of a significant number of components, and questions like how much space to allocate for each, what kind of detector to use, and which configuration allows the best PID/reconstruction, are often real dilemmas that need to be resolved without increasing costs.

In addition, the detector requirements are typically more stringent for multipurpose experiments like EIC, and best decisions require large-scale simulations of the major physics processes.

For all these reasons, learning algorithms (*e.g.*, AI-based) can be extremely useful in making faster and more efficient decisions. Bayesian Optimizers (BO) [Jon18, Sno12] are particularly suitable for optimizing the EIC detector design and can be deployed for a variety of critical R&D efforts over the next years.

BO's search for the global optimization over a bounded domain χ of black-box functions, formally expressed as $x^* = \arg \min_{x \in \chi} f(x)$, where f can be a noisy non-differentiable black-box function, which is expensive to evaluate. The aim of a BO is to keep the number of iterations required to identify the optimal value relatively small. When applied to detector design, each point explored corresponds to a different detector configuration. The function f can be thought of as a figure of merit that is to be optimized (*e.g.*, related to PID performance). Typically gaussian processes are used in building a surrogate model of f , but other regression methods, such as decision trees, can also be used.

We have explored BO in the optimization of the design of the dual-RICH. In a preliminary work (shown in

Fig. 2.2.2), six main parameters were considered to model the design (radial and longitudinal positions of mirror center, mirror radius, along with vertical and longitudinal positions and rotation of detector tiles with respect to the mirror center). The objective function chosen for the optimization corresponds to the N_σ (described in Sec. 2.1.2 and quantifying the separation power between pions and kaons). The sample of particles used for this detector design covers a larger phase-space than the one shown in Fig. 2.2.1, with polar angles spanning from 5 to 15 degrees and large momenta. Work is ongoing to extend the optimization to the transition regions between the aerogel and gas, as well as TOF and aerogel, including a more general parametrization of the detector.

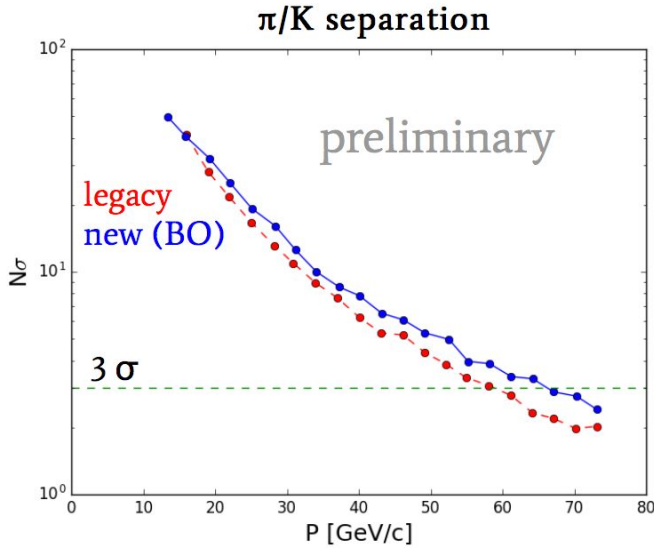


Figure 2.2.2: Comparison between the legacy (cf. Fig. 2.2.1) and a new design for the dRICH based on bayesian optimization. The new design shows (in the gas region) an improved separation between pions and kaons of at least $3 N_\sigma$ up to large momenta ($\sim 60 \text{ GeV}/c$).

This approach can be applied to design other detectors of EIC, and could in principle be generalized to a global detector design that combines different detectors, thus, maximizing the overall PID performance and reducing the costs of production.

2.2.2 Event-based reconstruction algorithm

A new event-based Cherenkov angle reconstruction method was introduced in 2018 to properly treat events with multiplicity larger than 1. The method essentially consists of two main steps: a single hit (detected photon) association followed by a global hypothesis (particle-types/tracks-radiators) selection based on the previous association. Each step is based on the optimization of a specific likelihood function that accounts for the angular correlation (the angle is estimated by the Inverse Ray-Tracing method) and the number of detected photons. The performances have been evaluated using deep-inelastic PYTHIA generated physics events, about 40% of which have multiple tracks and 50% of those have overlapping rings in dRICH.

The method has been refined and critically analyzed in the second half of 2018 and first half of 2019, especially in terms of the first-step likelihood function composition. Figure 2.2.3 shows the current main result: the optimal likelihood for hit association is essentially composed of the products of the confidence levels of the angular correlation (governed by the ERF function) of the photon to a single track-radiator and the anti correlation of the same photon relative to the other tracks-radiators. We are in the process of

finalizing an article describing this new reconstruction method and the results of the detailed analysis of the likelihood function.

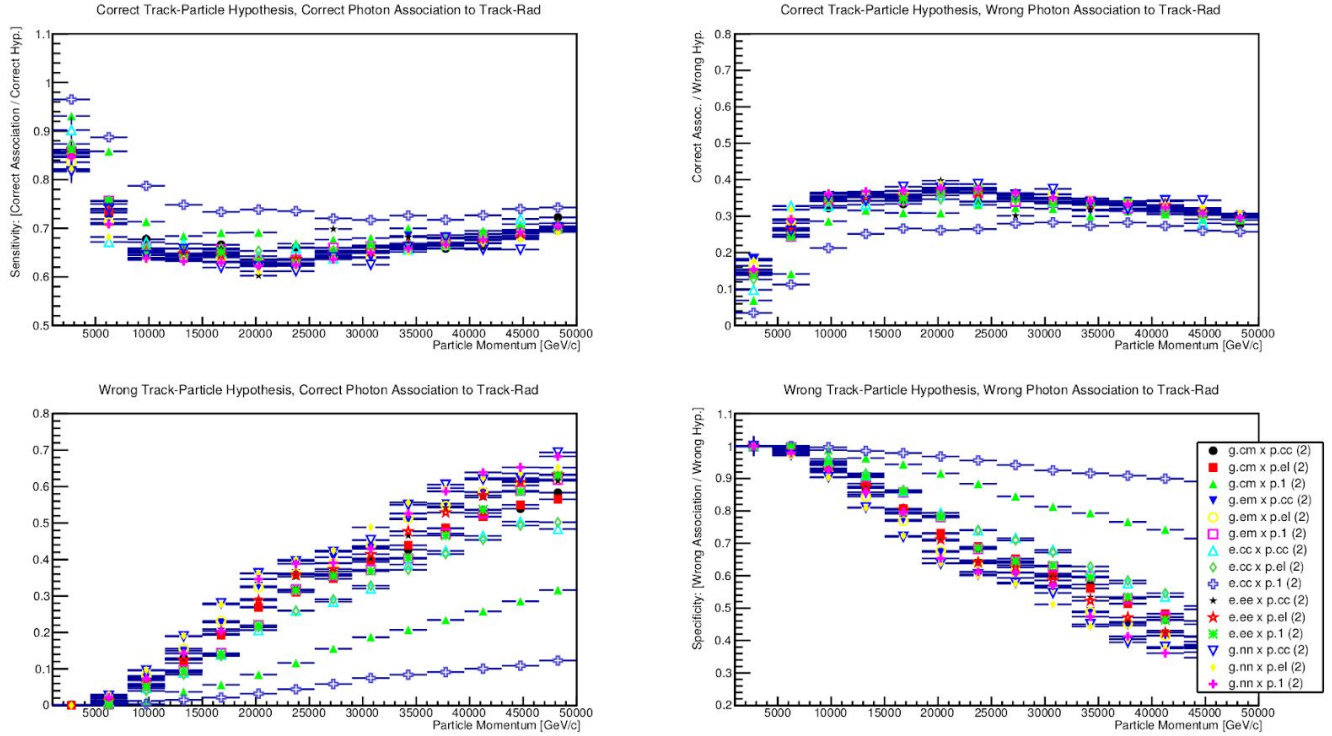


Figure 2.2.3: Analysis of the likelihood function composition used for hit association. The different points correspond to different likelihood compositions (shown in the legend). All plots show the success or failure rates as a function of particle momentum. The upper left and lower right plots show the rate of success and failure respectively for the correct and wrong particle hypotheses; they should be as large as possible. The remaining plots show the failure rate of reconstruction when the particle type hypothesis is correct (upper right) or wrong (lower left); they should be as small as possible.

2.2.3 dRICH prototype

The design of the dRICH has several critical aspects that need to be experimentally investigated: in fact, the performances of the dRICH largely depend on the effective number of Cherenkov photons produced in both radiators, as well as on the quality of the aerogel in terms of chromatic dependence of the refractive index; moreover, the impact of scintillation photons in “Freon” gases needs to be evaluated. All these aspects can only be addressed in a realistic prototype. For this reason a small scale prototype is under development. The design of the prototype is driven by the following main requirements:

1. reasonable number (order of 10) of photoelectrons for the gas ring per particle; this number depends almost linearly on the thickness (length) of the gas and therefore of the vessel;
2. catch both the aerogel ring (with a cone aperture of 11°) and the gas ring (with a cone aperture of 2.2°) in order to be able to estimate the angular resolution; this constraints the minimum transverse and longitudinal

sizes of the vessel;

3. compatibility with different photosensor solutions, starting with the ones already available within the eRD14, *e.g.*, four H13700 multianode PMTs (5x5 cm² each) or four S12642-1616PA matrices of 3x3 mm² area SiPMs, and related electronics;

4. isolation of aerogel and optical sensors from “Freon” gases;

5. specificities of the Fermi-Lab test beam facility (in particular mesons at different energies with transverse beam size of about 10 cm²), where the beam tests are expected to be performed;

6. possibility to reuse a 1-m long cylinder from the Stony Brook RICH (Klaus Dehmelt);

7. minimization of the vessel volume (to minimize the consumption of the expensive gas).

A consolidated design of the dRICH prototype is shown in Fig. 2.2.4.

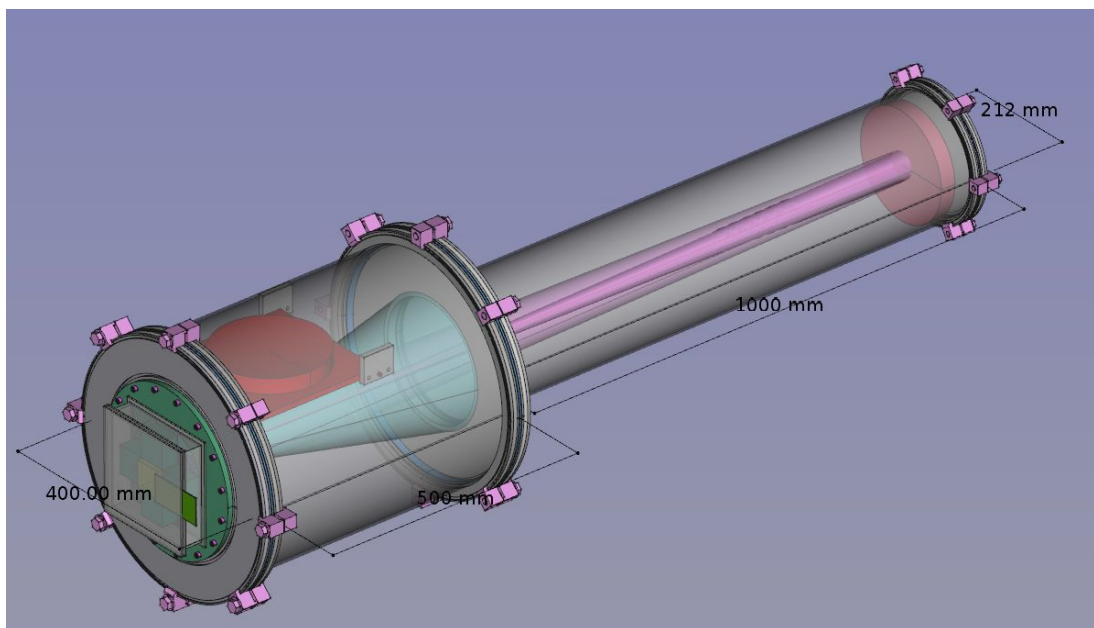


Figure 2.2.4: Consolidated 3D drawing of the dRICH prototype: the sensors (cyan) and aerogel (yellow) radiator are on the left, mounted onto the entrance flange (green) inside a dark box. The small gas mirror (red) is on the far right end. An insertable aerogel mirror (red) may intercept the aerogel photons and reflect them back to the PMTs.

The dRICH prototype design is being developed taking into account the following goals:

- mimic the properties and performance of the proposed dRICH components, and/or permit to derive them in a direct way;
- be cost effective (trade-off of small scale, flexibility and measurable quantities);
- be flexible enough to allow the use and test of different detector and components solutions.

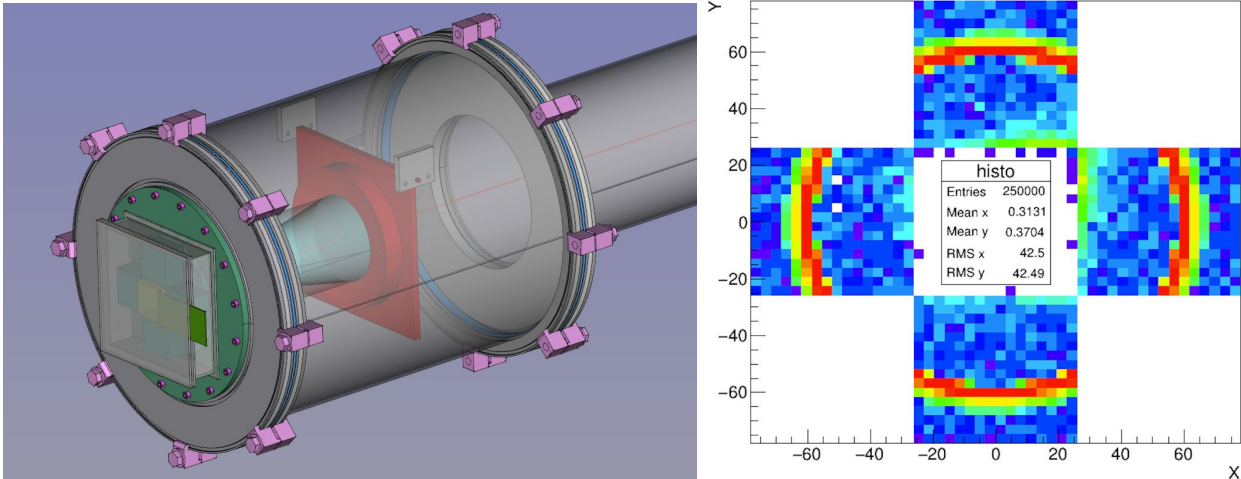


Figure 2.2.5: (Left) Detail of the dRICH prototype in the aerogel ring configuration. (Right) Simulated Cherenkov ring generated by the aerogel (on a log scale). The prototype is designed to image either the aerogel or gas Cherenkov ring at the center of the sensor array.

The prototype vessel is divided into two sections to minimize the dimensions while accommodating the different Cherenkov paths. The entrance flange houses a UV-transparent lucite foil (or quartz window) to isolate the inner gas volume while allowing the passage of the Cherenkov light. On its outer face, screw holes allow the insertion of a dark box with various sensors and an aerogel tile with possible additional UV filters. The focal planes of the mirrors coincide with the sensor entrance surface (a radius of 3 m and 0.6 m is adopted for gas and aerogel, respectively). Either the aerogel or gas Cherenkov photons are imaged at the center of the sensor array, depending on the position of the central rotatable mirror. The performance of each single radiator can be studied in detail and without interference, thus, optimising the usage of the limited instrumented area. The elements of the vessel are made of vacuum standards, to allow an efficient and safe gas exchange. A cap can be mounted on the entrance face with a bypass connecting the inner volume, to prevent pressure stress on the lucite foil during gas exhaust and exchange.

The sensor dark box and covered area follows the mRICH design and accounts for the available $5 \times 5 \text{ cm}^2$ sensors already successfully employed at test beams, but can also support other detector choices. The present configuration of the sensors guarantees the best coverage of the gas ring (radius of approx. 6 cm). The photo-sensor pixel size of 3 mm will keep the angular digitization (or pixel) error comparable to the other errors, allowing for the assessment of the intrinsic sources of uncertainties of the various radiators, and will reduce multiple photoelectrons in a single pixel for the gas ring (which will help to more accurately estimate the number of Cherenkov photons).

The proposed prototype configuration has been modeled and simulated in GEMC/Geant4. An example of a simulated configuration is shown in Fig. 2.2.5. The prototype allows the study of the Cherenkov resolution as a function of the optical properties of the radiators and filters. The prototype shall confirm and validate the dual radiator approach to cover the momentum range of few GeV/c – multi tens of GeV/c . Moreover, the radiator performance will be studied in terms of number of photons as well as angular uncertainties, possibly

for different aerogel thicknesses, gas types, and wavelength filters between solid and gas radiators (depending on aerogel availability). The chromatic dispersion of the aerogel, the expected dominant error in EIC configuration, can be studied with the insertion of optical filters, a method successfully employed in the past [Per16], as shown in Fig. 2.2.6. Of particular interest is the study with a meson beam at momenta intermediate between the two radiators working ranges.

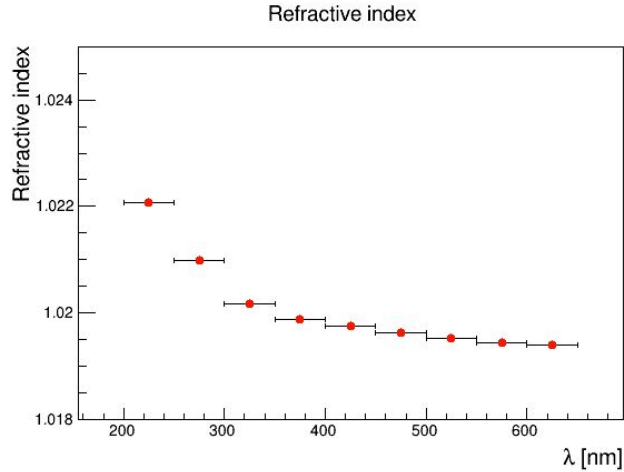


Figure 2.2.6: Simulation of a series of measurements with optical filters, to record only the photons in selected intervals of wavelengths and measure the chromatic dispersion of the aerogel. For each point, a statistics of 1000 events is assumed.

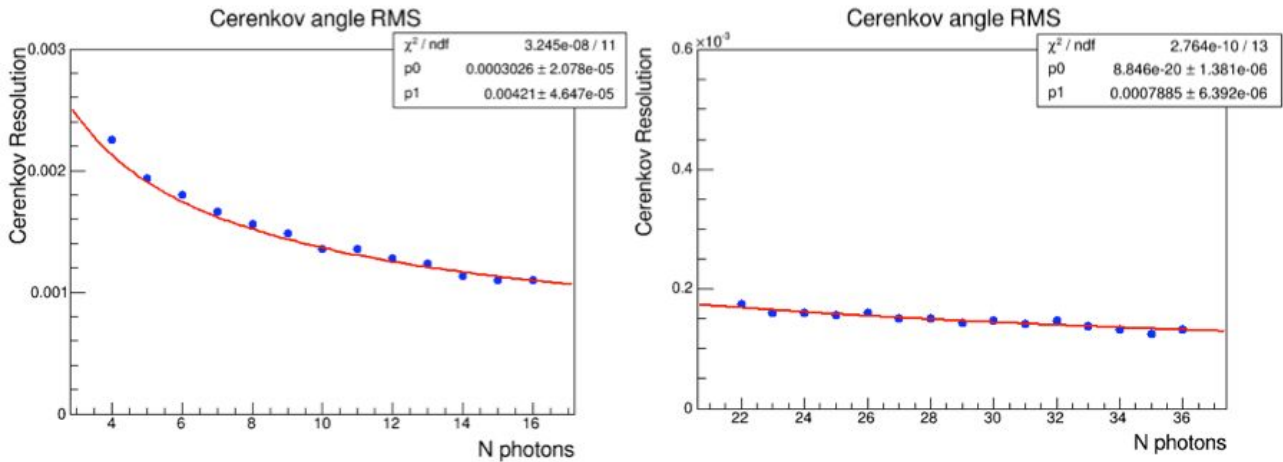


Figure 2.2.7: The expected performance of the dRICH prototype: Cerenkov angle resolution as a function of the number of detected photons for aerogel (left) and C_2F_6 gas (right) for UV sensitive H13700.

The expected number of detected photons is 9.4 for the aerogel and 27.9 for the gas. The resolutions are summarized in Table 2.2.1. The uncertainties are similar to the ones expected in the EIC configuration,

except for the pixel error with the aerogel radiator that, despite being larger due to the adapted imaging (reduced path of photons), is still smaller than the chromatic error and can be safely controlled by simulations.

1 p.e. Error (mrad)	Aerogel	C ₂ F ₆ Gas
Chromatic error	3.2	0.51
Emission	0.5	0.5
Pixel	2.5	0.42

Table 2.2.1: Main sources of uncertainty of the single-photon Cherenkov angle measurement with the dRICH prototype.

The dRICH prototype is exploiting all the synergies with the mRICH activities, as well as with other eRD14 initiatives: the photosensors and DAQ are shared between the two dRICH and mRICH prototypes; test-bench facilities derived from CLAS12 RICH are going to be used for radiators and PMT characterizations. The investigation of the gas performances will be useful also to consolidate the BNL gas RICH approach.

The minimal budget for the dRICH prototype consists of the mechanical tank, the gas, and related issues (one gas cylinder/2000 USD is expected to last for a single run; proper recirculation is required for safety/environmental reasons), the mirror, sensor supports, and UV filters.

The INFN manpower assigned to the mRICH activity will also be leading the dRICH prototype realization.

2.2.4 FY19 Progresses and Achievements

1. Application AI based methods (Bayesian approach) to the optimization of the dRICH geometrical configuration.
2. Completion of the analysis of the event-based Cherenkov angle reconstruction algorithm; submission of a paper for publication.
3. Finalization of a realistic design of the dRICH prototype.
4. Extension of the dRICH simulations to the prototype case in order to optimize the prototype design.
5. Start of prototype construction and procurement of its components.
6. Start of preparation of the aerogel/gas “long term” characterization tests and first beam test.

2.2.5 Proposed dRICH R&D Activities

1. Complete the prototype.
2. Perform a prototype test beam, possibly with a pre-test, to verify prototype functionality (coordinate with the mRICH).
3. Validation of the Monte Carlo simulation based on GEMC.

4. Improve dRICH model based on the test results and re-estimate expected performances (tune relevant parameters used in the Monte Carlo to carry on the past years analysis/development and consolidate the performances of the proposed detectors).
5. Continue long-term aerogel/gas characterization tests.

2.2.6 dRICH R&D Deliverables

FY20:

1. Results from the prototype test beam.
2. Validated MonteCarlo based on GEMC.
3. Assessment of the aerogel/gas interplay.

References

[Per16] S.A. Pereira et al, Eur. Phys. J. A (2016) 52: 23.

[Jon18] D.R. Jones et al., "Efficient global optimization of expensive black-box functions." J Global Optim 13.4 (1998): 455-492.

[Sno12] J. Snoek et al., R. P. (2012). "Practical bayesian optimization of machine learning algorithms". In NeurIPS (pp. 2951-2959).

2.3 Modular Aerogel RICH (mRICH)

Contacts: X. He <xhe@gsu.edu>, M.Contalbrigo <mcontalb@fe.infn.it>

The state-of-the-art designs of imaging Cherenkov detectors, such as proximity focusing detectors², or mirror-based imaging detectors³ require substantial volumes to be able to identify particles with momentum close to 10 GeV/c, due to the requirements imposed by the optical elements in the case of mirror-based detectors, or the desired ring separation in the case of proximity focusing devices. In the endcap regions of the proposed EIC detector, such space is not available. A more compact and modular design is required to fit into the available space and to still provide hadron PID capability with momentum coverage from 3 GeV/c to 10 GeV/c and e/π separation at lower momenta below 2 GeV/c.

² E. Torassa, Nucl. Instr.. Meth. **A824**, 152 (2016).
M. Tabata et al., Nucl. Instr.. Meth. **A766**, 212 (2014).

³ M. Adinolfi et al., Eur. Phys. J. **C73**, 2431 (2013).
A. Augusto Alves Jr et al., J. Instrum. **3**, s08005 (2008).
J. Engelfried et al., Nucl. Instr.. Meth. **A502**, 285 (2003).
J. Engelfried et al., Nucl. Instr.. Meth. **A431**, 53 (1999).
M. Contalbrigo et al., Nucl. Instr.. Meth. **A639**, 302 (2011).
R. A. Montgomery, Nucl. Instr.. Meth. **A732**, 366 (2013).

The mRICH consists of four components. A block of aerogel serves as the Cherenkov radiator. Immediately following is an acrylic Fresnel lens, which focuses the ring image and acts as a UV filter⁴. A pixelated optical sensor is located in the image plane, and the gap between the lens and the image plane is bounded by four flat mirrors. The device is shown in Fig. 2.3.1 (left). Also shown in Fig. 2.3.1 (right) is an event display of a 9 GeV/c pion traveling toward the center of the mRICH detector using the Geant4-based GEMC simulation framework.

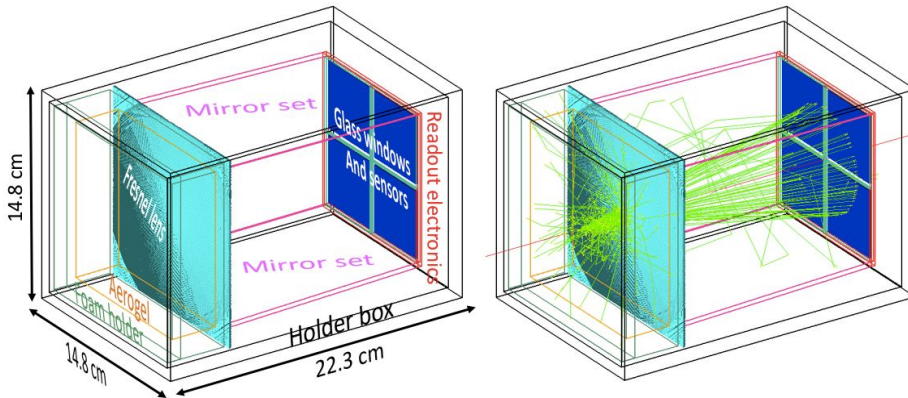


Figure 2.3.1: **Left:** The mRICH detector layout and its components. **Right:** An event display of a single 9 GeV/c pion traveling toward the center of the mRICH detector.

Two mRICH prototypes have been successfully tested at Fermilab. The first test was performed in 2016 for verifying the working principle of the design and the results have been published in NIM A. The second prototype was tested in 2018 to study PID performance with an improved design and a smaller pixel size of the photosensors.

2.3.1 FY19 Progress and Achievements

In FY19, the main activities include: (1) analysis of the second mRICH beam-test data taken at Fermilab in June of 2018; (2) implementation of the mRICH detector in the Forward sPHENIX experiment simulation; (3) study of the mRICH performance in the EIC detector designs using Pythia events.

Data Analysis of the 2nd mRICH Prototype Beam Test

Figure 2.3.2 shows the optical components of the second mRICH prototype built at Georgia State University (GSU). The second mRICH beam test took place from June 25 to July 6, 2018 at Fermilab. Three run configurations were used during the test: (1) 120-GeV/c proton beam incident perpendicularly to the mRICH in its active region to verify the ring image size, the number of detected Cherenkov photons, and the image-focusing property (see pixelated cumulative ring image on left in Fig. 2.3.3); (2) 120-GeV/c proton beam incident at an angle of 11° (see pixelated cumulative ring image in the middle plot of Fig. 2.3.3); and (3) meson beams at 2.0, 5.0 and 8.0 GeV/c (see pixelated cumulative ring image on right in Fig. 2.3.3). Very preliminary results from the ongoing analysis are selected for this report and shown in Figures 2.3.4, 2.3.5, 2.3.6 and 2.3.7. The signal time duration (or time over threshold) is related to the measured charge. The single-photon signal peaks at time durations around 50 ns, with a tail at shorter durations in case of incomplete multiplication in the H13700 dynodes. The excess of signals at durations around 30 ns is due to optical (in the sensor) or electrical (in the front-end) cross-talks. The excess at durations larger than 70 ns corresponds to large signals generated by the charged particle.

⁴ D.E. Fields et al., Nucl. Instr.. Meth. **A349**, 431 (1994).

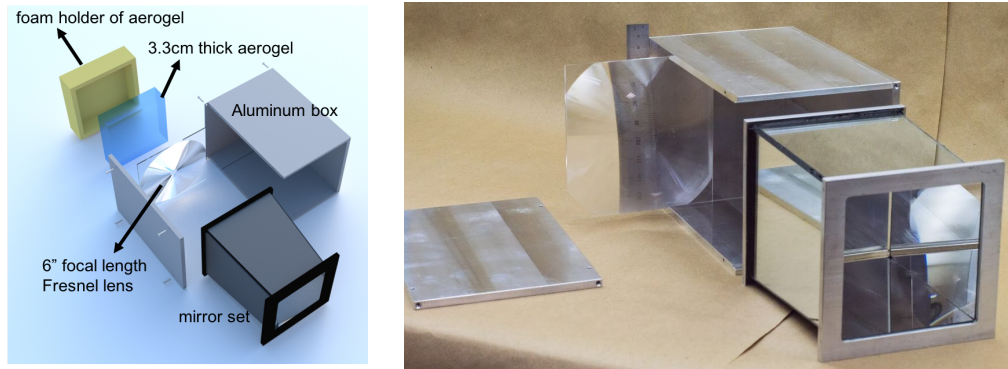


Figure 2.3.2: (left) 3D rendering of the second mRICH design; (right) second mRICH prototype components and assembly.

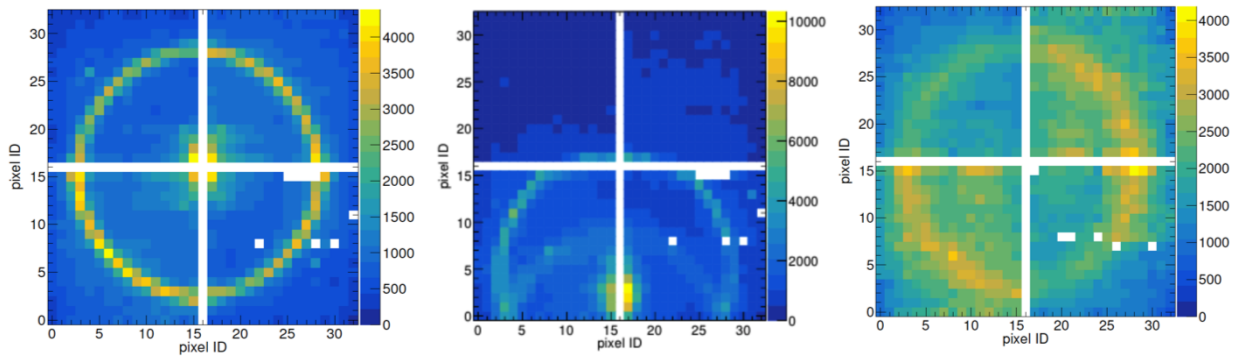


Figure 2.3.3: (left) Cumulative ring images formed from the 120-GeV/c primary proton beam incident on the center of mRICH. The white gaps show the PMT frames; (middle) ring images from the 120-GeV/c primary protons incident at an angle of 11° toward the lower section of mRICH; (right) images from an 8-GeV/c meson beam (mostly pions with a small mixture of kaons). The challenge of this analysis is to determine the beam position, since our beam hodoscope readout was not ready for this test.

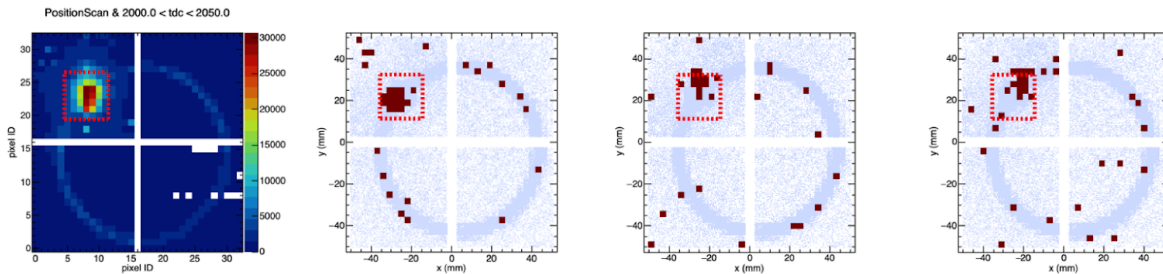


Figure 2.3.4: Event-by-event analysis of 120-GeV/c proton beam incident near the central region of the upper-left quadrant in the sensor plane. The pixelated cumulative images are shown in the left plot, which is followed by the images of three randomly picked single events. The red-dashed rectangular box indicates the region of the beam spot for this run. The shaded near-circular patterns in the three images on right are generated with a GEANT4-based simulation.

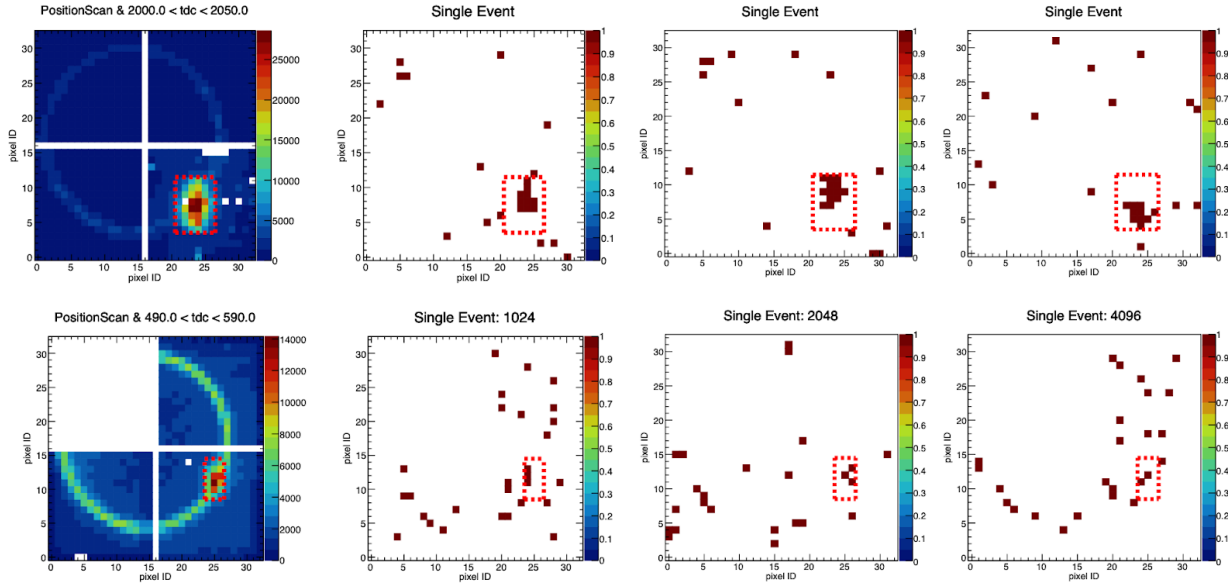


Figure 2.3.5: Comparison study of beam-spot (in the dotted box region) effects on Hamamatsu H13700 multi-anode PMTs (**top** row) and SiPM matrix (**bottom** row). The first column shows the accumulated ring images from a 120-GeV/c proton beam incident toward the lower left quadrant of the sensor plane. The other three columns show randomly picked single event photon hits samples. It is noted that there is no significant beam-spot pixel patterns observed on the SiPM matrix sensors (**lower** row) as it is seen on the H13700 sensors (**upper** row).

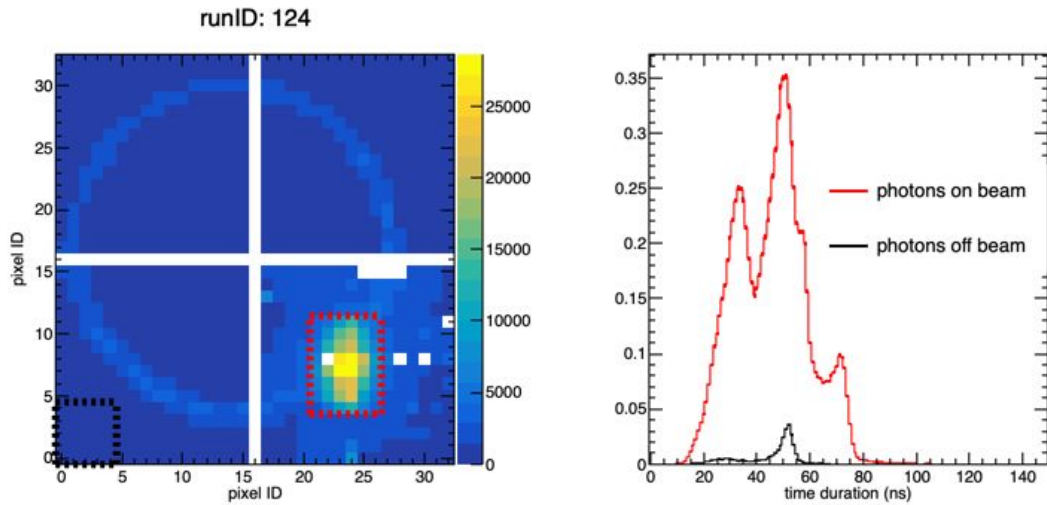


Figure 2.3.6: Timing structure (“time duration” = TDC time over threshold) comparison study of beam-spot (in the dotted box region) effects on Hamamatsu H13700 multi-anode PMTs. The red histogram in the right plot contains the events within the red boxed region in the cumulative image plot on the left, while the black histogram contains the events in the black boxed region at lower left corner. A detailed analysis of these data is ongoing.

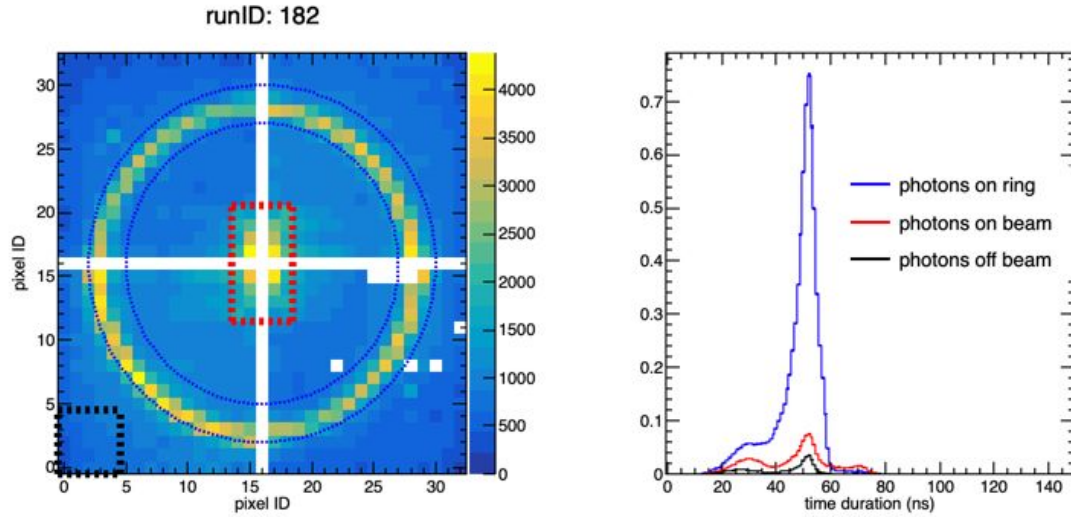


Figure 2.3.7: Timing structure (“time duration” = TDC time over threshold) comparison study of beam spot (in the dotted box region), ring-region, and the background region (black dotted-line region) from the Hamamatsu H13700 multi-anode PMTs. The red histogram in the right plot contains the events from the red boxed region in the cumulative image plot on the left, while the black histograms contains the events from the black boxed region in the lower left corner. A detailed analysis of these data is ongoing.

mRICH in the Forward sPHENIX Experiment

In order to validate the mRICH PID performance in real experiments before EIC comes online, an implementation of the mRICH detector array in the Forward sPHENIX was proposed in a recent Letter of Intent to BNL (as shown in Fig. 2.3.8). The addition of the mRICH detector to the Forward sPHENIX will not only enhance the physics capabilities of the sPHENIX experiment but will also make the sPHENIX detector a realistic detector for future EIC experiments. The mRICH implementation in the forward region is the first step of upgrading sPHENIX with PID capability.

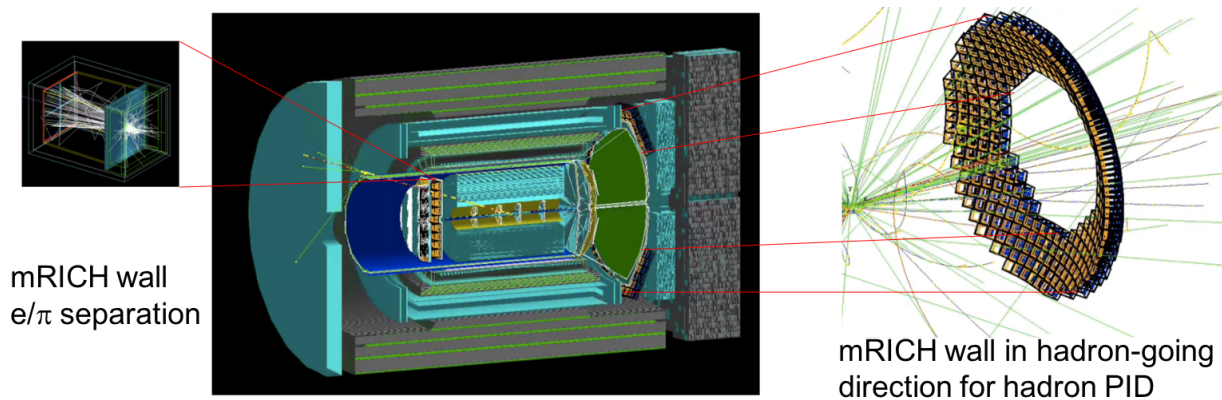


Figure 2.3.8: Conceptual design of the Forward sPHENIX with the mRICH detector arrays.

mRICH Performance in the EIC Detector Designs Using Pythia Events

Xu Sun (a post-doc at GSU), together with Zhiwen Zhao (Duke University), is leading the development of PID algorithms with mRICH using a log likelihood method. As an example, Fig. 2.3.9 shows ring-image patterns that have been generated from realistic Geant4 simulations of 5-GeV/ c pions, kaons, and protons. A systematic study of this PID method is currently ongoing.

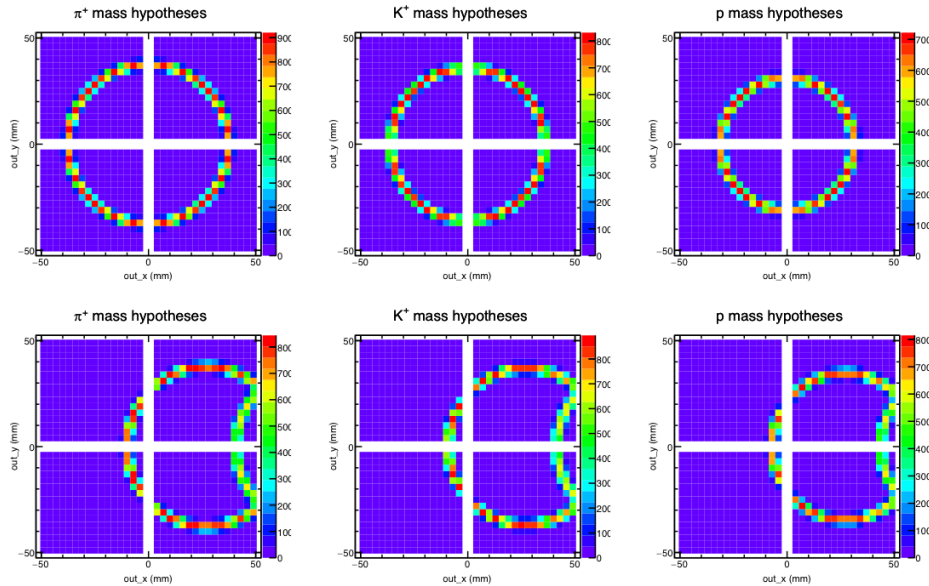


Figure 2.3.9: Cherenkov ring-image patterns generated in a Geant4 simulation. A log likelihood method uses these patterns to provide the PID information. The top row shows the image patterns from pions, kaons, and protons at 5 GeV/ c . These particles enter perpendicularly to the front of the mRICH module at the center. The bottom row shows the image patterns when the particles enter at an angle of 10°.

2.3.2 Proposed mRICH R&D Activities

In FY20, the proposed activities aim to finish the data analysis of the second mRICH beam test and to publish the results, as well as to perform other planned mRICH R&D tasks. In parallel, a joint beam test with the dRICH prototype will be organized to focus on the design readout chain connecting the new front-end chip (SiREAD-based readout and associated firmware) and the SSP protocol. Such a beam test will also provide the chance to continue the detailed study of the mRICH optical performance. Specifically, we will work on

- Data analysis of the second mRICH beam test (ongoing effort).
- Study of radiation hardness of the Fresnel lens (led by G. Kalicy).
- Development of an optical characterization system to measure the lens and aerogel block properties (students project at GSU funded by internal sources).
- Simulation study of mRICH performance in the Forward sPHENIX experiment at BNL (ongoing effort).
- Simulation study of mRICH performance in the electron endcap of JLEIC (ongoing effort).
- Organize a joint dRICH/mRICH beam test. Plan for an electron beam (at 2 GeV) test.

2.3.3 mRICH R&D Deliverables

FY20:

- Publication of the results of the second beam test of the mRICH prototype.
- Report on the performance of an mRICH array in EIC-like experiments.
- Report on the results of a detailed study of the radiation hardness of the Fresnel lens.

2.4 High-Performance DIRC (hpDIRC)

Contacts: G. Kalicy <gkalicy@jlab.org>, J. Schwiening <J.Schwiening@gsi.de>

A radially-compact detector based on the DIRC (Detection of Internally Reflected Cherenkov light) principle, shown in Fig 2.4.1a, is a very attractive solution for the EIC detector, providing particle identification (e/π , π/K , K/p) over a wide momentum range. The DIRC detector is a special type of RICH counter using rectangular-shaped radiators made of synthetic fused silica that are utilized also as light guides to transport Cherenkov photons to an expansion volume, where the photons are recorded by an array of photon sensors. During the photon transport, the emission angle of Cherenkov photons with respect to the particle track is maintained and can be reconstructed from the measured 3D parameters: the image location on the detector surface (x, y) and the time of arrival of each photon (t).

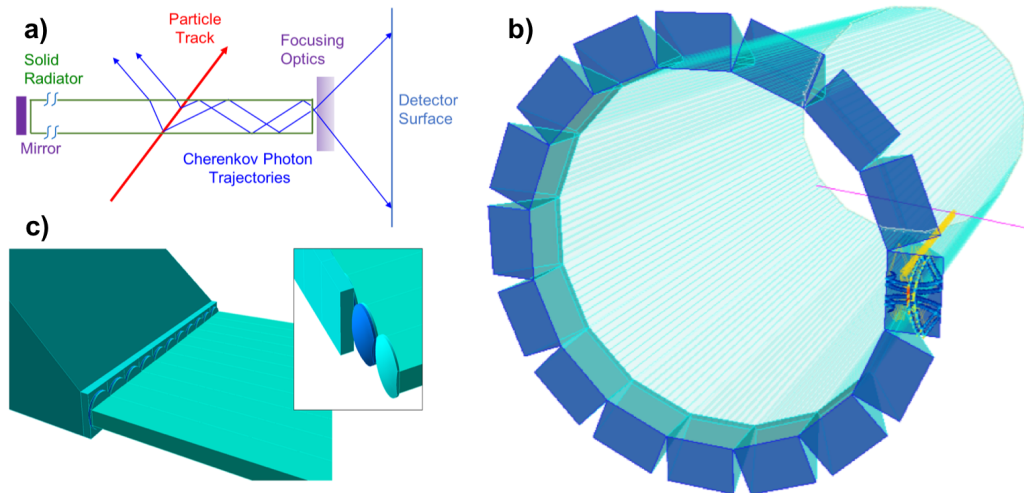


Figure 2.4.1: a) Schematic of the DIRC principle. b) Geant4 geometry for the simulation of the High-Performance DIRC where one can see the accumulated Cherenkov photon hit pattern for charged kaons. c) The fused silica prism expansion volume, a row of spherical three-layer lenses with high index of refraction (no air gaps) and the radiator bars. The insert shows the individual lenses and layers of the spherical lens system.

2.4.1 Summary

The objective of the DIRC R&D undertaken by the EIC PID consortium is to extend the PID capabilities of DIRC counters well beyond the state-of-the-art (e.g., Belle-II and PANDA). The past R&D activities funded by this program (initially eRD4, later eRD14) demonstrated the feasibility of a High-Performance DIRC

(hpDIRC) to provide 3σ separation of π/K up to 6 GeV/c, e/K up to 6 GeV/c, e/π up to 1.7 GeV/c, and K/p up to 10 GeV/c. The implementation of the High-Performance DIRC into a Geant4 simulation is shown in Fig. 2.4.1b. Key elements in achieving this performance are innovative focusing optics (shown in Fig 2.4.1c) and a time-based reconstruction algorithm. The ultimate goal of the ongoing program is to demonstrate this performance in a test beam with a prototype that is representative of the intended EIC hpDIRC configuration (small-pixel photosensors, high-resolution timing, advanced optics, *etc.*). Milestones towards achieving this goal include the design, characterization, and validation of a radiation-hard lens as well as the detailed simulation of the hpDIRC design and the development of the reconstruction algorithms. The last phase of the project will involve the validation of the simulated performance of the High-Performance DIRC design with the full system prototype in particle beams.

In the past fiscal year our major activities were: (1) the purchase of two custom-made 3-layer lenses using sapphire and PbF_2 as the middle layer, respectively, replacing the NLaK33 glass; (2) the radiation hardness study of five materials with doses of up to 750 krad at BNL in the ^{60}Co source; (3) the beam test of the PANDA Barrel DIRC prototype at CERN validating the potential for a significant reduction in the number of sensors required to cover the detector plane; (4) the parameterization of the current baseline hpDIRC design for the fast simulation of the EIC detector.

The EIC DIRC R&D program benefits greatly from the synergy with the PANDA DIRC R&D program, which has involved know-how, hardware, and software contributions. A key near-future component of the EIC DIRC program will be the transfer of the PANDA Barrel DIRC prototype to the U.S., which reflects the long-term interest of the GSI DIRC group to remain involved in the EIC project.

2.4.2 FY19 Progress and Achievements

Characterization and performance evaluation of 3-layer spherical lens prototypes

Procurement of new prototype lenses

After sapphire and PbF_2 were shown to be sufficiently radiation hard for the hpDIRC lens, the next challenge for FY19 was to demonstrate that these materials can be processed by the optical industry to produce high-quality lenses. Both materials are very challenging to machine by the optical industry (due to the toxicity of the lead and the hardness of the sapphire) and most companies do not want to work with these materials. However, we were able to identify two vendors, one in China and one the U.S., who accepted the challenge to build the prototype lenses. After discussing the design and fabrication process, including a site visit to the U.S. vendor, the orders have been placed and the lenses are currently in production. The delivery of the finished prototypes is expected this FY, no later than in September 2019.

Earlier in FY19 the GSI group procured a 3-layer spherical lens prototype with S-LAH97 (lanthanum crown glass) as the middle layer from the same U.S. vendor. The design, intended for the PANDA Barrel DIRC, is square, has polished sides, similar to the sapphire prototype lens currently in production. This S-LAH97 lens was recently sent to CUA to be evaluated in the laser setup at ODU. A comparison of the optical properties of the old and new spherical lens prototypes, including the two new lenses, is an important step in establishing the feasibility of the radiation-hard 3-layer lens.

Radiation hardness measurement of materials for lens prototypes with ^{60}Co

The determination of the radiation hardness of materials is an important aspect of the EIC DIRC R&D. Synthetic fused silica, which is used for most of the optical components in all DIRC systems, was already extensively tested for the BaBar and PANDA DIRC counters and proved to be radiation hard. However, the middle layer of the 3-layer lens was made, in all prototypes up to now, of a high-refractive index lanthanum crown glass (NLaK33, S-YGH51 or S-LAH97), and our first radiation tests strongly suggested that this material may not be suitable for the final design. Several materials were studied as potential alternatives to lanthanum glasses, and so far sapphire and PbF_2 are the leading candidates. All potential candidates have to be tested for radiation hardness.

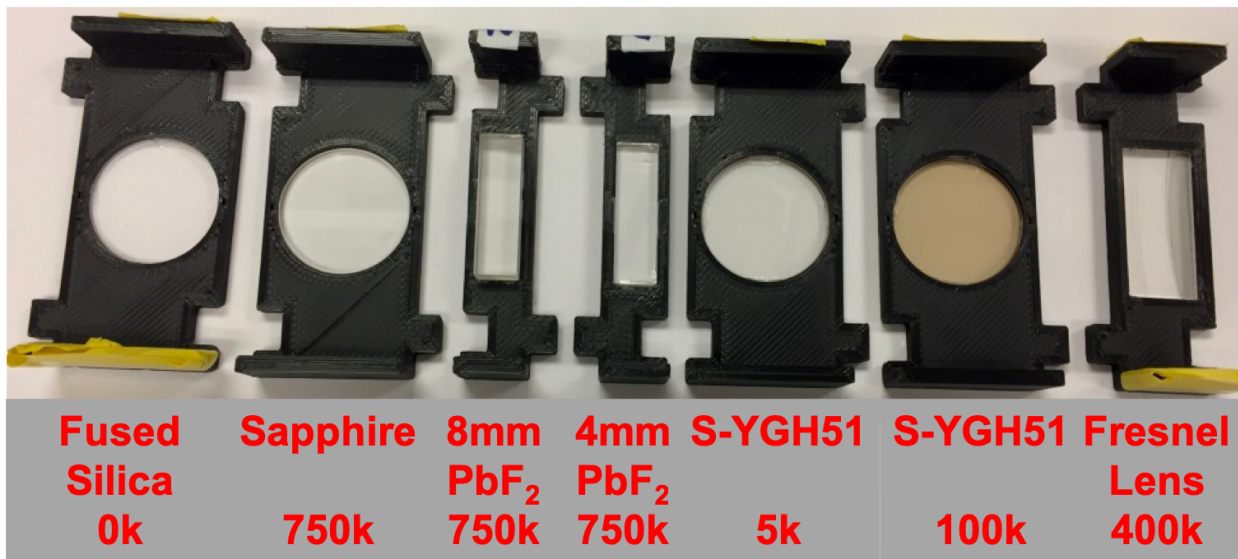


Figure 2.4.2: Samples of materials after irradiation in a ^{60}Co source with corresponding deposited doses.

A commonly used source for studies of radiation hardness of optical materials is ^{60}Co . Following the July 2017 and January 2018 recommendations by the R&D review committee, we prepared a dedicated setup for radiation hardness measurements with the ^{60}Co source at the BNL radiation facility. Samples of PbF_2 , sapphire, S-YGH51, as well as acrylic glass, used for the current mRICH Fresnel lens prototype, were exposed to accumulated doses of up to 750 krad. Fig 2.4.2 shows a photo of samples tested at BNL after the completion of the irradiation program, as well as a Fused Silica sample, never irradiated and used as a reference in the transmission measurements. A visible colour change was observed only for the S-YGH51 sample.

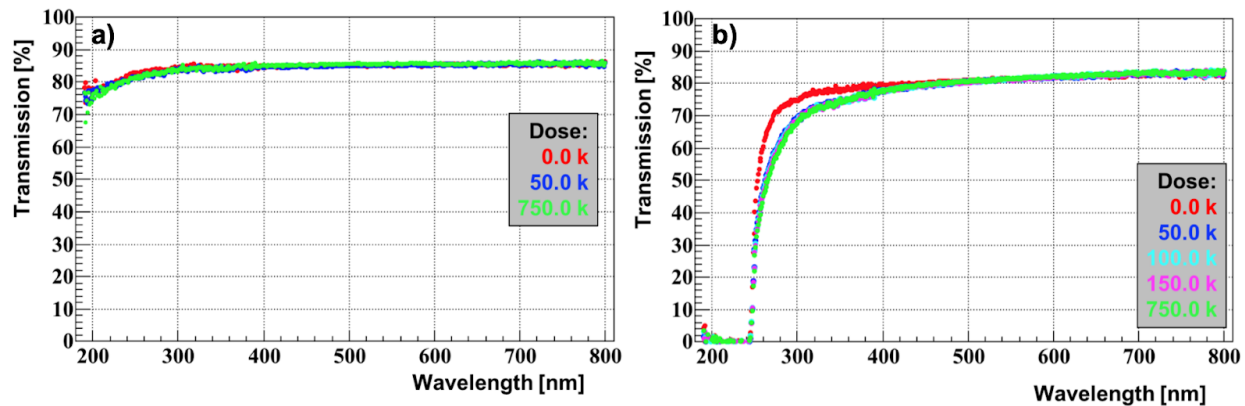


Figure 2.4.3: Measured transmission (not corrected for Fresnel losses) through the 2 mm-thick sapphire (a) and 8mm-thick PbF₂ (b) sample as a function of wavelength for selected amounts of deposited gamma ray dose from ⁶⁰Co.

The radiation damage is quantified by measuring the transmission in the 190-800 nm range in a monochromator. Two light sources with different measurement precision are used in the process, resulting in a precision of $\pm 0.5\%$ for the 390-800 nm range and $\pm 1.2\%$ below 390 nm. The results of the radiation hardness test for a 2 mm-thick sapphire sample are shown in Fig. 2.4.3a. Only three transmission measurements are shown: before irradiation, after the first 50 krad irradiation step, and after irradiation with the full dose. There is no significant transmission loss even after the dose of 750 krad. Figure 2.4.3b shows results for the 8 mm-thick PbF₂ sample. We observe a small transmission loss below 400 nm. The saturation of the absorption band happened, however, already below the first 50 krad step and we observed no further changes, even after reaching 750 krad.

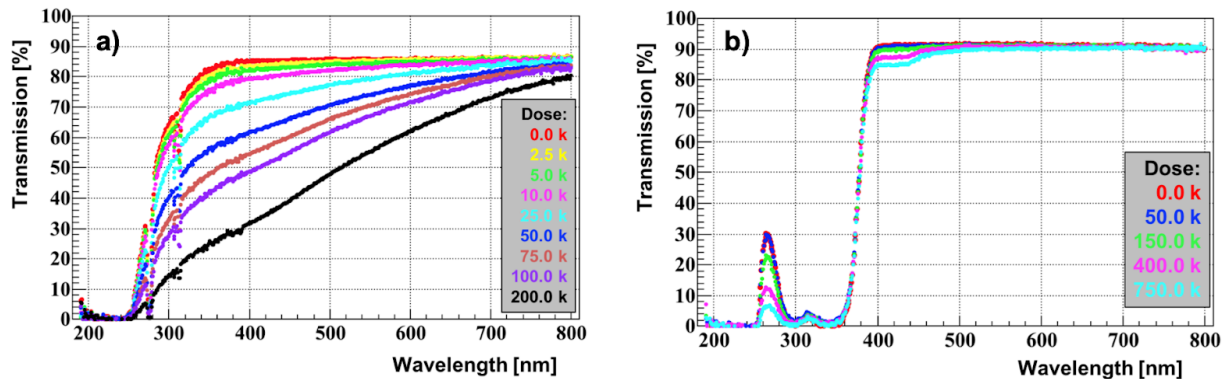


Figure 2.4.4: Measured transmission (not corrected for Fresnel losses) through the 2 mm-thick S-YGH51 glass (a) and 2 mm-thick Fresnel lens (b) sample as a function of wavelength for selected amounts of deposited gamma ray dose from ⁶⁰Co.

The results for the 2 mm-thick S-YGH51 Lanthanum crown glass sample are shown in Fig. 2.4.4a. Smaller irradiation doses for each step were selected based on earlier calibration measurements. We observe a significant deterioration of transmission for the full wavelength range. After 200 krad deposited dose we observe a transmission drop from 85% to 32% at 400 nm. The loss rate appears to be approximately linear,

0.5% per krad at 300-400 nm and 0.25% per krad at 500 nm. As reported earlier, the S-YGH51 glass is recovering part of the transmission loss with time. A detailed quantification of the recovery process is in progress. Figure 2.4.4b shows results for the 2 mm-thick acrylic mRICH lens sample. A small drop of transmission was observed below 500 nm but in general this material proved to be surprisingly radiation hard even after a dose of 750 krad.

Mapping the focal plane of lens prototypes

A special laser setup was built at the Old Dominion University lab to map the shape of the focal plane of prototype lenses by rotating the lens through two parallel laser beams. The intersection point of the two laser beams determines the focal length. The lens is being placed inside a 30 x 40 x 60 cm³ glass container filled with mineral oil (with a refractive index very close to fused silica) to simulate the focusing behavior of the lens placed between the bar and the prism. The 3-layer lens prototypes were supported by a special 3D-printed holders that made it possible to map out the focal plane in all three dimensions. The spherical 3-layer lens prototype in the setup with green laser shining through it is shown in Fig. 2.4.5a. Three of the prototype lenses produced the desired flat shape of the focal plane for the beams close to the center of the lens, in good agreement with Geant simulations, as previously reported. This setup was successful in determining the shape of the focal plane, but requires several modifications to increase the range of incident angles, improve the precision of the measurement, and limit the systematic uncertainties, in order to publish the results. The proposed modifications are shown as a CAD drawing in Fig. 2.4.5b. The longer oil tank would be made of plexiglass and placed on a scissor lift table (red on the fig) that will lower the tank to gain access to the optical elements, suspended above the tank, and then lift it up again. This will simplify the calibration of the setup and changing of the lenses. The rotation stage for the lens and the screen will be redesigned and fixed to the stable support structure above the tank. A camera with a special filter will be placed behind the tank to allow a more precise determination of the focal length and speed up the measurement significantly.

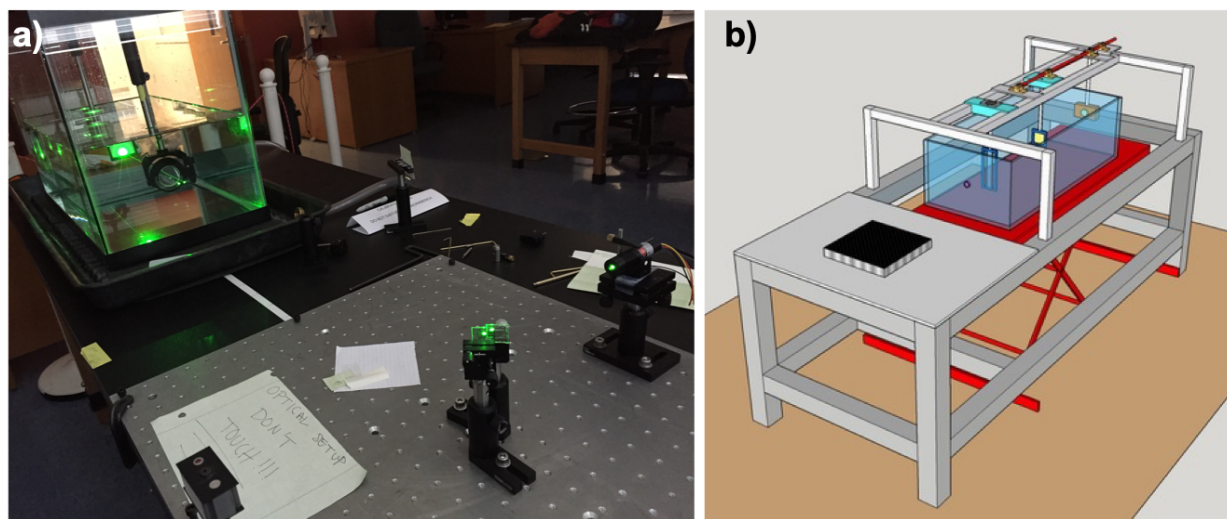


Figure 2.4.5: Laser setup to map the lens focal plane: (a) photo of current setup, (b) CAD drawing of the improved

redesigned setup.

Parametrization of the High-Performance DIRC for fast simulations

The High-Performance DIRC is an important part of all three proposed EIC central detector concepts. The increasing interest in EIC physics studies with Monte Carlo data demonstrates the need for (1) a parametrization of the High-Performance DIRC baseline design performance to be used as input to the fast EIC detector simulations and (2) the implementation of a more realistic DIRC detector design in the full simulation framework. Since the differences in the various hpDIRC designs is only moderate, any hpDIRC parameterization will be useful for all three detector concepts. Therefore, we decided to prioritize task (1) in this FY and preliminary results are shown in Fig. 2.4.6. The full Geant4 simulation of the current hpDIRC baseline design was used to determine the photon yield and the Cherenkov angle resolution per photon and to calculate the Cherenkov track resolution (CTR) as a function of the polar angle and momentum of the charged particle (see Fig. 2.4.6 (a)). The fast simulation combines the calculated CTR value for a given particle momentum and polar angle with the assumed tracking resolution to perform a Gaussian smearing of the expected Cherenkov angle, to compare it to the expectation and to calculate the PID probabilities for the different particle hypothesis. In addition, the fast simulation returns the deviation of the smeared Cherenkov angle from the expected values in units of CTR. Fig. 2.4.6 (b) shows the derived π/K separation power in standard deviations as a result of the fast reconstruction. A special C++ class was designed and released to the EIC software community.

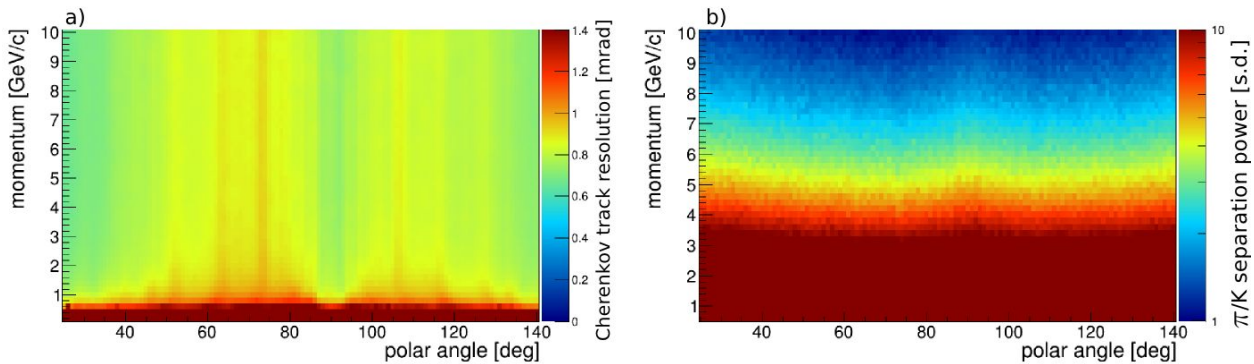


Figure 2.4.6: Cherenkov track resolution in Geant4 simulation as a function of the particle polar angle and momentum (a) and the derived π/K separation from the fast reconstruction for a tracking resolution of 0.5 mrad (b).

Validation of reduced sensor coverage with prototype in particle beams

Although this activity was not funded during the current period, the results of our collaboration with the PANDA Barrel DIRC group, and the outcome of their 2018 beam test at CERN, should be noted.

Experimental validation of the new design ideas are important for the DIRC in the EIC R&D program. Since not all of the required components of the high-performance DIRC baseline design are available yet (such as sensors with small pixels, fast readout electronics, full-length radiators, *etc*) the collaboration with the PANDA Barrel DIRC group is used to evaluate the performance of the specific design options for the

High-Performance DIRC.

The test beam at CERN in July/August 2018 was primarily focused on the validation of the PID performance of a cost-saving PANDA Barrel DIRC design option with reduced MCP-PMT coverage. The prototype featured a single narrow synthetic fused silica radiator bar, coupled to the 3-layer spherical lens, which was coupled to the synthetic fused silica prism expansion volume with a 33° opening angle, similar to the 2017 setup. However, while the 2017 prototype featured a 3×4 array of MCP-PMTs covering the entire backplane of the prism expansion volume, the 2018 prototype, shown in Fig. 2.4.7a, used a 2×4 MCP-PMT array, covering only $\frac{2}{3}$ of the prism backplane. An example occupancy plot for the new sensor arrangement is shown in Fig. 2.4.7b. The data analysis is still ongoing but first results are very encouraging. Figure 2.4.7c shows the π/p separation power at 7 GeV/c as a function of the beam polar angle. The observed PID performance of the 2×4 MCP-PMT array meets the PANDA requirements. Although the observed lower photon yield, caused by the limited sensor coverage, is expected to lead to a loss of π/p separation power, the measured performance in 2018 was consistently similar to or better than in 2017. A possible explanation is that a loss of photons in the region of overlapping hit patterns, near the sides of the prism, has a reduced impact on the PID performance for the time-based imaging reconstruction. The direct comparison to 2017 is, however, complicated by the fact that several parameters were changed. The laser pulser calibration method was improved for 2018 and the performance of the TRB/PADIWA-based readout electronics was about 10% better in 2018. Further analysis is needed to separate the effects of the photon yield and the timing precision.

However, due to the substantial cost savings, the 2×4 MCP-PMT array design has been selected for the PANDA Barrel DIRC construction and a similarly reduced sensor coverage should be considered for the hpDIRC as well.

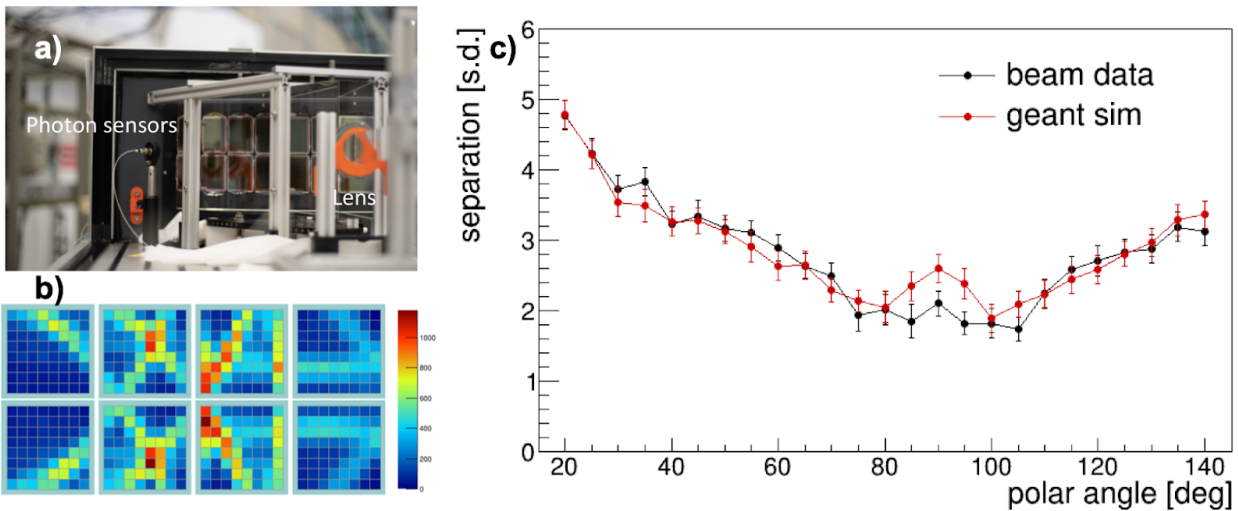


Figure 2.4.7: a) Photo of the MCP-PMT arrangement in the PANDA Barrel DIRC 2018 prototype at CERN. b) Distribution of the number of detected hits per MCP-PMT pixel from 50k pions at a polar angle of 20° and a momentum of 7 GeV/c; c) π/p separation power at 7 GeV/c beam momentum as a function of the polar angle.

Feasibility study for a “mini-DIRC” for near-beam ion identification

While the focus of the consortium has been until now been on PID in the central detector (including the endcaps), PID is also needed for the forward near-beam which detect scattered light ions and heavy-ion fragments. Identification of ions is important for achieving both key EIC physics goals (such as imaging of nuclear glue with positive identification of light ions, and new topics such as discovery of rare isotopes produced in electron scattering on heavy-ions). A forward magnetic spectrometer, integrated with the accelerator, can measure the magnetic rigidity of ions ($\sim M/Z$ or A/Z). However, an independent measurement of Z is needed to extract A and Z independently. Since all ion fragments travel at the same velocity, TOF techniques are of limited use (in the EIC there is no need to use TOF for disentangling multiple vertices in a single bunch crossing as at the LHC). One possible approach is dE/dx , which is proportional to Z^2 . This works well for light ions, and could even be part of the information provided by the trackers in the Roman pots, but for heavy ions the amount of material needed to distinguish, $Z=82$ from $Z=81$ would be substantial. Thus, it is preferable to use a DIRC-like Cherenkov detector, which provides both a compact size, large photon yield, and good timing resolution. The number of photons produced in fused silica is about $1,000 * Z^2$ per cm. Most of these are lost, but based on DIRC simulations, half a cm of fused silica should provide 100,000 useful photons, which is an order of magnitude more than is required to reach an uncertainty in Z^2 of 1% ($Z=81$ from $Z=82$ are separated by 2.5% in Z^2). The bar would have similar transverse dimensions as a Si-tracker in the Roman pot, and could be placed behind the last one. The main challenge is to find a readout for the thin bar which can count the photons with a precision of at least 1%. Since the simulations involved would be very similar to those for the high-performance DIRC, we propose a small pilot study in FY20 to evaluate the feasibility of such a detector. The work would be carried out by the DIRC postdoc.

2.4.3 Proposed hpDIRC R&D Activities

In response to the prioritization of the hardware activities by the committee for FY19, most of the software activities were postponed and will have to be addressed in FY20. The proposed hpDIRC PostDoc will support not only the postponed simulation studies and ongoing activities like the lens evaluation and radiation hardness studies, but also will be crucial for the prototype activities in terms of both software and hardware. In particular, the hired person will be responsible for the prototype simulation and reconstruction as well as the commissioning of the readout electronics and DAQ and the study of the beam instrumentation requirements for the beam test. In the future the PostDoc is expected to lead the analysis of the prototype data. The experience from the prototype simulation will be applied to improve the current hpDIRC design.

The current hpDIRC implementation in Geant is based on the properties of available commercial MCP-PMT sensors. However, the latest generation of MCP-PMTs, currently being tested for the PANDA experiment, features a significantly higher photon detection efficiency (PDE) with a useful wavelength range extended much further into the UV. Upgrading the properties of the sensors and of the glue used in the bar assembly will make use of the enhanced UV transmission offered by the sapphire in the new 3-layer lens prototype, which should improve the PID performance.

Following the initial hpDIRC design implementation, it is now crucial to study the effect of different bar sizes, focusing system options, expansion volume shapes and dimensions, as well as sensor types

(MCP-PMTs vs. SiPMs) and pixel sizes on the DIRC performance to identify a credible and cost-efficient baseline design for the High-Performance DIRC. The implementation of this design in the full EIC central detector simulation frameworks is an important step to facilitate the study of the combined PID performance of the eRD14 detector systems. Other important simulation activities are the study of the mitigation of chromatic dispersion effects using fast timing and the potential use of the DIRC for precise event timing.

The production of a radiation hard 3-layer lens is an essential step for the High-Performance DIRC R&D process. Two prototype lenses with the middle layers made of PbF_2 or sapphire are in production with the delivery scheduled for September 2019. An additional prototype with LAH97 glass as a middle layer was purchased by PANDA DIRC group and sent to CUA for tests. The optical performance of all three prototype lenses will be evaluated in FY20. The laser setup for 3D mapping of focal plane will be upgraded to improve precision and completeness of the measurement by adding studies of the optical aberrations using off-center laser beams. We believe that this improvement will benefit the quality of the measurements and allow a better NIM publication summarizing this study of the various prototype lenses.

Detailed radiation hardness test of PbF_2 and sapphire, among a few other materials, will be performed in July 2019 using the ^{60}Co source at BNL. Studies will include birefringence as well as radio-, UV- and visible luminescence. In FY20 the radiation hardness study will be expanded by adding neutron irradiation. Radiation hardness studies of with gamma and neutron sources will be summarized in the publication.

The next step in the development of readout electronics will require a sensor with small pixels. The only commercially available MCP-PMT candidate is the PHOTONIS XP85122-S with a pixel pitch of 1.6 mm. Given the current funding situation, we previously decided to prioritize the lens development for FY19 and postponed the sensor procurement. However, with a clear plan for the hpDIRC prototype in place, the procurement of the sensor is the main hardware priority in FY20. The sensor will be procured through the High-B sensor-evaluation program (see Chapter 4.1.2). Its gain, timing resolution, and ion-feedback rate will be characterized at JLab in summer of FY20. It will then be sent to the Hawaii electronics group for validation of the fast readout electronics. The availability of the sensor in FY20 has another timely benefit, which is the possibility to compare in detail its timing and charge-sharing/crosstalk properties to those of the newly developed LAPPDs. The comparison between the performance of various photon sensors that are viable candidates for the EIC-PID detectors is an important aspect of the program carried out by the EIC-PID consortium.

Synergetic Activities Supported by External Funding

The synergy with the PANDA Barrel DIRC project not only provided access to the prototype and the CERN test beams in 2015, 2016, 2017, and 2018 but includes several planned mid- and long-term contributions from the GSI DIRC group to the EIC DIRC project. With the submission of the PANDA Barrel DIRC TDR in 2017 the activity focus of the GSI DIRC group on PANDA shifted to the mechanical design and the R&D for the detector assembly. Both activities are directly relevant to the EIC DIRC design.

After conclusion of the beam tests of the PANDA Barrel DIRC, components of the prototype have become available for use by the EIC DIRC effort in FY20 on the basis of a long-term loan or an in-kind contribution.

The mechanical prototype structure, as well as at least one narrow bar, one wide plate, one prism expansion volume, a set of PHOTONIS XP85012 MCP-PMTs and PADIWA/TRB readout electronics for initial tests, will be transported to the U.S. for future prototype beam tests at Fermilab or BNL. This will significantly reduce the financial investment required to set up the first prototype for the test of lenses, sensors, and readout electronics with particle beams (this would be a deliverable in FY21/FY22). In FY18 we started to investigate the administrative process required for a loan agreement between GSI and CUA (the U.S. receiving institution). This activity continued in FY19 with the goal of completing the transfer in FY20. Development of the LAPPD sensors and readout is well in line with hpDIRC prototype timeline. The 32x32 channel version of this sensor will be crucial to start work on the readout electronics prior to the assembly of the complete prototype. The first step of the hpDIRC prototype will be to reproduce the PANDA results in a reference measurement, using the PANDA optics and XP85012 MCP-PMTs (with 6.5mm pixel pitch). The ultimate goal is to assemble an EIC DIRC prototype with proper pixel-size sensors and appropriate geometry to validate the simulated performance and to directly measure the PID performance.

Summary of Proposed activities

FY20

Software

- Develop the prototype simulation, evaluate performance, and determine requirements for beamline instrumentation needed to achieve performance goals.
- Study the PID performance of the current hpDIRC design for different time resolution/tracking resolution scenarios and the improved photodetection efficiency of the latest MCP-PMT sensors.
- Implement plate geometry with and without focusing.
- Optimize the current hpDIRC design: adjust prism angle and limit sensor coverage based on PANDA prototype results.
- Study feasibility of “mini-DIRC” for near-beam ion identification

Hardware

- Transfer of the PANDA DIRC Prototype to the U.S.
- Set up the prototype DAQ system and commission the PHOTONIS XP85012 MCP-PMTs with TRB/PADIWA-based readout electronics.
- Upgrade of the lens characterization setup.
- Characterization of the new prototype lenses.
- Radiation hardness study with neutrons.

FY21

- First studies of hpDIRC prototype with particle beams.
- Investigation of the potential use of DIRC for high-precision event timing.
- Investigation of chromatic dispersion mitigation in the context of different photocathode materials and readout timing precision.
- Development of analytical version of time-based imaging.
- Optimization of design in coordination with the other eRD14 PID systems within full EIC central detector simulation framework.

- Study PID performance of the baseline design in the presence of backgrounds.

2.4.4 hpDIRC R&D Deliverables

FY20

- Completion of PANDA Barrel DIRC prototype transfer to U.S.
- Validation of prototype DAQ for PHOTONIS XP85012 MCP-PMT array with TRB/PADIWA-based readout electronics.
- Completion of Geant simulation package for the hpDIRC prototype in beam test environment.
- Upgraded laser setup to characterize the optical properties of the lens prototypes.
- Performance evaluation of the three new prototype lenses in laser setup.
- Detailed radiation hardness study of candidate lens materials, including PbF_2 and sapphire, using both neutron and gamma sources.
- Publication describing the performance validation of the focusing lens-based optics using the DIRC prototype in particle beams.

3. Lepton (electron) Identification

Contacts: C. Hyde <chyde@odu.edu>

The focus of the funded activities of the eRD14 Consortium is on hadron-species identification. However, we have not neglected electron and muon identification. At an Electron-Ion Collider, detection and identification of the scattered electron is a critical requirement. Also, many important processes involve particle decays to leptons (*e.g.*, $J/\psi \rightarrow e^+e^-$). The baseline system for e/π identification is the electromagnetic calorimeter (EMcal), which is included with 4π coverage in all the EIC model detectors. However, the pion suppression achievable in the EMcal is limited primarily from charge-exchange events (πp to $\pi^0 n$), resulting in an electromagnetic shower indistinguishable from one initiated by an electron ($e p$), and associated with a charged track. Although different types of EMcals have been considered for different parts of the EIC detectors, in general a good EMcal will provide e/π background suppression by up to about 1:100 for a single track, or $1:10^4$ for dilepton productions (*e.g.*, J/ψ). This can be improved with a shower-shape analysis in a high-granularity EM calorimeter, but at the cost of a loss of electron efficiency. Figure 3.1 illustrates the trade-off between PID detection efficiency *vs.* purity of PID, for a fixed PID separation of two species by $N\sigma$. The inclusion of a hadronic calorimeter (HCal) behind the EMcal will only partially improve the e/π identification, since charged pion events that charge-exchange in the EMcal will be mostly contained in the EMcal, and will not give large signals in the HCal. In order to reach kinematics where pion backgrounds are high, additional e/π ID detectors will be needed.

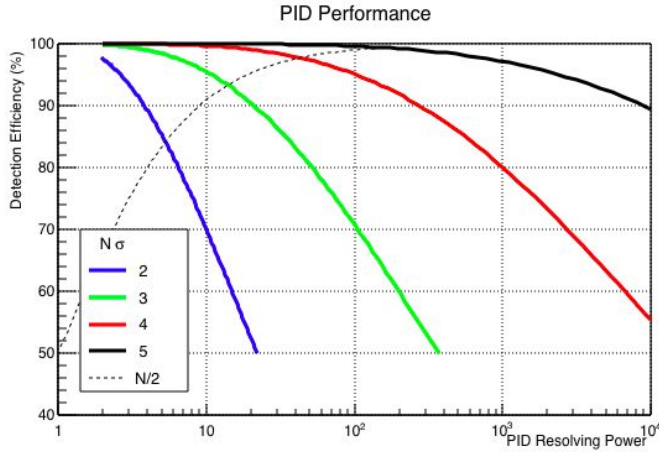


Figure 3.1: Contours of constant PID separation, $N\sigma$, in the plane of PID efficiency vs. resolving power *vis-a-vis* the unwanted species. The dashed line corresponds to making the PID separation at the midpoint between the two particle-species distributions.

3.1 Electron ID

The twin roles for lepton ID (identification of the scattered electron and of leptonic decays of hadrons such as J/ψ) impose different requirements in terms of coverage in both momentum and angular range. The main challenge for the identification of the scattered electron comes from low-momentum (1-2 GeV) pions in the electron-side endcap and the central barrel. As shown in Figures 3.3 and 3.2 (left), this background rises rapidly at lower momenta, while the EMcal pion rejection factor is at best constant, and in reality likely to get slightly worse. However, the combination of an EMcal and a Cherenkov detector such as the mRICH or DIRC can offset the rising in pion background, making it possible to detect and identify scattered electrons with lower momenta, effectively extending the kinematic reach of the EIC.

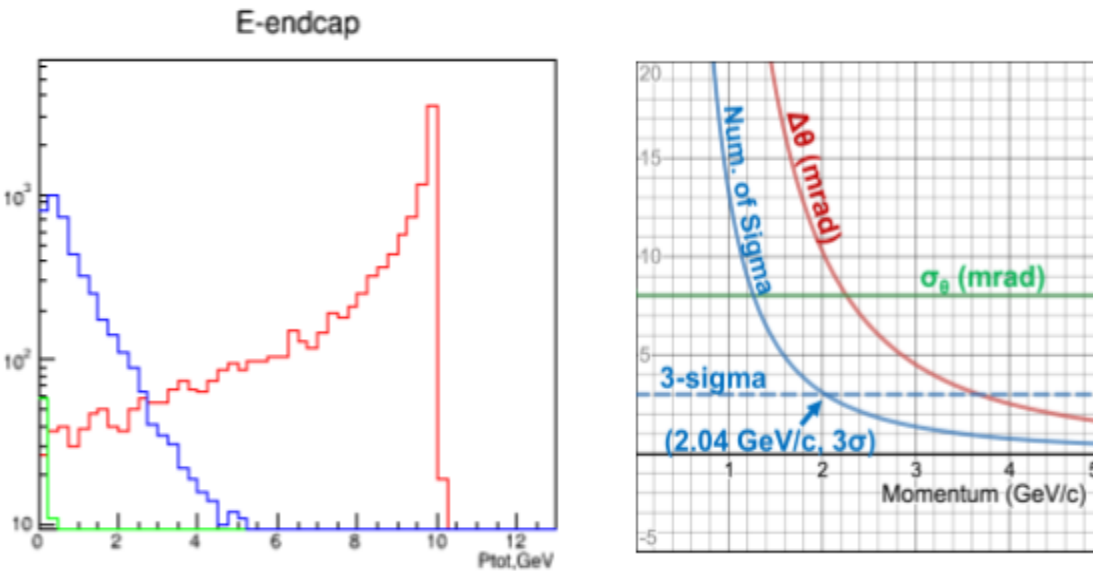


Figure 3.2 Left: Electron-endcap momentum distributions of scattered electrons (red), negative pions (blue), and secondaries (green) for collisions of 10 GeV electrons on 100 GeV protons (a common BNL / JLab kinematic) from Pythia in a bin of $1 < Q^2 < 10 \text{ GeV}^2$ for the electrons (pions include photoproduction). **Right:** e/π discrimination beam-test performance achieved with the mRICH (section 2.3). The green line is the per-photon resolution (mrad). The red line is the $e-\pi$ separation (mrad). The blue line is the achieved separation in experimental σ of the Cherenkov radii.

If implemented in the electron endcap, the mRICH (see section 2.3) will provide additional e/π discrimination, as illustrated in Fig. 3.2 (right). Figure 3.2 (right) shows that while the additional e/π discrimination is 3-sigma at 2 GeV, it rises to 13-sigma at 1 GeV. Following the dashed line of Fig 3.1, the combination of EMcal and mRICH can ensure less than 1% pion contamination in the electron sample over the entire momentum range of Fig. 3.2 (left).

Figure 3.3, similar to Fig. 3.2, shows the particle multiplicities in the negative pseudo-rapidity side (electron-endcap side) of the central barrel region. Below 2 GeV/c, e/π discrimination is again challenging.

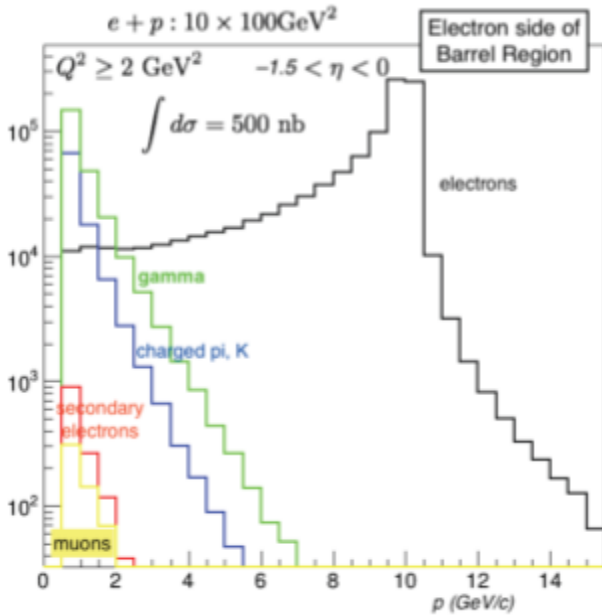


Figure 3.3: Central barrel region, negative-pseudorapidity (electron endcap side): momentum distributions of scattered electrons (black), photons from hadron decays (green), charged π/K (blue), electrons from hadron decays (red), and muons (yellow). The particles are produced in DIS of 10 GeV electrons colliding with 100 GeV/c protons. The events are selected for $Q^2 \geq 2 \text{ GeV}^2$.

Figure 3.4 outlines the e/π separation achievable with the DIRC. At 2 GeV/c, multiple scattering in the DIRC itself limits the tracking resolution to 1.5 mrad, and this degrades to 2.5 mrad at 1.3 GeV/c. The DIRC will still provide 5:1 e/π resolving power over this momentum range, with electron efficiency > 85%. This will provide an electron sample with less than 1% pion contamination for all momenta above $\sim 1.3 \text{ GeV}/c$.

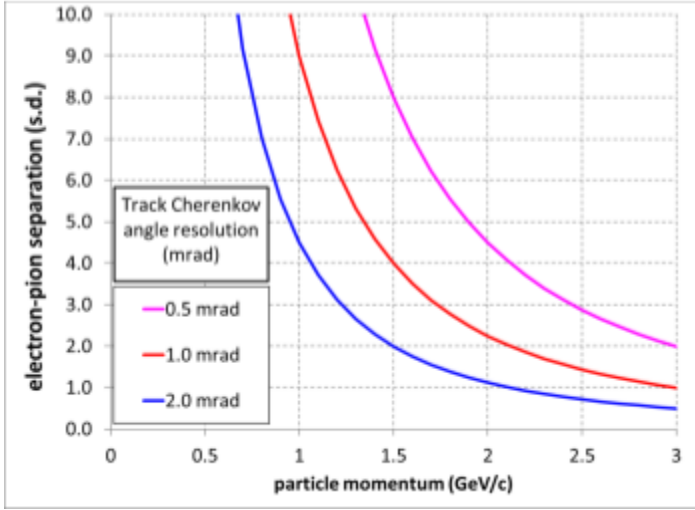


Figure 3.4: e/π separation in the DIRC in units of standard deviations (s.d.) as a function of particle momentum for different values of the track Cherenkov angle resolution σ_{track} . The EIC DIRC is aiming for a track Cherenkov angle resolution of 1 mrad or better, providing a 3 s.d. π/K separation at 6 GeV/c and an e/π separation of 3 s.d. at 1.7 GeV/c and 9 s.d. At 1 GeV/c (neglecting multiple scattering).

In the hadron endcap, Fig. 2.1.5 demonstrates $\geq 3\sigma$ e/π separation up to 19 GeV/c by the proposed dual-RICH. For the C_2F_6 gas alone, $\geq 3\sigma$ e/π separation is achieved over the range 5–19 GeV/c. Thus, in the ion endcap, with the dual-RICH together with the EMCAL, $10^3:1$ e/π separation per track is achievable at $\sim 95\%$ electron efficiency up to 19 GeV. This is sufficient for identifying, for instance, decays of charmonium.

3.2 Muon ID

Muon identification is important for di-lepton production (both inclusive and vector meson decays, *e.g.*, J/ψ) and for semi-leptonic decays of heavy-flavor hadrons. Every EIC detector concept includes some form of hadron calorimetry in the ion downstream endcap of the central detector. However, the different proposals differ significantly in the central barrel region. We are assessing the Belle (and its Belle-II upgrade) K_{Long} – Muon (KLM) detector as a modest-cost option for instrumenting the solenoid return yoke. This has shown good performance for muon ID and modest performance for measuring the energy of high-energy neutrons and K-long mesons.

4. Photosensors & Electronics

The specific requirements that the DIRC and the RICH detectors must fulfill within the scope of the EIC pose unique constraints on sensor and electronics performance different from any previous DIRC and/or RICH implementation. Table 1 below lists the minimum requirements on DIRC, mRICH, and dRICH photosensors. Specifically, the small pixel size of 2–3 mm and the immunity to magnetic fields of magnitude in the range 1.5–3 T are unique constraints. The main objective of this R&D effort during the proposed funding period is to identify and assess suitable photosensor and electronics solutions for the readout of the EIC Cherenkov detectors, both for the full EIC detector and for prototypes in beam tests. Depending on the evaluation outcome, design optimization studies of those photosensor and electronics parameters that are found lacking in the evaluated samples but critical for operations in the EIC environment, will be carried out. In addition to supporting the adaptation of developing photo-sensor technologies for the EIC Cherenkov detectors (such as LAPPDs and GEMs) the goal is to identify a cost-efficient common readout solution that is shared within the

EIC-PID consortium. Ultimately, in the long term, this R&D work will allow us to make a recommendation about the best photo-sensors and electronics solutions for the PID detectors in EIC implementation.

Sensor requirements and options

The consideration of possible photosensor solutions for each detector component is driven by the operational parameters of the detector, with cost optimization in mind. The table 4.1 below summarizes the performance parameters that photosensors for the hpDIRC, mRICH, and dRICH must satisfy.

Parameter	hpDIRC	mRICH, dRICH
Gain	$\sim 10^6$	$\sim 10^6$
Timing Resolution	≤ 100 ps	≤ 800 ps
Pixel Size	2–3 mm	≤ 3 mm
Dark Noise	≤ 1 kHz/cm ²	≤ 5 MHz/cm ²
Radiation Hardness	Yes ⁵	Yes ⁶
Single-photon mode operation?	Yes	Yes
Magnetic-field immunity?	Yes (1.5–3 T)	Yes (1.5–3 T)
Photon Detection Efficiency	$\geq 20\%$	$\geq 20\%$

Table 4.1 A list of performance requirements for the photosensors for the EIC PID Cherenkov detectors.

The key parameters of the photodetectors for the mRICH are small pixel size, resistance to magnetic field, and low cost (due to its large sensor area). Depending on the mRICH location, the requirement for radiation hardness will vary. The detector does not require good PMT timing resolution. GEMs with a photocathode sensitive to visible light, with their good radiation hardness and good position resolution, would be a very good and cost-effective solution for the mRICH. SiPMs could be used where their radiation hardness is sufficient. MCP-PMTs such as LAPPDs with pixelated readout could be considered as possible photosensors for mRICH detectors if they have sufficient resistance to magnetic fields. In the final EIC detector, it is possible to use different photosensors in different locations (LAPPDs could, for instance, be use near the beam where the radiation is high and SiPMs away from the beam, where the angle of the magnetic field changes more rapidly).

The key parameter of the photodetectors for the dRICH is the small pixel size. Although the relative sensor area (normalized to the absolute detector area) of this detector is small, due to the large absolute detector area, cost is also an important parameter. Good sensor options for the dRICH would be similar to the ones for mRICH (keeping in mind that due to the location of the sensors, the requirement for radiation hardness is not as important for the dRICH).

The key parameters of the photodetectors for a DIRC are fast timing, small pixel size, and a moderate to low dark count rate (DCR). Magnetic-field tolerance is required if the DIRC readout is located within the magnetic field of the solenoid. SiPMs might be possible to use for a DIRC if future developments lower their DCR to an acceptable level. Currently, the only photodetectors satisfying these requirements are MCP-PMTs (including LAPPDs with pixelated readout). Excellent timing resolution (~ 100 ps RMS) is in particular required for the high-performance DIRC if a time-based PID reconstruction method is adopted for the geometry based on wide radiator plates. Such timing resolution is satisfied by currently commercially

⁵ The EIC radiation levels can be inferred from current operations at RHIC, and will depend on the sensor location.

available MCP-PMTs, however, development of electronics with good time resolution for small signals may be required.

4.1 Sensors in High-B fields

Contacts: Y. Ilieva <jordanka@physics.sc.edu>, C. Zorn <zorn@jlab.org>

The integration of the three Cherenkov detectors in the central detector involves setting their photo-sensor readouts in the non-uniform fringe field of the solenoid. While an out-of-field readout option for the DIRC may be feasible, an in-field readout is the only option for the two RICH detectors. The objective of this activity, thus, has been to assess the gain and the timing performance of available photosensors in high magnetic fields (due to the maximum field of 5 T attainable by the magnet, we can do the assessment from 0 T up to the field magnitude at which the sensor performance breaks down) and for various relative orientations between the sensor and the magnetic field, and to reasonably support (as needed for the R&D) further design optimization studies of these sensors. The long-term goal of the research is to recommend sensor options for Cherenkov-detectors readout in the magnetic field of the solenoid magnet.

4.1.1 FY19 Progress and Achievements

In the past year, the main focus of the activities was the gain, efficiency, and ion-feedback evaluation of a multi-anode Planacon MCP PMT with a pore size of 10 μm . This choice is primarily based on our previous measurements of single-anode sensors, which showed that the best multi-anode MCP-PMTs candidates for EIC application are the ones with the smallest pore size. Currently, the smallest pore size of commercially available multi-anode MCP PMTs is 10 μm and there are two manufacturers that have been producing such sensors, Hamamatsu and Photonis. Photek has also very-recently developed a small-pore-size multi-anode sensor, which we plan to potentially test in FY21.

In Summer 2018 we took efficiency and ion-feedback data with a 10 μm -pore-size Planacon MCP PMT. Our results for the efficiency were presented in detail in the December-2018 progress report. The analysis of the ion-feedback data was finalized in the first part of FY19 and the results are reported here. Figure 3.2.4 shows several examples of waveforms illustrating the method used to extract the ion-feedback rate. The four panels show several different shapes of waveforms: of a signal without ion-feedback (delayed) signal and small-amplitude noise (top left), of a signal without ion-feedback signal and a large-amplitude noise (top right), and of a signal with ion-feedback signal and a small and a large noise on bottom left and right, respectively. The figures also show the time interval that is probed for a signal ($t < 96$ ns) and the one probed for a delayed ion signal ($t > 100$ ns), as well as the threshold amplitude, A_{thr} , above which signals are counted. The ion-feedback rate is determined as

$$Rate = N_{ions}/N_{signals}$$

where $N_{signals}$ is the number of waveforms for which an amplitude above A_{thr} is observed in the signal time interval, whereas N_{ions} is the number of signal waveforms for which also an amplitude above A_{thr} is observed in the ion-signal time interval. One can see that the value of A_{thr} critically affects the estimate of the ion-feedback rate. Given the changing noise amplitude between the various waveforms and the large variation of signal and ion-signal amplitudes, it is clear that any choice of a fixed value of A_{thr} would

introduce an error in the estimate of the ion-feedback rate.

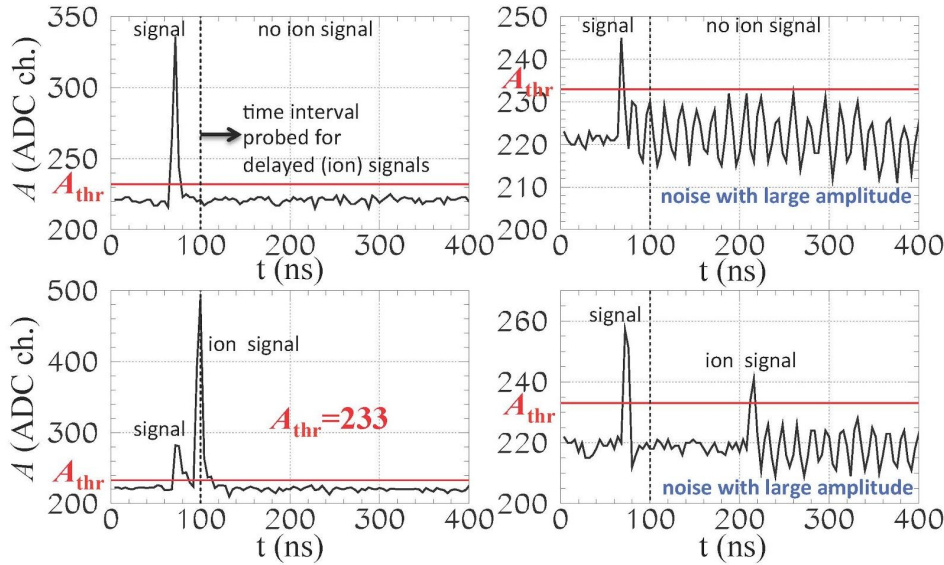


Figure 3.2.4: Examples of various types of signal waveforms, with and without an ion signal and different noise amplitudes. The solid red line shows an amplitude threshold of 233 ADC ch. superimposed on each waveform. Signals and ion signals with small amplitudes, below the threshold, will be missed in the estimate of ion-feedback rate, whereas large noise may be counted as an ion signal if it exceeds the threshold.

To avoid this problem, for each setting (HV, B , θ) we estimated the ion-feedback rate for a large number of values of A_{thr} , starting from the pedestal value of 220 ADC ch, and extrapolated the linear high-end of the correlation $Rate(A_{thr})$ down to the pedestal. This procedure is shown in Fig. 3.2.5 for the setting of $B = 0.3$ T and HV = -2.6 kV. The extrapolated value of $Rate$ at $A_{thr} = 220$ ADC ch. is our best estimate of the true ion-feedback rate that would be measured were the noise amplitude 0 V. Figure 3.2.6 shows the dependence of the ion-feedback rate on HV and B-field. At all HV, the ion-feedback rate is below 2%. The results suggest that the backscattering is primarily driven by high voltage, whereas the B-field dependence is relatively weak.

During the rest of FY19, we will perform first time-resolution measurements of the same 10- μ m Planacon MCP PMT as a function of (B , θ). In Summer of 2019 we will

- study the timing resolution of a 10- μ m Planacon for various B-fields as a function of the high voltage between the photocathode and the first MCP, between the two MCPs,
- If time permits, we will take data for various high voltages across the three stages in the PMT. The goal of this study is to identify the extent to which the gain and efficiency can be recovered by varying separately the high voltages across the three stages.

Note on high voltage and signal amplification: The gain studies we have carried out in the past years aimed to map the **upper limits** of the response of a given MCP-PMT in high B-fields (beyond which the signal amplitude is not viable). For this purpose, both, an increased HV and a variable external amplification were employed. In the past years, we have presented to the committee the gain performance of PMTs at the very upper limit of HV and amplification. For example, for the Planacon 10- μ m pore-size sensor, the results at the highest B-fields (2.2 T at $\theta=0^\circ$ or 1.5 T at $\theta=20^\circ$) presented in 2017, were only possible at -2.7 kV and with x20x200 amplification. At a lower HV, no viable signals were observed, independent of external amplification. Ultimately, considerations of PMT lifetime, efficiency, uniform response over a range of relative orientations with respect to the direction of the B-field, *etc.*, that limit the values of the operational

parameters will likely lower the B-field for operations below the established upper limits. Thus, the upper limits serve to define the operation-exclusion boundaries in (B, θ) space. Once we understand what the exclusion boundaries are and how they are affected by various parameter changes, we will be able to identify realistic operational parameters.

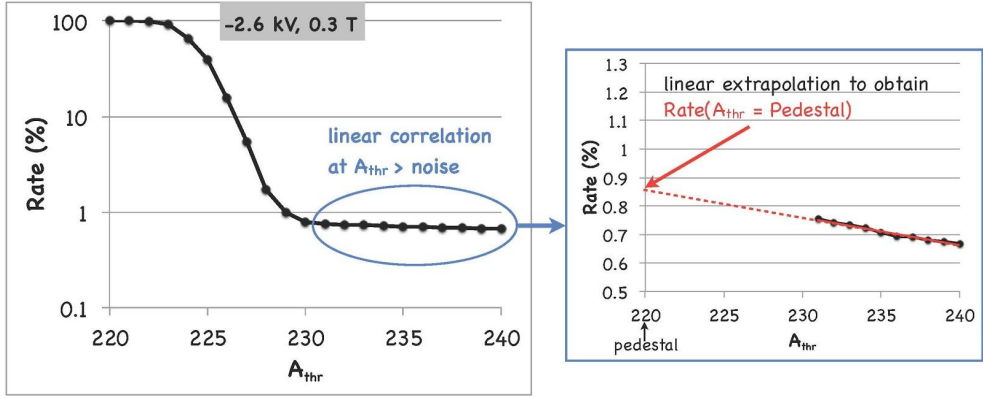


Figure 3.2.5: Illustration of the procedure applied to obtain a best estimate of ion-feedback rate. **Left:** Ion-feedback rate for various values of A_{thr} . When A_{thr} is low, due to the finite amplitude of the noise, all signals are also counted as ion signals and the rate is about 100%. When A_{thr} increases, the noise is less likely to be counted as a signal and the ion rate decreases. The area above $A_{thr}=233$ corresponds to A_{thr} being higher than the noise for all types of waveforms. Further increase of A_{thr} eliminates small-amplitude ion signals and the rate slowly decreases. A zoomed-in figure of the linear portion of the dependence $Rate(A_{thr})$ is shown on the **Right**, as well as a linear extrapolation to the pedestal. The value $Rate(A_{thr}=\text{pedestal})$ is our estimate of the true ion-feedback rate, corresponding to an ideal waveform with no noise.

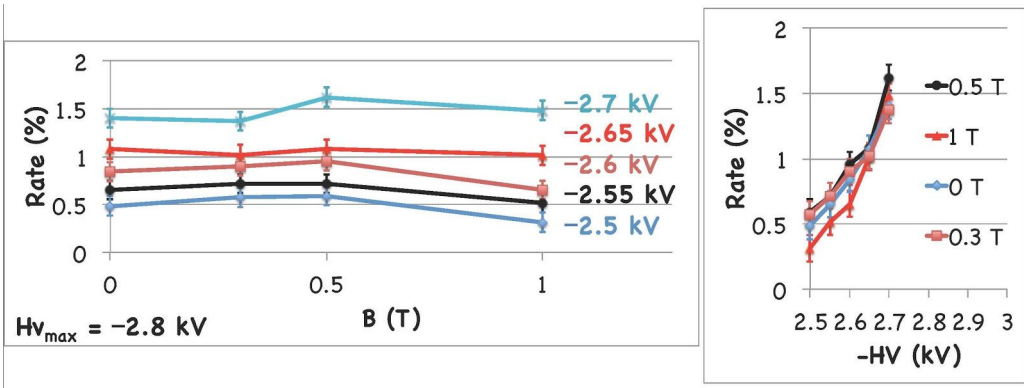


Figure 3.2.6: Estimates of backscattering rate (normalized to number of signals) as a function of B-field magnitude (**left**) and high voltage (**right**) at $\theta=0^\circ$. The back scattering seems to be driven by HV, while the dependence on the B-field magnitude is relatively weak. The ion-feedback rate is below 2% for all fields and HV values. Taking 1.5% as the upper limit of ion-feedback rate below which the sensors should be operated, a HV of up to -2.65 kV, which is 95% of the maximum operational $HV_{max} = -2.8$ kV, is acceptable for a safe operation of the MCP-PMT.

4.1.2 Proposed High-B R&D Activities

The main focus of our work in for FY20 will be on the detailed characterization of a new-generation 10- μm multi-anode Planacon in magnetic fields from 0 T up to the maximum field where the gain measurements show that the PMT performance breaks down. To that extent, we will purchase one sample of the latest-generation Planacon, XP85122-S. This unit has several improved characteristics that are relevant for the EIC-PID program, compared to the unit we tested in 2017 – 2019. The PMT has a smaller pixel size,

which is critical for the validation of the hpDIRC prototype performance, and has an atomic-layer-deposition (ALD) photocathode that reduces ion-feedback. Tests performed by the PANDA DIRC group, however, suggest that the sensor has worse High-B immunity than its non-ALD counterpart. Given that XP85122-S is currently the only commercially-available MCP PMT with a pixel size that satisfies the requirements for the Cherenkov detectors, it is critical that its performance is mapped for a wide range of (B, θ, φ, HV) . This new Planacon MCP PMT will not only be used for evaluation in the High-B tests, but also, as part of the readout of the hpDIRC prototype (the program and timelines of the prototype are discussed in Chapter 2.4.3) and for the validation of the SiREAD readout of this type of PMT (the plans for validation bench tests are discussed in Chapter 4.3.2). In FY20, we will begin a full scan of the gain, efficiency, timing, and ion feedback as a function of (B, θ, φ, HV) . Specifically, the motivation for the timing-resolution measurements is given below.

Given the large gain variations with (B, θ, φ) observed in the measurements we have performed up to date, and the solenoid field non-uniformity in the area where the installation of the DIRC⁶ readout is considered, it is clear that the gain across the readout will not be uniform. Since the timing resolution of an MCP-PMT depends strongly on the amplitude of the output signal, *i.e.* the sensor's gain, the evolution of the sensors timing response with (B, θ, φ, HV) needs to be considered. A theoretical model of the electron avalanche development in the MCP suggests that the transit time spread (TTS) of a straight-channel MCP should not depend on the component of the field parallel to the channel axis⁷. No theoretical input exists regarding the effect of transverse fields. Actual timing measurements of chevron-stacked MCPs exist only for magnetic fields up to 2 T. The study done for the development of the BELLE II TOP counter evaluated the timing resolution of a multi-anode Hamamatsu sensor up to 1.5 T for a fixed orientation of the sensor axis relative to the field and found no significant changes⁸. A more comprehensive study was done for the development of the PANDA DIRC as the timing performance was evaluated not only for varying fields but also for varying orientations between the sensor and the field axes⁹. Within the uncertainties of their measurements, the latter study found only a small deterioration of the time resolution towards higher fields. As this study covered a range of fields up to 2 T only, there are no data mapping MCP-PMT timing response above 2 T and it is not known if the observed small deterioration would follow a progressive trend at higher fields. While, based on the published low-field measurements, one expects the timing resolution to deteriorate (if indeed) as the field increases much less than the gain, given the requirement of 100 ps or better timing resolution for the hpDIRC, it becomes important to evaluate MCP-PMT timing characteristics with (B, θ, φ, HV) . Naturally, timing measurements strongly relate to the gain measurements and will also follow up with sensor design optimization as well as with advancements in performance of timing readout electronics. Extending the functionality of the High-B test setup to allow for precise timing measurements is also a natural synergistic activity with the LAPPD project.

The requested budget in the 60% and 80% scenario includes the cost of the cryogens required to cool the magnet and operate it over 2 weeks of measurements, of small components, such as boards, holders, connectors, *etc.* needed to readout the sensor and operate it in the dark box, a partial cost of a 10- μ m multi-anode Planacon MCP PMT, and of travel of USC personnel (one faculty, one graduate, and one

⁶ DIRC is explicitly mentioned here, since excellent timing resolution is key for the DIRC time-based PID method..

⁷ G.W. Fraser, Nucl. Instr. Meth. A **291**, 595 (1990).

⁸ S. Hirose, Nucl. Instr. Meth. A **766**, 163 (2014).

⁹A. Lehmann *et al.*, Nucl. Instr. Meth. A **595**, 173 (2008).

undergraduate students) needed to prepare for and perform the measurements. The remaining cost of the Planacon MCP PMT will be covered by carry-over funds in the USC High-B account. The carry-over are funds that we were able to save by capitalizing on several opportunities where we could reduce the cost of travel to JLab on the R&D account (sharing lodging at JLab by the students whenever possible, partial support from other sources in FY 19 for Y. Ilieva, shared travel cost from/to Columbia whenever possible). We note that the increased budget for LHe, compared to past years, is due to the 25% increase of LHe cost by the JLab supplier in FY19. Similar increase is anticipated in FY20, and the budget reflects those increases. The 100% budget includes salary support for a second USC undergraduate student. The second undergraduate student working on the project will provide needed manpower to maintain longer shifts, take and analyse more data and overall to yield a larger output of the FY20 activities. The need for more USC personnel is due to colleagues relocating for new appointments and not being able to take shifts and perform data monitoring and analysis during the measurements with a cold magnet. Purchasing a 10- μm Planacon in FY20 is well aligned in time with the activities on the hpDIRC prototype, the development and characterization of pixelated LAPPD, and the development of readout electronics for all Cherenkov prototypes based on SiREAD chips.

Our goal for the future effort of the High-B program is to achieve an MCP-PMT design and operational parameters that are optimized for successful application in the Cherenkov PID detectors in the high magnetic field of the central detector at EIC. This effort involves (a) Characterization in High-B of a variety of suitable commercially-available multi-anode MCP-PMTs as a function of various operational parameters, (b) Development and implementation of a simulation of an MCP-PMT in the design process. For this component, we will profit from the simulation effort in the LAPPD project that began in FY19.

Proposed R&D Activities

FY20

- Evaluation of the gain, ion-feedback, and timing resolution of a multi-anode 10- μm pore-size Planacon XP85122-S as a function of (B, θ, φ, HV) .
- Comprehensive gain and timing studies of XP85122-S with changing $HV_{\text{Cathode-MCP1}}$, $HV_{\text{MCP1-MCP2}}$, $HV_{\text{MCP2-Anode}}$.

FY21

- Evaluation of the gain, ion-feedback, and timing resolution of a multi-anode 10- μm pore-size Photek sensor as a function of (B, θ, φ, HV) .
- Comprehensive gain and timing studies of Photek sensor with changing $HV_{\text{Cathode-MCP1}}$, $HV_{\text{MCP1-MCP2}}$, $HV_{\text{MCP2-Anode}}$.

The proposed activities of the program are based on our results from the previous years of the program. As our efforts continue to develop, we will continue to benefit from the expertise of our PANDA GSI collaborators and from the established collaborations with MCP-PMT manufacturers, such as Photek, Photonis, and Hamamatsu as we proceed with the evaluation of their sensors.

4.1.3 High-B R&D Deliverables

FY20

- Report on multi-anode PMT (Planacon) performance as a function of (B, θ, φ, HV) .

- Publication of our 2014 – 2018 results.

4.2 LAPPD™ MCP-PMTs

Contacts: J. Xie <jxie@anl.gov>, M. Chiu <chiu@bnl.gov>

The LAPPD collaboration has successfully commercialized the standard new type MCP-PMT using atomic layer deposition technique as LAPPD™, with the same very high performance as existing MCP-PMTs, but at a significantly lower cost. For the EIC detector R&D, the effort aims to adapt the LAPPDs to the EIC requirements, which include pixelated readout and acceptable performance in high magnetic fields. With these adaptations, the LAPPDs can be used for the readout of DIRC, dRICH and mRICH subsystems as well as for TOF applications.

4.2.1 FY19 Progress and Achievements

4.2.1.1 Magnetic field tolerance, fast timing

In FY2019, the magnetic field tolerance of the ALD coated low cost MCP-PMT/LAPPD has been significantly improved to a level of over 1.5 Tesla, an order of magnitude higher than the first version Argonne MCP-PMT. The magnetic field tolerance comparison of four different ANL version MCP-PMTs were shown in Figure 4.2.1. Further improvement of magnetic field tolerance is possible with even smaller pore size (Incom is developing 6 μm pore size) MCPs. The angle dependence and biased voltage dependence of MCP-PMT performance in magnetic field were also tested, data were taken and currently under analysis.

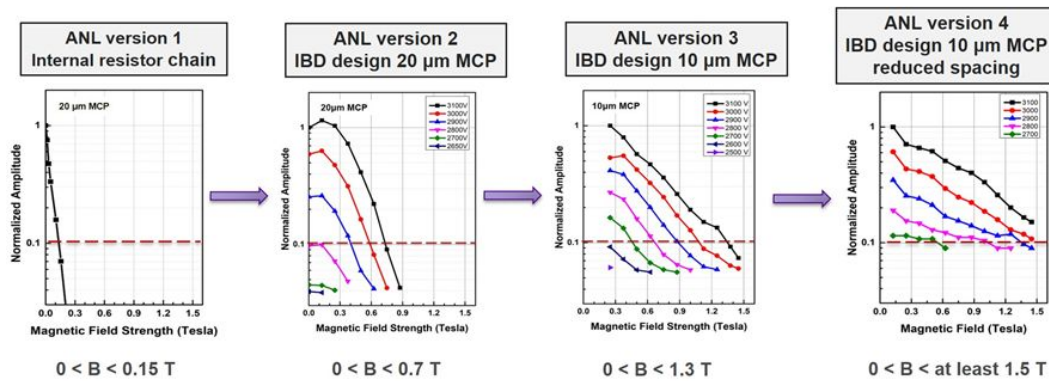


Figure 4.2.1: Comparison of magnetic field tolerance of four different versions of Argonne developed MCP-PMTs. The magnetic field tolerance was improved an order of magnitude from 0.15 T to over 1.5 T. Version 1) Internal resistor chain design with 20 μm pore size MCPs; 2) Independent biased design with 20 μm pore size MCPs; 3) Independent biased design with 10 μm pore size MCPs; 4) Independent biased design with 10 μm pore size MCPs and reduced spacing.

Using the ePHENIX field map, the magnetic field strength at the proposed locations of the mRICH and a forward pSTOF in ePHENIX was determined to range up to a maximum of 0.6 T. Both these detectors could

potentially use commercial LAPPDs as their photosensor. The recent advances in magnetic-field tolerance for the Argonne MCP-PMT design show that future LAPPDs could be made with the required field tolerance for the above proposed detectors, if they incorporate the Argonne design modifications (smaller pores and smaller gap between MCPs).

With smaller pore size MCPs, the timing characteristics of the MCP-PMTs were also improved, as listed in Table 4.2.1. The rise time was improved from 536 ps to 390 ps, time resolution reaches RMS of 106 ps and σ of 20 ps. The version 4 with reduced spacing design is supposed to have better timing resolution than version 3, but the results give worse timing in this specific tube unexpectedly. Further study will be performed on version 3 and 4 tubes to investigate the reason of the worse timing resolution.

Table 4.2.1: Geometry and performance comparison of various version Argonne developed MCP-PMTs

		ANL Version 2 Standard 20 μ m MCP-PMT	ANL Version 3 10 μ m MCP-PMT without reduced spacing	ANL Version 4 10 μ m MCP-PMT with reduced spacing
MCP	Pore size	20 μ m	10 μ m	10 μ m
	Length to diameter ratio (L/d)	60:1	60:1	60:1
	Thickness	1.2 mm	0.6 mm	0.6 mm
	Open area ratio	60 %	70 %	70 %
	Bias angle	8°	13°	13°
Detector geometry	Window thickness	2.75 mm	2.75 mm	2.75 mm
	Spacing 1	3.25 mm	2.25 mm	2.25 mm
	Spacing 2	1.75 mm	2.0 mm	0.7 mm
	Spacing 3	2.0 mm	4.0 mm	1.1 mm
	Shims	0.3 mm	0.3 mm	0.3 mm
	Tile base thickness	2.75 mm	2.75 mm	2.75 mm
MCP-PMT stack	Internal stack height	9.70 mm	9.75 mm	5.55 mm
	Total stack height	15.20 mm	15.25 mm	11.05 mm
Gain Characteristic	Gain	1.35×10^7	3.05×10^6	2.0×10^7
Time Characteristic	Rise time	536 ps	439 ps	390 ps
	Timing distribution RMS	204 ps	106 ps	190 ps
	System resolution	70.0 ps	37.2 ps	43 ps
	Time resolution	63 ps	20 ps	30 ps
	Differential time spread	11 ps	7 ps	5 ps
	Spatial resolution along strip	0.83 mm	0.53 mm	0.38 mm
Magnetic Field	Magnetic field tolerance	0.7 Tesla	1.3 Tesla	Over 1.5 Tesla

4.2.1.2 Pixel MCP-PMT readout with glass/quartz anode plate

In order to achieve the promise of the LAPPD as a useful photodetector for the ring imaging PID detectors (RICH, DIRC, and mRICH) at the EIC, a pixelated readout is essential. An elegant solution may be to use a capacitively coupled readout. In this solution, instead of an internal pad layer with signal feedthroughs, a resistive anode is created at the bottom of the MCP stack. The signals can then be capacitively coupled to a PCB with pads on the outside of the sealed MCP-PMT. This allows the user to optimize the pad design for the specific application. Another advantage is that with capacitive coupling, signals will be shared among pads, allowing for interpolation of the position and therefore potentially improving the position resolution beyond the pitch width over $\sqrt{12}$ that is standard for a single pad hit. This could allow for larger pad sizes while still achieving a desired resolution, which reduces the channel count and saves on cost and power. However, a disadvantage with charge sharing is that the cluster size increases, and thus one has to be careful

of occupancy effects. This is a concern for the DIRC, and less of a concern for the mRICH and gaseous RICH detectors.

To better understand the above effects, a capacitively-coupled MCP stack-up was installed into an MCP vacuum system, and placed in a beam of 120-GeV protons at the Fermilab test beam, as shown in Fig. 4.2.2a. Placing the stack in a vacuum system is very useful in the development phase since one can interchange different elements, such as the resistive anode, without going through the difficulty of building a sealed PMT. We could thus cycle through different elements to determine the ideal stack-up design. In this vacuum setup, since there is no high QE photocathode, signals are produced via ionization in the MCPs which then initiate the secondary electron avalanche. We read out the capacitively coupled MCP stack-up with 16 pads of 2x2, 3x3, 4x4, and 5x5 mm² pitch, as shown in the lower right inset of Fig. 4.2.2a. In Fig. 4.2.2b one can see the digitized waveforms from the CAEN DT5742 readout, showing the signals spread across 4 channels from one incoming proton track. This can be contrasted to our results from last year with direct coupling of the pads to the MCP stack, where only one pad would show a signal due to the small size of the electron cloud which is collected onto the pad. The signals from capacitive coupling are narrow and with a rise-time that is only a little slower than with direct coupling.

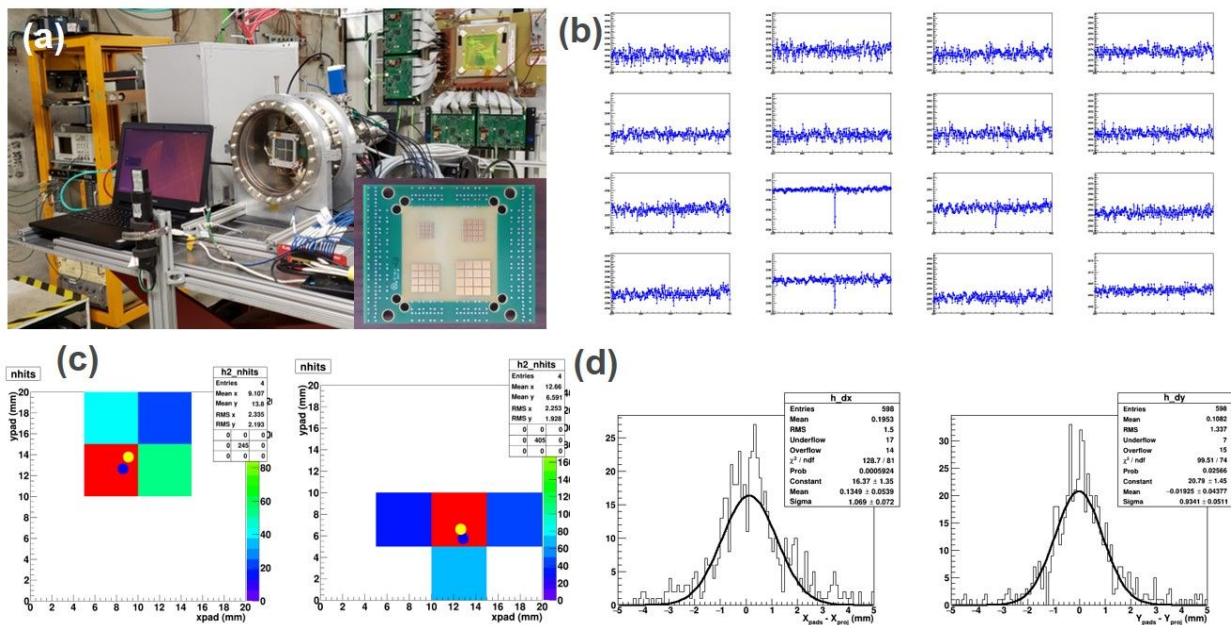


Figure 4.2.2: (a) MCP vacuum system installed at Fermilab test facility for capacitively-coupled pixel readout testing. Inset: the simple PCB board designed with 2x2, 3x3, 4x4 and 5x5 mm² pixels; (b) Signal waveforms for a single event on 4x4 mm² pads. The charge is mainly confined in one pixel, with small charge sharing at adjacent pixels; (c) Charge distribution example of two events from a 5x5 mm² pad run, with the cluster mean (yellow dot) and track projection (blue dot); (d) Position resolution of 5x5 mm² pad run: left: x-axis, right: y-axis.

The hit position on the MCP stack-up was derived using a simple mean of the charge amplitudes in each pad. To determine the position resolution one can achieve using capacitive coupling, we tracked the protons using the Fermilab Test Beam Facility’s MWPCs. The track fit was then projected onto the MCP stackup. The distribution of the difference between the track projection and the location determined from the pads for a

5x5 mm² run is shown in Fig. 4.2.2d for both the x and y directions on the pad. Table 4.2.2 shows σ_x and σ_y from runs with the 4 pad sizes tested. The sigmas are all around 1 mm, and generally get smaller with smaller pad sizes. We believe the increase in sigma for the 2x2 mm² run occurs because of losses of signal off the edge of the pads, since the 2x2 pads only cover 8x8 mm² (the beam spot from 120 GeV protons is itself around 3-4 mm wide in the horizontal direction).

The MWPCs consists of four X-Y hodoscope planes, with 1 mm pitch wires in each plane. Our preliminary estimates of the projection resolution using the MWPC is about 0.6 mm, but this has not been accounted for in Table 4.2.2 pending further refinements in our analysis. Our results show that a capacitive coupling design through glass enables pixelated readout for the LAPPD MCP-PMTs, and can achieve position resolutions that are better than with directly coupled pixel readout, even though using larger pad sizes, due to the charge sharing effect. When taking into consideration the cluster sizes from charge sharing using this scheme, and estimates of the occupancy for the RICH, mRICH, and DIRC detectors at the EIC, there should be no problem with overlapping clusters for the lower occupancies in the RICH and mRICH detectors, but that there may be a problem for the DIRC. This requires further study in simulation and also in optimizing the cluster size of a capacitively coupled MCP-PMT.

Table 4.2.2: Pixel readout results with different pixel sizes.

Run#	Pixel Size	<nhits>	Fraction of protons that leave Hits in MCP	σ (x)	σ (y)
196	5x5 mm ²	1.9	0.269	1.1 mm	0.97 mm
168	4x4 mm ²	2.2	0.265	0.81 mm	0.76 mm
149	3x3 mm ²	2.2	0.153	0.94 mm	0.95 mm
137	2x2 mm ²	2.5	0.157	1.4 mm	1.7 mm

Having demonstrated that capacitive coupling through glass works in the MCP vacuum system, for the next fiscal year we propose to build sealed capacitively coupled MCP-PMTs using the ANL 6 cm² tube facility. Various pad designs coupled to the capacitively coupled MCP-PMT will be tested in the FNAL test beam and with laser. The possibility exists that the novel zig-zag designs investigated by the eRD6 group, which has been able to achieve 100 μ m resolution with 2 cm pads, could achieve similar results for the capacitively coupled MCP-PMT. Such resolutions would enable better PID performance in ring imaging detectors, since improvements in measurement of the ring angle translates directly to better determination of the particle type.

4.2.1.3 MCP-PMT simulation

Following the committee's suggestion, we initiated the MCP-PMT simulation effort with SIMION software. Secondary electron emission process was first established with simple cylinder pore model, but with potential gradient defined (can be scaled). The simulation of the secondary electron emission process within a single MCP pore is shown in Fig. 4.2.3. The amplified electron shower from individual initial electron shows reasonable transit time relative to the initial electron hit, and the transit times are consistent pulse to pulse, indicating the principle of the simulation model is reasonable.

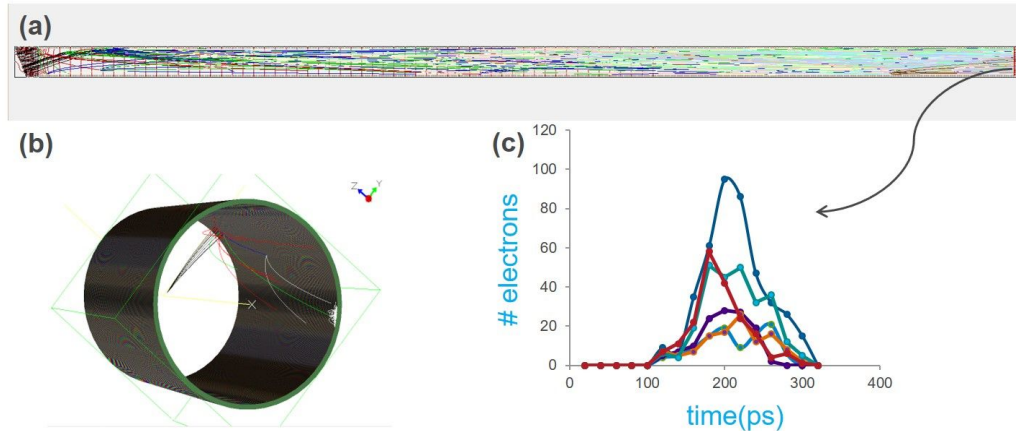


Figure 4.2.3: Single MCP simulation with SIMION software. (a) Side view of the secondary electron emission process in a single pore with multiple electrons, colors represent different “generations” of electrons as they are amplified down the pore; (b) 3-D view of the secondary electron emission process in a single pore at the beginning of the pore; (c) Dependence of a series of simulated detection pulses on the time relative to the initial electron time, each curve is a histogram of the electron shower for that initial electron hit. Note that time is shorter but times are consistent pulse to pulse.

With the establishment of the secondary electron emission process within a single pore, a full MCP-PMT geometry was constructed. We are actively working towards a full pulse simulation and later to introduce a magnetic field in the process as well. This MCP-PMT simulation effort should help us understand better the factors that affects MCP-PMT performance at different conditions, providing directions for us to further improve the design of MCP-PMTs.

4.2.2 Proposed MCP-PMT/LAPPD R&D Activities

FY20

- Produce 6cm MCP-PMTs with capacitive-coupling pixelated readout through glass
- Integrate magnetic field tolerant design with glass pixelated readout
- Test the glass pixel MCP-PMT with different pixels, evaluate its charge sharing and cross talk
- Test 20cm ceramic LAPPD, compare advantages/disadvantages of glass pixel vs. ceramic pixel
- Complete MCP-PMT simulation, introduce magnetic field in MCP-PMT simulation, understand the principle of MCP-PMT operation in high B field
- Further enhance work with electronics, DIRC, dRICH and mRICH to prepare the integration of MCP-PMT/LAPPDs on sub-systems

FY21

- Integrate Hawaii electronics with MCP-PMT/LAPPDs
- Evaluate the MCP-PMT/LAPPD performance with Hawaii electronics
- Study MCP-PMT/LAPPD afterpulse and ion feedback
- Test MCP-PMT/LAPPD with electronics package on beamline
- Possible MCP-PMT with 6 μm pore size to further enhance magnetic field tolerance

4.2.3 LAPPD R&D Deliverables

FY20

- 6cm MCP-PMT with capacitive-coupling pixelated readout through glass
- MCP-PMT simulation package
- Publications on glass capacitive coupling MCP-PMT and simulations

FY21 (tentative)

- Integration of Hawaii electronics with MCP-PMT/LAPPD
- Bench test and beam test of the sensor package
- Publication of papers on experimental results

4.3 Readout Sensors and Electronics for Detector Prototypes

Contacts: G. Varner <varner@phys.hawaii.edu>, M. Contalbrigo <mcontalb@fe.infn.it>

The development of advanced, high-performance RICH and DIRC detectors poses new demands on photosensors and requires new readout electronics. All eRD14 Cherenkov systems envision using small pixels (2–3 mm), while the DIRC also needs to obtain good timing (< 100 ps RMS) with the relatively small pulses produced by MCP-PMTs. While initial prototype tests have been made with larger pixels and poorer timing to validate Monte Carlo simulations, which were then used to infer the performance of the systems developed for the EIC, future prototypes will have to be able to directly demonstrate the desired PID performance. To achieve this, new readout electronics has to be developed. In addition, while a demonstration of the PID performance can be achieved using simpler sensors (*e.g.*, MAPMTs for the two RICH detector prototypes), the final EIC application will impose additional constraints, such as operation in the magnetic field of the solenoid as well as a minimization of the total system cost. Thus, it is also important to develop the capability to test alternative sensor solutions and up-to-date readout architectures.

To address the slightly different requirements and timelines of the various systems, we have developed a common consortium-wide strategy that provides a complete solution while maximizing synergies and minimizing cost. The Hawaii group has taken the main responsibility for the development of the front-end electronics (ASICs and boards), while INFN together with JLab has the lead on integration for both the sensors and back-end / DAQ. The development has been staged, from almost ready-to-go systems to provide a reliable reference based on a consolidated technology to innovative solutions optimized for the EIC prototypes. For the front end, the older MAROC-based system that was used in the first mRICH test beam (and is also used for CLAS12 RICH and GlueX DIRC) has been adapted for sensors (MAPMTs, SiPMs) with smaller pixels. This provides a fallback solution, and allows to explore different cooling options for the SiPMs. A new front-end is also being developed based on the waveform sampling TARGETX chip (first version ready for the 2018 mRICH beam test at Fermi Lab), which will be integrated on a board directly matching the footprint of the sensors. In contrast to MAROC, TARGETX can also provide the high-resolution timing required by high-performance DIRC detectors using time-based reconstruction algorithms. Ultimately, TARGETX would be replaced by the lower-power, higher-performance SiREAD chip. EIC experience with TARGEX would facilitate proper integration of the new chip. Nalu Scientific, LLC, a Hawaii-based small business specializing in System-on-Chips for particle physics, in collaboration

with the University of Hawaii has recently concluded a Phase I SBIR project to develop the SiREAD chip. The prototype 32 channel waveform sampling and digitizing SiREAD was fabricated and is currently under test. Figure 4.3.1 shows the fabricated SiREAD together with preliminary SiPM readout signals.

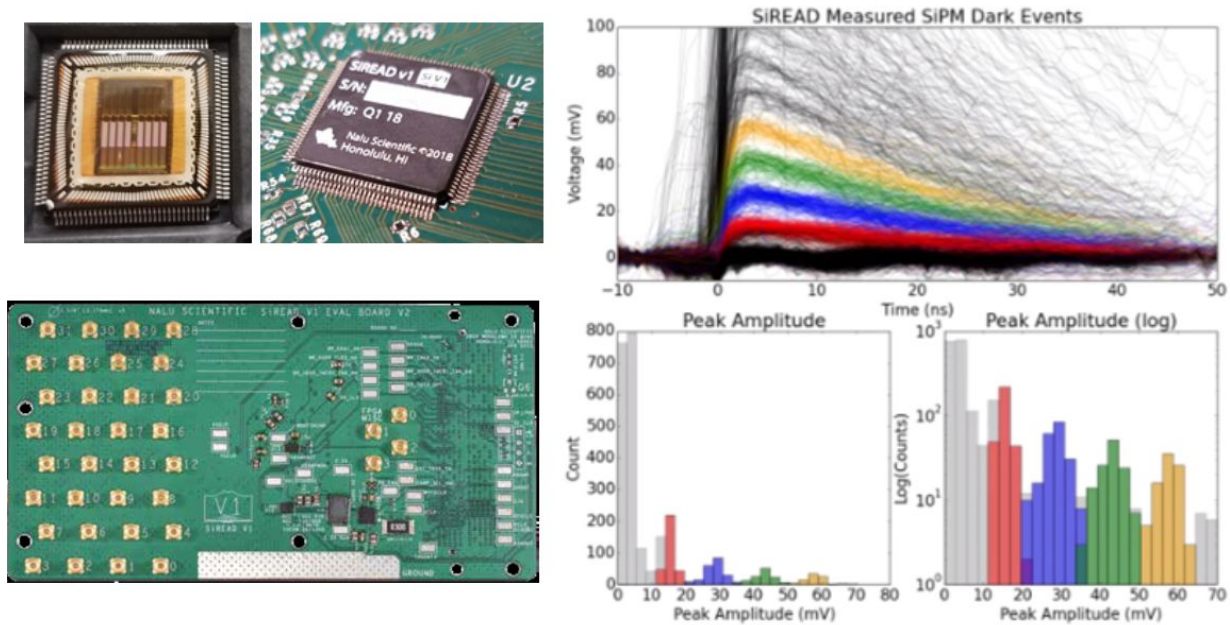


Figure 4.3.1: Micrograph of the fabricated prototype SiREAD (**top left**). Prototype SiREAD on the evaluation PCB (**top middle**). Superimposed dark count waveforms recorded from a SiPM using the SiREAD operating at 1 Gsa/s (**right**). High channel count evaluation PCB for SiREAD with 32 dedicated MMCX connectors (**bottom left**).

The SiREAD effort will also benefit from the ASoC (higher performance System-on-Chip), which has now received SBIR II funding. We hope that SiREAD will be available for instrumenting the hpDIRC prototype with small-pixel MCP-PMTs once the prototype is moved to the U.S. in FY20 specifically for the EIC R&D effort. For the back end we plan to use an adaptation of the data acquisition (DAQ) developed for CLAS12. The latter will be integrated with all three front ends and will be able to collect data from multiple sensors, and evolved in time to support cost-effective solutions and novel streaming readout approaches. The new mRICH and dRICH prototypes, while allowing the performance study with more and more realistic optical components, will also serve as demonstrators during the development of the dedicated readout electronics, *i.e.*, TARGETX / SiREAD- based readout with common DAQ.

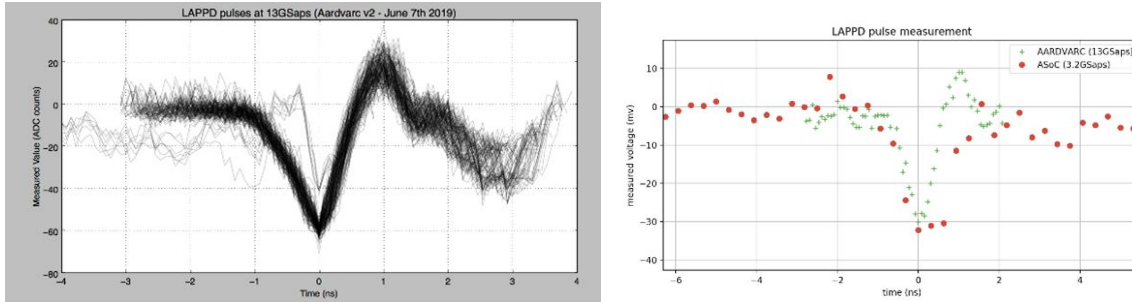


Figure 4.3.2: Super imposed reading out a LAPPD fabricated by Incom using Nalu Scientific’s high sample rate AARDVARC chip (**left**). Readout of a single LAPPD pulse using a AARDVARC and ASoC chip for comparison of various sample rate (**right**).

Staff at Nalu Scientific have been collaborating with Incom in MA on testing Nalu’s readout chips on LAPPDs. Figure 4.3.2 shows some results from this effort. While Nalu’s 13 GSa/s digitizer chip was used for this application, the concept can be expanded to lower resolution LAPPDs too.

The use of sensors with a small pixel size (2–3 mm) should allow to validate the PID performance of the mRICH, dRICH, and hpDIRC prototypes. The H13700-03 MAPMTs acquired in FY17 by GSU provide the baseline solution for testing the optics of the RICH prototypes, a goal for which tolerance to magnetic fields is not required. SiPMs represent an innovative solution with several advantages potentially interesting for EIC (such as robustness, low bias voltage, cost-effective industrial production, magnetic-field compatibility, low material budget), but also some limitations (high noise, low radiation hardness). For the DIRC, MCP-PMTs with a similar footprint will be required to provide the desired timing performance. This is also the type of sensor that would be used in a final DIRC application.

4.3.1 FY19 Progress and Achievements

The large number of sensor's channels to be readout imposes a compact, modular, and fast data acquisition system (DAQ). In addition, DAQ needs to provide single channel timing information (~few hundreds ps resolution or better) and possibly charge information (the smaller gas rings show a simulated photon multiplicity on a single pixel of approx. 1.3). The Hawaii group has been developing new front-end chips based on SiREAD, suitable for SiPM. The chip will be readout by a proper porting of the recent DAQ system developed for the CLAS12/RICH, and based on a powerful optical link between the generic programmable FPGA front-end board and the VSX sub-system processor back-end board. This synergy would speed up and simultaneously reduce development costs.

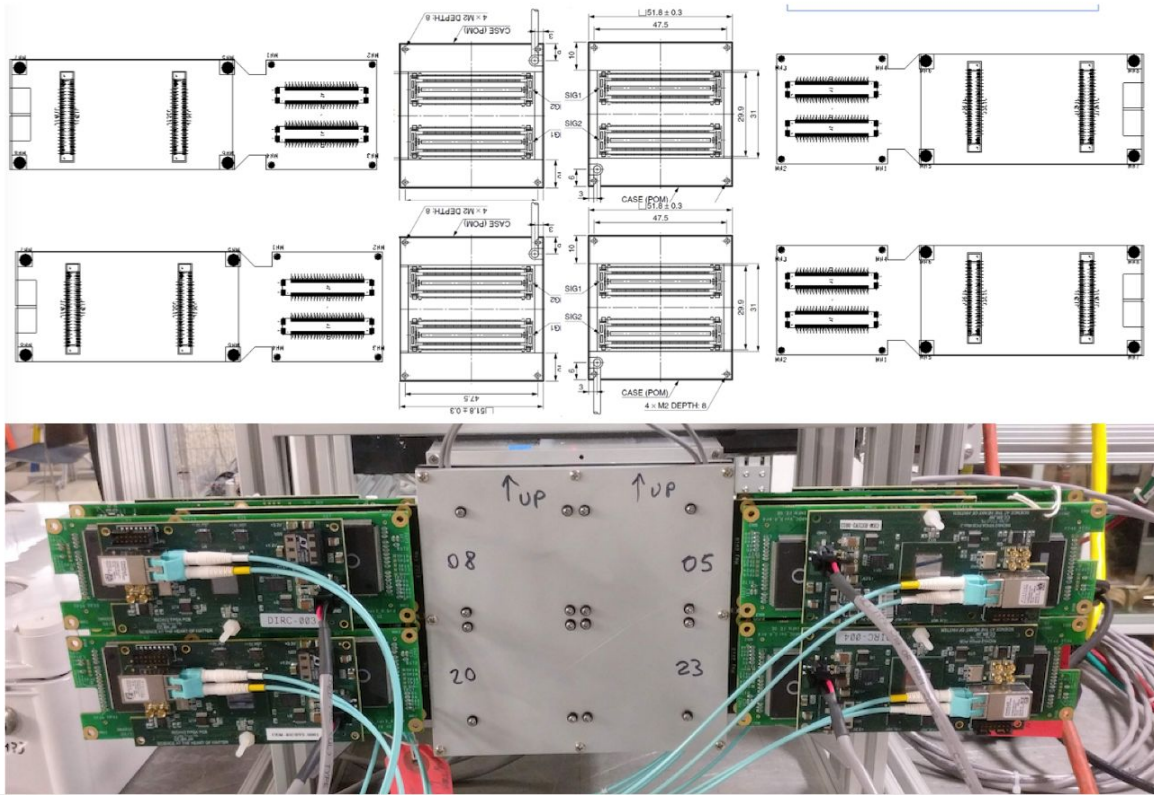


Figure 4.3.3: Adaptation of the CLAS12 readout electronics to the H13700 sensors. The adapter boards distribute the 256 channels of one sensor over two 128 channel MAROC boards mounted on opposite side (front and back).

The electronics developed for CLAS12 has been designed to readout MAPMTs and to be compatible with SiPMs. It can efficiently readout small (a fraction of 160 fC equivalent charge) and fast (of the order of 10 ns rise time) signals. An adapter board is designed to match the layout and impedance of the photo-sensor, while routing the channel outputs to the MAROC inputs. A FPGA board loads the chip configuration and organizes the readout information in ethernet or optical link connection with the back-end. This modular design can be adapted to different sensor sizes, pixelization and types. In order to match it to the H13700 sensors with 3 mm pixel size, an adapter board distributing the 256 channels (16x16) over two MAROC readout units was realized for the last mRICH test beam, see Fig.4.3.3. To match with S12642-1616PA matrices of 3x3 mm² MPPCs, an adapter board with decoupling capacitors and a cooling plate has been realized and is under test. In order to be able to readout several units during the mRICH prototype test beams, both a stand-alone TCP/IP direct link to a desktop and a complete CLAS12 DAQ VSX/VME chain, using the JLab SSP protocol, have been successfully operated with dedicated stand-alone data acquisition software.

The proposed back end and DAQ based on the SSP protocol will be compatible with both the current CLAS12 (MAROC-based) front end electronics, and the new (TARGETX, SiREAD) electronics developed by U. Hawaii. A preliminary positive assessment of the SSP DAQ firmware compatibility has been

performed by the Hawaii group. Being designed to serve a complete detector, such a DAQ system is suitable for EIC, but represents an over-sophisticated and costly solution during the prototyping phase. The INFN and JLab groups aim to realize a simplified version to be distributed among the Consortium groups. Such a basic system is under development at JLab. The funding request covers the adaptation to the Consortium needs and ensures the availability of a dedicated and flexible DAQ solution over the extended EIC R&D time period.

The INFN groups have already experience in studying the performance of SiPM in the single-photon regime for Cherenkov applications. Promising results were obtained but additional work is needed to prove a realistic working conditions in single-photon mode, taking into account the high dark count rate and the performance degradation resulting from irradiation. There is a wide interest in studying mitigation measures to improve the radiation tolerance of SiPM. The majority of the tests were dedicated to the calorimetry application, where the most important feature is linearity over a wide range of multi-photon signals. The case of single-photon detection requires special attention and dedicated measurements. The INFN group intends to extend the preliminary studies done for the high-intensity JLab environment [Con14, Con15, Bal17] to a whole program for the EIC case. This implies the contact with groups studying SiPM for Cherenkov applications in hostile environments [Tsa16, Cal19] and the collaboration with other EIC R&D Consortiums, in particular eRD21 for the estimate of the background levels, and eRD1 for the study of SiPM tolerance to radiation. Dedicated meetings have been already planned at the EIC R&D meeting at Stoney Brook and at the DIRC Workshop in Germany this year.

The characterization of the readout solutions with standard and innovative sensors requires a benchmark assessment that is most effectively obtained on laboratory test benches. To this end, the INFN group intends to setup two permanent stations with a pico-second pulsed laser working in a single-photon regime and a complete readout chains (see Fig. 4.3.4). A station was developed at JLab for the CLAS12 RICH and can be adapted to the EIC sensors and electronics. It employs a light diffuser to illuminate the whole surface of a large-area sensor while keeping a single-photon regime in each pixel. A second station is being realized in Italy with an existing laser source and a focalized beam, in order to be able to scan the sensor surface. The stations will be used to characterize and compare the photo-sensor performance in conjunction with the alternative readout solutions, to study the sensor response at various levels of irradiation with and without mitigation measures (e.g. cooling and annealing) and to validate different DAQ architectures.

Highly integrated, low-power, and high-performance readout of 256-anode, 50-mm photosensors is being studied at the University of Hawaii, which has extensive experience in developing electronics for modern PID systems, such as the Belle II TOP DIRC. The proposed system can be adapted to read out all the photosensors (MaPMT, MCP-PMT, SiPM) that are being considered for the various RICH and DIRC detector prototypes being developed by the EIC PID consortium.

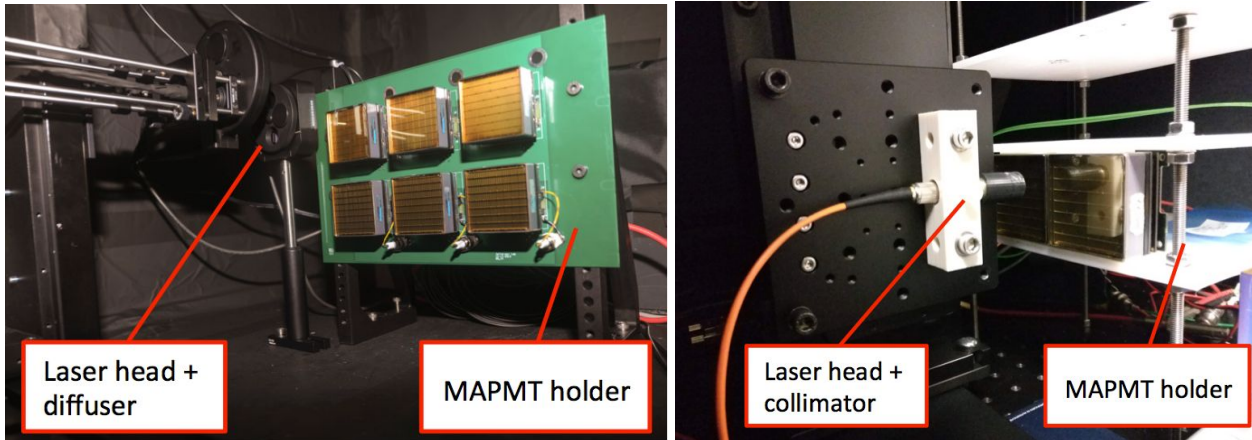


Figure 4.3.4: (Left) Existing laser test bench at JLab with a standardized MAROC readout. (Right) Laser test bench under development in Italy.

A compact board stack mates in the envelope directly behind the photosensors, permitting seamlessly abutting together an array of such devices. Each board stack consists of an interface board, which mates directly to the photodetector high-density signal connectors and hosts the waveform sampling ASICs, as well as a digital interface node. A simple and standard power and serial interface allows groups of these 256-anode devices to be collected into a single ethernet acquisition node. The first version of this readout will use a TARGET family ASIC, which has been successfully deployed in 10's of thousands of channel quantities for applications such as large muon systems or atmospheric gamma Cherenkov camera readout. Pairs of these 16-channel ASICs are mounted onto tiny DIMM cards, mounted onto the interface board. As a second phase, reduced power and further compactness will be realized by upgrading to the 64-channel SiREAD ASIC, when it becomes available. Both the TARGET and SiREAD ASICs are developed by the Hawaii group (TARGET at University of Hawaii, and SiREAD as a commercial product at Nalu Scientific). The high-speed sampling used by both chips provides the timing resolution required for the DIRC and can provide readout of waveforms during test beam conditions, which can be helpful for interpreting the data. Funding is requested for \$20k of a graduate student time to complete the layout of the 3 boards, coordinate their assembly, verify functionality of first prototypes, and characterize their performance. The cost of the fabrication and population of these first prototypes is estimated as \$10k, including printed circuit board and component costs.

In the first year of the Readout Sensors and Electronics for Prototyping activities, the goal was to instrument a 4-PMT modular RICH prototype. The PMTs are challenging in that these 2" PMTs have a rather dense anode array of 256 signal channels each. As a first stage, the readout makes use of the existing TARGETX family of 16-channel transient waveform digitizing ASICs. This compact solution benefits from integrating all trigger, sampling and analog-digital conversion functionality in the same ASIC. Therefore a relatively compact 4x4 array of these chips is able to instrument each PMT. To further speed development, a standard control and readout programmable logic unit, the SCROD, which was developed for the Belle II muon system upgrade has been adopted. While this reduced significant the initial prototyping costs, the form factor is not compatible with a final, tiled-array of readout photosensors. All the requisite boards have been

fabricated and will be tested in the Fermilab test beam facility. The complete system diagram is shown in Fig. 4.3.5.

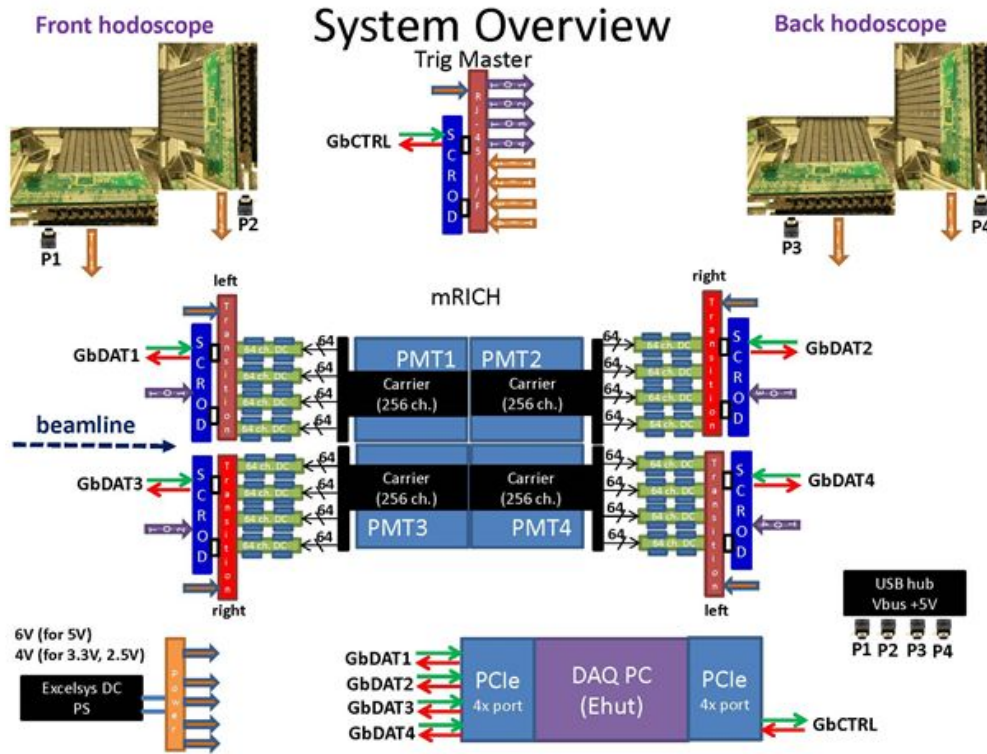


Figure 4.3.5: Overview of the 1k channel modular RICH prototype readout, which is built upon the TARGET ASIC and SCROD control and readout module.

SiREAD Parameter	Specifications
Channels	64
Sampling rate	1-4 GSa/s
Storage samples/ch	4096
Analog bandwidth	0.7-1.1 GHz
RMS voltage noise	<1mV
Dynamic range	10-11 bits
Signal voltage range	2.1 V
ADC on chip	12 bits
Readout	Serial LVDS
Power consumption	20-40 mW/ch

Table 4.3.1: SiREAD specifications.

A photograph of the first PMT assembly is shown in Fig. 4.3.6. Also shown in Fig. 4.3.6 (right) is a new building block (64 channel card card) that is based on Nalu Scientific’s SiREAD chip. The Hawaii team has fabricated and populated the board and is currently developing readout firmware for it. In order for these 4 PMTs to abutt, the design has them arrayed in a ‘pinwheel’ configuration, as shown in Fig. 4.3.7. This is something that will be addressed by the higher integration density of the future SiREAD ASIC and next-generation FPGA board.

To further reduce cost and further integration, compactness and reliability the next stage of development will implement the SiREAD ASIC. In addition to increasing channel density from 16 to 64 channels, most of the state-machine control infrastructure provided by the companion FPGA will be integrated as “system on chip” functionality. This significantly reduces the digital interconnection burden and will

make the system more scalable and make better utilization of a reduced number of gigabit fiber optic links used for control and data acquisition.

Details of the SiREAD are provided in Fig. 4.3.1 and Table 4.3.1. For the programmable logic upgrade, the plan is to use an FPGA capable of supporting the high-speed serial interface control and readout of numerous SiREAD. One straw-man design has this single FPGA readout out 16x 64-channel SiREAD, or 4 PMTs worth in the density presented above.

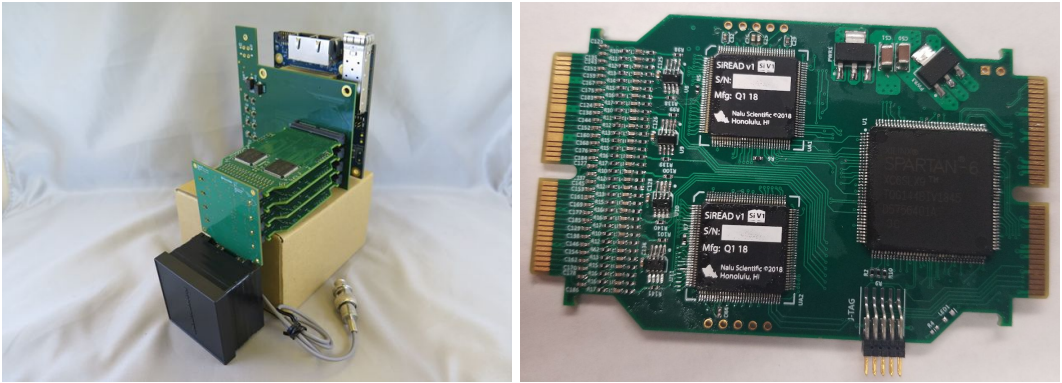


Figure 4.3.6: Photograph of the first generation of 256-anode 2" PMT readout for use in the Fermilab beam test facility (left). Photograph of the 64 channel SiREAD based (2x SiREAD rev.1) readout card as a building block for the 256 MA-PMT readout (right).

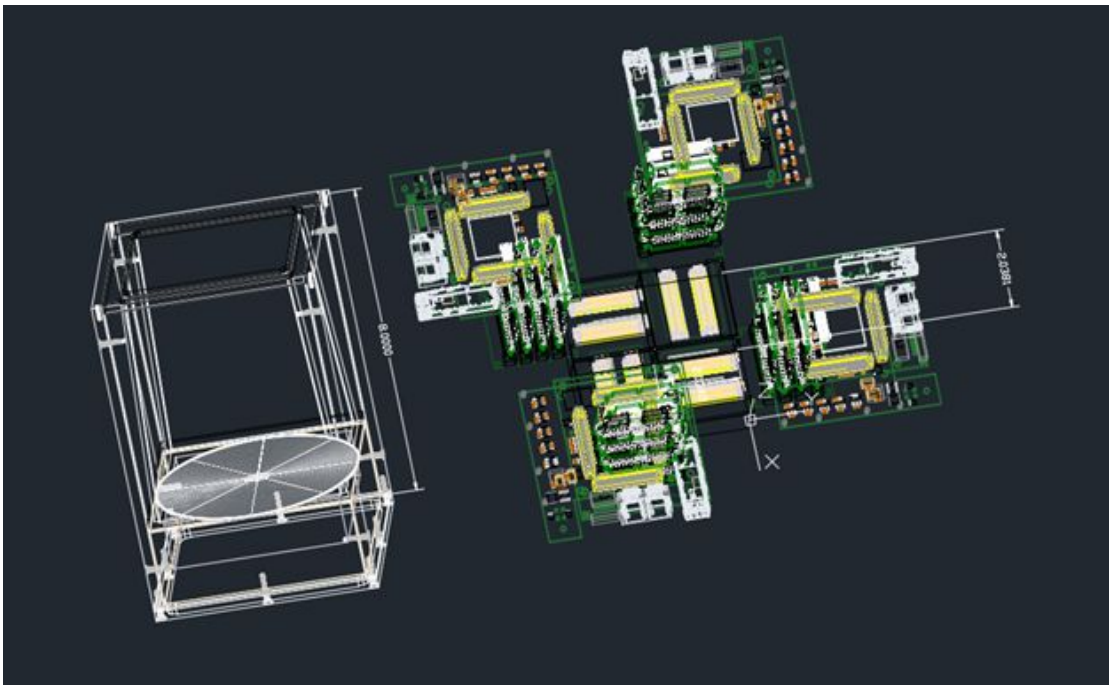


Figure 4.3.7: Prototype readout configuration, where a 'pinwheel' configuration has been used to permit the 2x2 PMT array to be abutted. While the initial design had the readout directly behind the PMT, because the current SCROD form-factor could not fit in the envelope behind the PMT, it was decided to use a Carrier board, which would offset the TARGETX and other cards and permit a simpler mechanical support and light-sealing. Next generations of the readout

will use increased integration density to permit a low-profile readout that will fit within the envelope behind the photosensor and allow indefinite tiling of photosensors and their readout.

4.3.2 Proposed R&D Activities

FY20

- Characterization of performance and validation of cost for compact and lower power readout variant using the SiREAD ASIC.
- Adapt SiREAD based readout firmware to operate with the SCROD FPGA
- Second generation firmware and improved data throughput for front-end to back-end communication.
- Modular and scalable 256-channel building block readout based on the SiREAD ASIC.
- Integration of the SSP DAQ protocol with the SiREAD front-end chips.
- Development of a portable DAQ system derived from the CLAS12 RICH readout.
- Development of pulsed-laser test stations.
- Study SiPM single-photon detection performance in the EIC environment.

References

[Con14] M. Contalbeigo et al., Nucl. Instrum. And Meth. A 766 (2014) 22.

[Con15] M. Contalbrigo, Nucl. Instrum. And Meth. A 787 (2015) 224.

[Bal17] I. Balossino et al., Nucl. Instrum. And Meth. A 876 (2017) 89.

[Tsa16] T. Tsang et al., J. Instrum. 11 (2016) P12002.

[Cal19] M. Calvi et al., Nucl. Instrum. And Meth. A 922 (2019) 243.

5. Budget

5.1 Budget Request

As our baseline (100% level), we request \$515.6k for FY20, but also provide budgets reduced by 20% and 40%, labelled “80%” and “60%” in the tables below. We also provide guidance on our plans beyond FY19 in each section above, but do not include summaries in this section beyond FY20. However, please note that in some cases items which would not be funded in the reduced-budget scenarios would be shifted into FY21. All budget items include overhead at the receiving institution. Breakdown of the request by project and institution can be found below for all three funding levels. The consortium funds have been distributed among participating institutions so as to minimize overhead and maximize flexibility. The SoWs will be submitted with wording reflecting the possibility for institutions to fund collaborators at other institutions, for instance to cover travel costs.

5.2 Dual-Radiator RICH (dRICH)

	<u>100%</u>	<u>80%</u>	<u>60%</u>
Postdoc, INFN/JLab, 4 months (Luca Barion)	\$13k	\$13k	\$13k
Postdoc, INFN/JLab, 12 months (Aram Movsisyan)	\$20k	\$10k	
Prototype components	\$15k	\$10k	\$5k
Travel	\$4k	\$2k	\$2k
<i>Total</i>	\$52k	\$35k	\$20k

5.3 Modular Aerogel RICH (mRICH)

	<u>100%</u>	<u>80%</u>	<u>60%</u>
Postdoc, INFN/JLab, 2 months (Luca Barion)	\$7k	\$7k	\$7k
Postdoc GSU (Xu Sun)	\$27.3k	\$20.5k	\$13.7k
Grad student, GSU	\$32k	\$27.3k	\$19.8k
Materials, GSU	\$4.5k	\$1.5k	\$1.5k
Travel and Conference fee, INFN/GSU	\$7.5k	\$7.5k	\$7.5k
<i>Total</i>	\$78.3k	\$63.8k	\$49.5k

5.4 High-Performance DIRC (hpDIRC)

	<u>100%</u>	<u>80%</u>	<u>60%</u>
Postdoc, CUA, 50%	\$60k	\$60k	\$45k
Lens characterization components	\$25k	\$15k	\$7k
Prototype shipment	\$15k	\$15k	\$15k
Prototype DAQ/monitoring equipment	\$24k	\$8k	\$8k
Radiation Hardness test	\$1k	\$1k	\$1k
Travel, CUA/GSI	\$9k	\$9k	\$6k
<i>Total</i>	\$134k	\$108k	\$82k

5.5 Sensors in High-B Fields

	<u>100%</u>	<u>80%</u>	<u>60%</u>
LHe and materials for high-B run, JLab	\$9.7k	\$9.7k	\$9.7k
Undergraduate student, USC	\$10.8k	\$5.4k	\$5.4k
Travel, USC	\$12.3k	\$10.5k	\$10.5k
Planacon MCP PMT 10 μ m pore size (partial cost)	\$6.5k	\$6.5k	\$6.5k
<i>Total</i>	\$39.3k	\$32.1k	\$32.1k

5.6 MCP-PMT, LAPPD

	<u>100%</u>	<u>80%</u>	<u>60%</u>
Staff effort for manufacture and test pixel MCP-PMTs	\$75k	\$70k	\$60k
MCPs and pixel tile assemblies	\$15k	\$15k	\$10k
MCP-PMT simulations	\$20k	\$10k	
Travel to Incom, meetings and conferences	\$10k	\$5k	\$5k
<i>Total</i>	\$120k	\$100k	\$75k

5.7 Readout Sensors and Electronics for Detector Prototypes

	<u>100%</u>	<u>80%</u>	<u>60%</u>
Front-end readout electronics, Hawaii	\$60k	\$48k	\$36k
Postdoc, INFN, 6 months (Luca Barion)	\$20k	\$20k	\$20k
Components, INFN	\$10k	\$5k	
Travel INFN	\$2k	\$2k	
<i>Total</i>	\$92k	\$75k	\$56k

5.8 Budget by project

	<u>100%</u>	<u>80%</u>	<u>60%</u>
dRICH	\$52k	\$35k	\$20k
mRICH	\$78.3k	\$63.8k	\$49.5k
hpDIRC	\$134k	\$108k	\$82k
high-B	\$39.3k	\$32.1k	\$32.1k
LAPPD	\$120k	\$100k	\$75k
Electronics	\$92k	\$75k	\$56k
<i>Total</i>	\$515.6k	\$413.9k	\$314.6k

5.9 Budget by institution

	<u>100%</u>	<u>80%</u>	<u>60%</u>
ANL	\$120k	\$100k	\$75k
INFN	\$94k	\$72k	\$50k
CUA (and GSI)	\$134k	\$108k	\$82k
GSU	\$68.3k	\$53.8k	\$39.5k
U. Hawaii	\$60k	\$48k	\$36k
JLab	\$9.7k	\$9.7k	\$9.7k
USC	\$29.6k	\$22.4k	\$22.4k
<i>Total</i>	\$515.6k	\$413.9k	\$314.6k

Appendices

Appendix A

List of R&D Publications and Presentations

2019 -- Publications

1. J. Xie *et al.*, *Fast-timing microchannel plate photodetectors: design, fabrication and characterization*, *Review of Scientific Instruments*, 90, 043109 (2019) <https://doi.org/10.1063/1.5063825>
2. M. Hattawy *et al.*, *Characteristics of fast timing MCP-PMTs in magnetic fields*, *NIMA*, 929, 84 (2019) <https://doi.org/10.1016/j.nima.2019.03.045>

2019 -- Presentations

1. A. Rowland, *Studies of the Gain of Small-Pore Size Microchannel Plate Photomultipliers in High Magnetic Fields*, poster presentation, Discover USC, Columbia, SC, April 26, 2019

2018 -- Publications

1. X. He, for the EIC PID Consortium (eRD14 Collaboration), *Ring Imaging Cherenkov Detector Technologies for Particle Identification in the Electron-Ion Collider Experiments*, 21st Particle and Nuclei International Conference (PANIC 2017), *International Journal of Modern Physics: Conference Series*, Vol. 46 (2018) 1960080. DOI: 10.1142/S2010194518600807.
2. J. Xie *et al.*, *Rate capability and magnetic field tolerance measurements of fast timing microchannel plate photodetectors*, 912, 85 (2018). <https://doi.org/10.1016/j.nima.2017.10.059>
3. G. Kalicy *et al.*, *High-performance DIRC detector for the future Electron Ion Collider experiment*, *Proceedings of DIRC2017*, *JINST* **13**, C04018 (2018). <https://doi.org/10.1088/1748-0221/13/04/C04018>
4. Y. Ilieva *et al.*, *Particle Identification for a future EIC detector*, *Proceedings of DIRC2017*, *JINST* **13**, C03018 (2018). <https://doi.org/10.1088/1748-0221/13/03/C03018>

2018 -- Presentations

1. X. Sun, for the EIC PID Consortium (eRD14 Collaboration), *Ring Imaging Cherenkov Detector for Particle Identification in the Electron-Ion Collider (EIC) Experiments*, RHIC/AGS Users Meeting, June 12 – 15, 2018.
2. J. Xie, *Development of Fast-timing MCP-PMT/LAPPD for Particle IDentification (PID)*, CPAD Instrumentation Frontier Workshop 2018, Providence, RI, December 9-11, 2018
3. J. Xie, *Development of MCP-PMT/LAPPD towards EIC application*, Electron Ion Collider User Group Meeting, Washington, DC, July 30-August 2, 2018
4. A. Rowland (EIC PID Consortium), *Studies of the Gain of Small-Pore Size Microchannel Plate Photomultipliers in High Magnetic Fields*, poster presentation at the Conference Experience for Undergraduates, 5th Joint Meeting of the APS Division of Nuclear Physics and the Physical Society of Japan, Waicoloa, HI, October 23 – 27, 2018

5. A. Rowland, *Studies of the Gain of Small-Pore Size Microchannel Plate Photomultipliers in High Magnetic Fields*, poster presentation, 85th Annual Meeting of the APS Southeastern Section, Knoxville, TN, November 8 – 10, 2018

2017 -- Publications

1. A. Del Dotto, C.-P. Wong *et al.* (EIC PID Consortium), *Design and R&D of RICH detectors for EIC experiments*, NIM A <https://doi.org/10.1016/j.nima.2017.03.032>
2. J. Wang *et al.*, *Design improvement and bias voltage optimization of glass-body microchannel plate picosecond photodetector*, Nuclear Science IEEE Transactions 64, 1871 (2017).
3. C.P. Wong *et al.*, *Modular focusing ring imaging Cherenkov detector for Electron-Ion Collider experiments*, NIM A 871, 13 (2017).

2017 -- Presentations

1. R. Dzhygadlo for the EIC DIRC Collaboration, *DIRC-based PID for the EIC Central Detector*, oral presentation at the DPG spring meeting, Muenster, March 27 – 31, 2017.
2. X. He for the EIC PID Consortium, *Ring Imaging Cherenkov Detector Technologies for Particle Identification in the Electron-Ion Collider Experiments*, PANIC2017, in Beijing, September 1 – 5, 2017.
3. Y. Ilieva for the EIC PID Consortium, *Particle Identification for a Future EIC Detector*, 2017 International Workshop on Fast Cherenkov Detectors - Photon detection, DIRC design and DAQ, August 7 – 9, 2017, Giessen, Germany.
4. G. Kalicy for the EIC PID Consortium, *The High-Performance DIRC for a Future EIC Detector*, 2017 International Workshop on Fast Cherenkov Detectors - Photon detection, DIRC design and DAQ, August 7 – 9, 2017, Giessen, Germany.
5. J. Xie, *Development of fast-timing microchannel plate photomultiplier*, Fall Meeting of the Division of Nuclear Physics of the American Physical Society (DNP 2017), Pittsburgh, PA, Oct. 2017 (Invited talk)

2016 -- Publications

1. Y. Ilieva *et al.*, *MCP-PMT Studies at the High-B Test Facility at Jefferson Lab*, JINST **11**, 2016; <http://dx.doi.org/10.1088/1748-0221/11/03/C03061>. Proceedings of the International Workshop on Fast Cherenkov Detectors - Photon detection, DIRC design and DAQ, November 11–13, 2015, Giessen, Germany.
2. G. Kalicy *et al.*, *High-performance DIRC detector for Electron Ion Collider*, submitted to JINST, 2016; Proceedings of the International Workshop on Fast Cherenkov Detectors - Photon detection, DIRC design and DAQ, November 11–13, 2015, Giessen, Germany.
3. J. Xie *et al.*, *Development of a low-cost fast-timing microchannel plate photodetector*, Nucl. Instrum. Meth. A 824 (2016) 159-161.
4. L. Allison: *High-performance DIRC detector for use in an Electron-Ion Collider*, Proceedings for ICHEP2016 (38th International Conference on High Energy Physics), August 3-10, 2016, Chicago, IL, submitted to Proceedings of Science.

2016 -- Presentations

1. H. Hamilton, *Testing of Advanced Particle Detectors for the Next Generation Particle Collider*, oral presentation at the Abilene Christian University Undergraduate Research Festival, 5 April 2016, Abilene, TX.
2. C. Towell, *Development of an Electron Ion Collider Detector Test Stand*, oral presentation at the Abilene Christian University Undergraduate Research Festival, 5 April 2016, Abilene, TX.
3. A. Del Dotto for the EIC PID consortium, *Design and R&D of RICH detectors for EIC experiments*, poster presented at RICH 2016, 9th International Workshop on Ring Imaging Cherenkov Detectors, Slovenia on September 5-9, 2016.
4. Z.W. Zhao for the EIC PID consortium, EIC RICH R&D, presentation at EIC User Group Meeting, January 2016.
5. L. Allison for the EIC DIRC Collaboration, *Particle ID with DIRC Detectors*, invited talk at ODU Nuclear Group Seminar, March 17, 2016.
6. G. Kalicy for the EIC DIRC Collaboration, *DIRCs*, invited talk at ODU Nuclear Group Seminar, December 4, 2016.
7. G. Kalicy for the EIC DIRC Collaboration, *DIRC@EIC*, presentation at EIC User Group Meeting, January 2016.
8. G. Kalicy: PID systems for the JLab EIC full-acceptance detector, ICHEP2016 38th International Conference on High Energy Physics, August 3–10, 2016, Chicago, IL.
9. J. Xie *et al.*, *Planar microchannel plate photomultiplier with VUV-UV-Vis full range response for fast timing and imaging applications*, accepted for RICH 2016, 9th International Workshop on Ring Imaging Cherenkov Detectors, Slovenia on September 5-9, 2016.
10. C.P. Wong, *Performance Study of a Prototype Modular RICH Detector for EIC Experiments*, oral presentation at 2016 Fall Meeting of the APS Division of Nuclear Physics, October 13–16, 2016, Vancouver, Canada.

2015 -- Publications

1. J. Wang *et al.*, *Development and testing of cost-effective, 6cm × 6cm MCP-based photodetectors for fast timing applications*, Nucl. Instrum. Meth. A 804 (2015) 84–93.

2015 -- Presentations

1. H. Hamilton, *Improved Timing Instruments for Particle Identification*, oral presentation at the Abilene Christian University Undergraduate Research Festival, March 31, 2015, Abilene, TX.
2. C. Towell, *Building Detectors to Study a New Phase of Matter*, oral presentation at the Abilene Christian University Undergraduate Research Festival, March 31, 2015, Abilene, TX.
3. E. Bringley *et al.*, *Experimental Setup and Commissioning of a Test Facility for Gain Evaluation of Microchannel-Plate Photomultipliers in High Magnetic Field at Jefferson Lab*, poster presentation at the University of South Carolina Discovery Day, 24 April 2015, Columbia, SC.
4. C. Barber, *Gain Evaluation of Micro-Channel-Plate Photomultipliers in the Upgraded High-B Test Facility at Jefferson Lab*, poster presentation at the Conference Experience for Undergraduates at the 2015 Fall Meeting of the APS Division of Nuclear Physics, October 28–31, 2015, Santa Fe, NM; BAPS.2015.DNP.EA.37.
5. H. Hamilton, *Testing of multigap Resistive Plate Chambers for Electron Ion Collider Detector Development*, poster presentation at the Conference Experience for Undergraduates at the 2015 Fall

- Meeting of the APS Division of Nuclear Physics, October 28–31, 2015, Santa Fe, NM; BAPS.2015.DNP.EA.9.
6. C. Towell, *Cosmic Test Stand Development for Electron Ion Collider Detector R&D*, poster presentation at the Conference Experience for Undergraduates at the 2015 Fall Meeting of the APS Division of Nuclear Physics, October 28–31, 2015, Santa Fe, NM; BAPS.2015.DNP.EA.20.
 7. Y. Ilieva for the EIC DIRC Collaboration, *MCP-PMT Studies at the High-B Test Facility at Jefferson Lab*, invited talk at the International Workshop on Fast Cherenkov Detectors - Photon detection, DIRC design and DAQ, November 11–13, 2015, Giessen, Germany.
 8. G. Kalicy for the EIC DIRC Collaboration, *High-performance DIRC detector for Electron Ion Collider*, invited talk at the International Workshop on Fast Cherenkov Detectors - Photon detection, DIRC design and DAQ, November 11–13, 2015, Giessen, Germany.
 9. L. Allison for the EIC DIRC Collaboration, *Studies of prototype 3-component lens in CERN test beam and on a test bench at ODU*, invited talk at the International Workshop on Fast Cherenkov Detectors - Photon detection, DIRC design and DAQ, November 11–13, 2015, Giessen, Germany.
 10. G. Kalicy for the EIC DIRC Collaboration, *DIRC detectors*, presentation at JLab seminar, Newport News, December 2015.
 11. G. Kalicy for the EIC DIRC Collaboration, *Photosensors tests at high B facility in JLab*, presentation at meeting with Photonis in Lancaster, PA, October 2015.
 12. G. Kalicy for the EIC DIRC Collaboration, *Photosensors tests at high B facility in JLab*, presentation on meeting with Hamamatsu at JLab, September 2015.
 13. G. Kalicy for the EIC DIRC Collaboration, *Developing DIRC Technology*, presentation at ODU Colloquium, Norfolk VA, April 2015.
 14. R. Dzhygadlo for the EIC DIRC Collaboration, *DIRC-based PID for the EIC Central Detector*, oral presentation at the DPG spring meeting, Heidelberg, March 23–27, 2015.
 15. C.P. Wong, *Simulation Study of RICH Detector for Particle Identification in Forward Region at Electron-Ion Collider*, oral presentation at APS April Meeting 2015, April 11–14, 2015, Baltimore, MD.

Prior 2015 -- Presentations

1. C. Nickle, *Experimental Setup for Magnetic-Field Tests of Small-Size Light Sensors at Jefferson Lab*, poster presentation at the Conference Experience for Undergraduates at the 2013 Fall Meeting of the APS Division of Nuclear Physics, October 23–26, 2013, Newport News, VA; BAPS.2013.DNP.EA.121.
2. E. Bringley *et al.*, *Experimental Setup and Commissioning of a Test Facility for Gain Evaluation of Microchannel-Plate Photomultipliers in High Magnetic Field at Jefferson Lab*, poster presentation at the Conference Experience for Undergraduates at the 4th Joint Meeting of the APS Division of Nuclear Physics and the Physical Society of Japan, October 7–11, 2014, Waikoloa, Hawaii; BAPS.2014.HAW.GB.140.
3. H. Hamilton, *Time of Flight Detector Development for Future Heavy Ion Experiments*, poster presentation at the Conference Experience for Undergraduates at the 4th Joint Meeting of the APS Division of Nuclear Physics and the Physical Society of Japan, October 7–11, 2014, Waikoloa, Hawaii; BAPS.2014.HAW.GB.149.

4. C. Towell, *Developing a High Precision Cosmic Test Stand for PHENIX Research and Development*, poster presentation at the Conference Experience for Undergraduates at the 4th Joint Meeting of the APS Division of Nuclear Physics and the Physical Society of Japan, October 7–11, 2014, Waikoloa, Hawaii; BAPS.2014.HAW.GB.147.